NASA Technical Memorandum 89002

Far-Field Acoustics of Supersonic Rectangular Nozzles With Various Throat Aspect Ratios

Michael K. Ponton
PRC Kentron, Inc.
Hampton, Virginia

James C. Manning and John M. Seiner
Langley Research Center
Hampton, Virginia

National Aeronautics
and Space Administration

Scientific and Technical Information Branch

1986

Summary

The acoustic data generated from a far-field study of four rectangular nozzles with various throat aspect ratios are presented. One nozzle tested (throat aspect ratio of 2.0) was designed for an exit Mach number of 1.66 and the remaining three nozzles tested (throat aspect ratios of 3.7, 5.8, and 7.6) were designed for an exit Mach number of 1.35. Results include plots of narrowband spectra and overall sound pressures.

Introduction

The impetus for studying rectangular nozzles is driven by the potential for improved fighter aircraft aerodynamic and propulsive performance by utilizing this type of geometry for their engines' exhaust ducts. Except for research (refs. 1 through 3) on resonance phenomena of choked rectangular jets with aspect ratios greater than 5, the authors know of no previously published far-field acoustic data gathered under anechoic conditions for low-aspect-ratio rectangular nozzles designed to produce supersonic shock-free flows.

The far-field acoustic properties of jets produced by four low-aspect-ratio (less than 10) rectangular nozzles were studied at the Langley Research Center. Three of these nozzles were designed to produce identical supersonic exit Mach numbers. The far-field acoustic data generated from studying the plumes of these nozzles under static (no external flow) conditions in an anechoic environment are presented in this report.

The data are organized to (1) show the narrowband spectra gathered by microphones at several spatial locations for various operating conditions and (2) show the directional properties of the overall sound pressures generated by the jet flows.

Symbols

A_e	nozzle exit area
A_t	nozzle throat area
AR	throat aspect ratio, w/h_t
h_e	nozzle height at exit, $(A_e/A_t)(w/\mathrm{AR})$
h_t	nozzle height at throat
M_d	nozzle design Mach number
OASP	overall sound pressure (root-mean-square pressure)
p_a	ambient pressure
p_e	static pressure at nozzle exit
R	radius from microphone arc to nozzle centerline at nozzle exit, 3.66 m
RH	relative humidity
SPL	sound pressure level
T_a	ambient temperature
w	nozzle internal duct width, 10.16 cm
ϕ	azimuthal angle
θ	microphone angle relative to downstream jet axis

Experimental Details

The far-field acoustic data were gathered in the Langley Anechoic Noise Facility (LANF)(ref. 4). This facility's interior dimensions are 8.2 by 8.4 by 7.5 m high from wedge tip to wedge tip. The LANF utilizes an air supply capable of supplying 7.7 kg/s of continuous dry unheated air. Electronically controlled valves maintain nozzle pressure ratios to within 0.3 percent of the desired set point. Pressure transducers used in the system to control the flow were calibrated each day.

Free field 1/4-inch microphones were positioned on a circular arc from $\theta = 22.5°$ to $135°$(with respect to the nozzle downstream jet axis, see left-hand side of fig. 1) at $7.5°$ increments. The radius from the microphone arc to the center of the nozzle exit was 3.66 m. The outputs from the 16 microphones were multiplexed and then fed directly into a Fast Fourier Transform analyzer and digital voltmeter. The multiplexers, analyzer, and voltmeter were computer interfaced to enable remote-controlled setup and data acquisition. Microphone calibrations were performed at the beginning of each week. Each nozzle being tested was positioned at various azimuthal angles, ϕ, with $0°$ being referenced to the large dimension of the nozzle. (See right-hand side of fig. 1.) A simple rotational device was used to accomplish the azimuthal settings. (See fig. 2.) Spectral data (analyzed to 60 kHz with a filter bandwidth of 60 Hz) were collected for nine azimuthal angles at five different pressure ratios. Sound pressure data, processed by a digital voltmeter, were obtained for the same 9 values of ϕ at 11 or 12 nozzle pressure ratios, dependent upon the particular nozzle tested.

Four nozzles with throat aspect ratios of 2.0, 3.7, 5.8, and 7.6 were tested. These nozzles are convergent divergent in a single plane utilizing wedge-shaped passages and having full sidewalls (i.e., sidewalls extending to the nozzle exit) as shown in figure 3. (See ref. 5.) Table 1 provides salient features of the nozzle designs.

Table 1. Geometry of Nozzles

AR	w, cm	h_t, cm	A_e/A_t	h_e, cm	M_d
2.0	10.16	5.080	1.300	6.604	1.66
3.7	10.16	2.746	1.089	2.990	1.35
5.8	10.16	1.752	1.089	1.908	1.35
7.6	10.16	1.337	1.089	1.456	1.35

Acoustic Results

Narrowband spectra were gathered for 16 microphone θ locations (22.5° to 135° in 7.5° increments), 9 nozzle ϕ positions (0°, 15°, 30°, 45°, 60°, 75°, 90°, 180°, and 270°), and 5 operating pressure ratios (p_e/p_a = 0.6, 0.85, 1.0, 1.25, and 1.45 for the nozzle with AR = 2.0 and p_e/p_a = 0.65, 0.85, 1.0, 1.25, and 1.45 for the nozzles with AR = 3.7, 5.8, and 7.6); this yielded 720 spectra for each nozzle configuration. However to conserve space, only eight θ locations (30° to 135° in 15° increments) are presented in this report. Note that the pressure ratio p_e/p_a is inferred from the nozzle design Mach number and the operating supply pressure located in a plenum upstream of the nozzle. Figures 4 through 7 contain the spectra for the nozzles with aspect ratios of 2.0, 3.7, 5.8, and 7.6, respectively. The spectra are presented from 120 Hz to 20 kHz, a range where most of the useful acoustic information exists. All the spectral data from 0 to 60 kHz are being maintained in computer files. Spectral corrections for atmospheric absorption have not been made; however, the relative humidity and ambient temperature are included for each spectrum to enable such corrections if deemed necessary.

Overall sound pressures are shown on directivity plots in figures 8 through 11 (again AR = 2.0, 3.7, 5.8, and 7.6, respectively) for the coordinate ϕ, azimuthal angle. The run conditions for the data plotted coincide with the ϕ positions used to gather spectral data and include 16 θ angles (22.5° to 135° in 7.5° increments), 12 pressure ratios for the nozzle with AR = 2.0 (p_e/p_a = 0.5, 0.6, 0.7, 0.8, 0.85, 0.9, 1.0, 1.1, 1.2, 1.25, 1.35, and 1.45) and 11 pressure ratios for the nozzles with AR = 3.7, 5.8, and 7.6 (p_e/p_a = 0.65, 0.7, 0.8, 0.85, 0.9, 1.0, 1.1, 1.2, 1.25, 1.35, and 1.45). Since a change in ϕ involves a nozzle rotation, each directivity plot contains data taken over several days.

Concluding Remarks

Far-field acoustic data acquired at the Langley Research Center are presented for four rectangular nozzles having throat aspect ratios of 2.0, 3.7, 5.8, and 7.6. The first nozzle (aspect ratio 2.0) was designed to produce an exit Mach number of 1.66 and the latter three nozzles (aspect ratios of 3.7, 5.8, and 7.6) were designed to produce an exit Mach number of 1.35. Narrowband spectra and overall sound pressures are given for numerous spatial locations and supersonic nozzle pressure ratios.

NASA Langley Research Center
Hampton, VA 23665-5225
October 31, 1986

References

1. Powell, Alan: On the Noise Emanating From a Two-Dimensional Jet Above the Critical Pressure. *Aeronaut. Q.*, vol. IV, pt. 2, Feb. 1953, pp. 103–122.
2. Hammitt, Andrew G.: The Oscillation and Noise of an Overpressure Sonic Jet. *J. Aerosp. Sci.*, vol. 28, no. 9, Sept. 1961, pp. 673–680.
3. Krothapalli, R.; Baganoff, D.; and Hsia, Y.: On the Mechanism of Screech Tone Generation in Underexpanded Rectangular Jets. AIAA-83-0727, Apr. 1983.
4. Hubbard, Harvey H.; and Manning, James C.: *Aeroacoustic Research Facilities at NASA Langley Research Center Description and Operational Characteristics.* NASA TM-84585, 1983.
5. Seiner, John M.; Ponton, Michael K.; and Manning, James C.: Acoustic Properties Associated With Rectangular Geometry Supersonic Nozzles. AIAA-86-1867, July 1986.

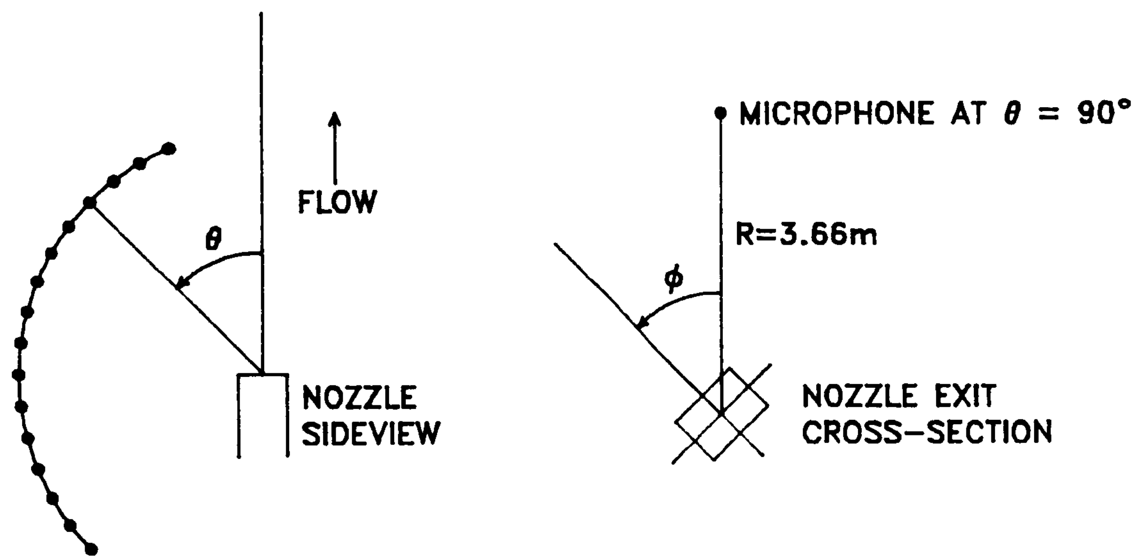

Figure 1. Reference of microphone angle θ and azimuthal angle ϕ.

ORIGINAL PAGE IS
OF POOR QUALITY

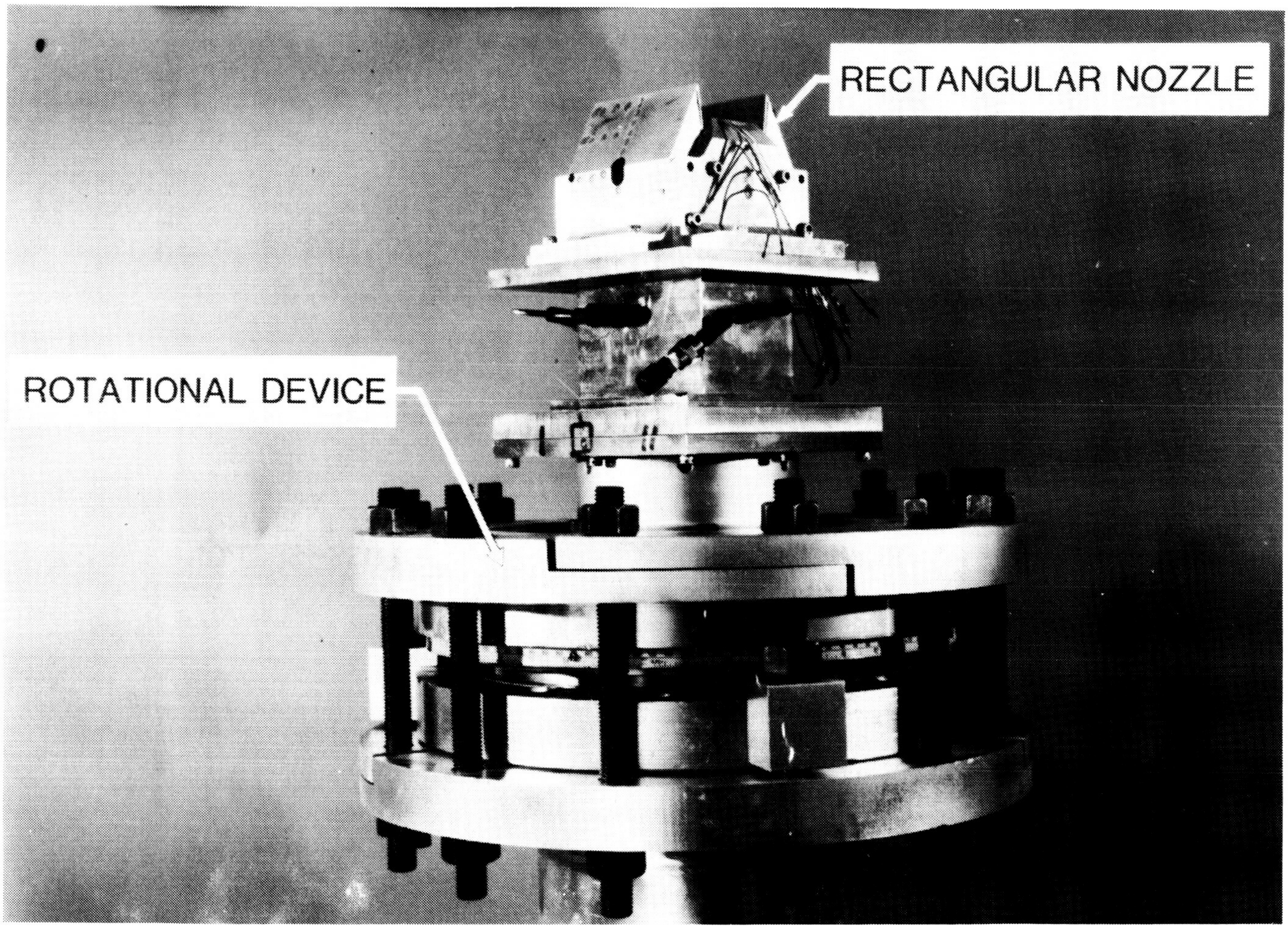

L-86-332

Figure 2. Device used to set azimuthal angle ϕ.

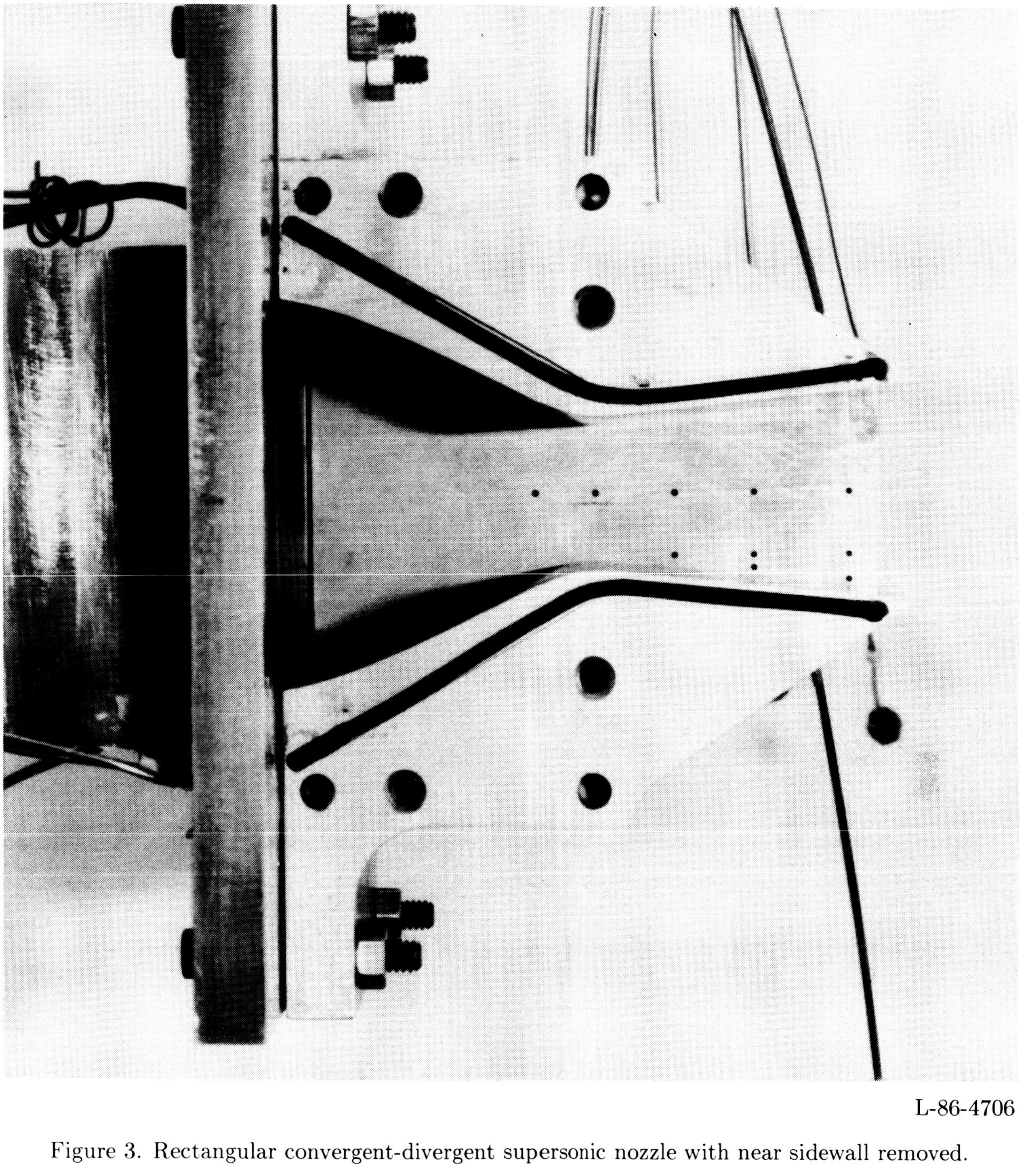

L-86-4706

Figure 3. Rectangular convergent-divergent supersonic nozzle with near sidewall removed.

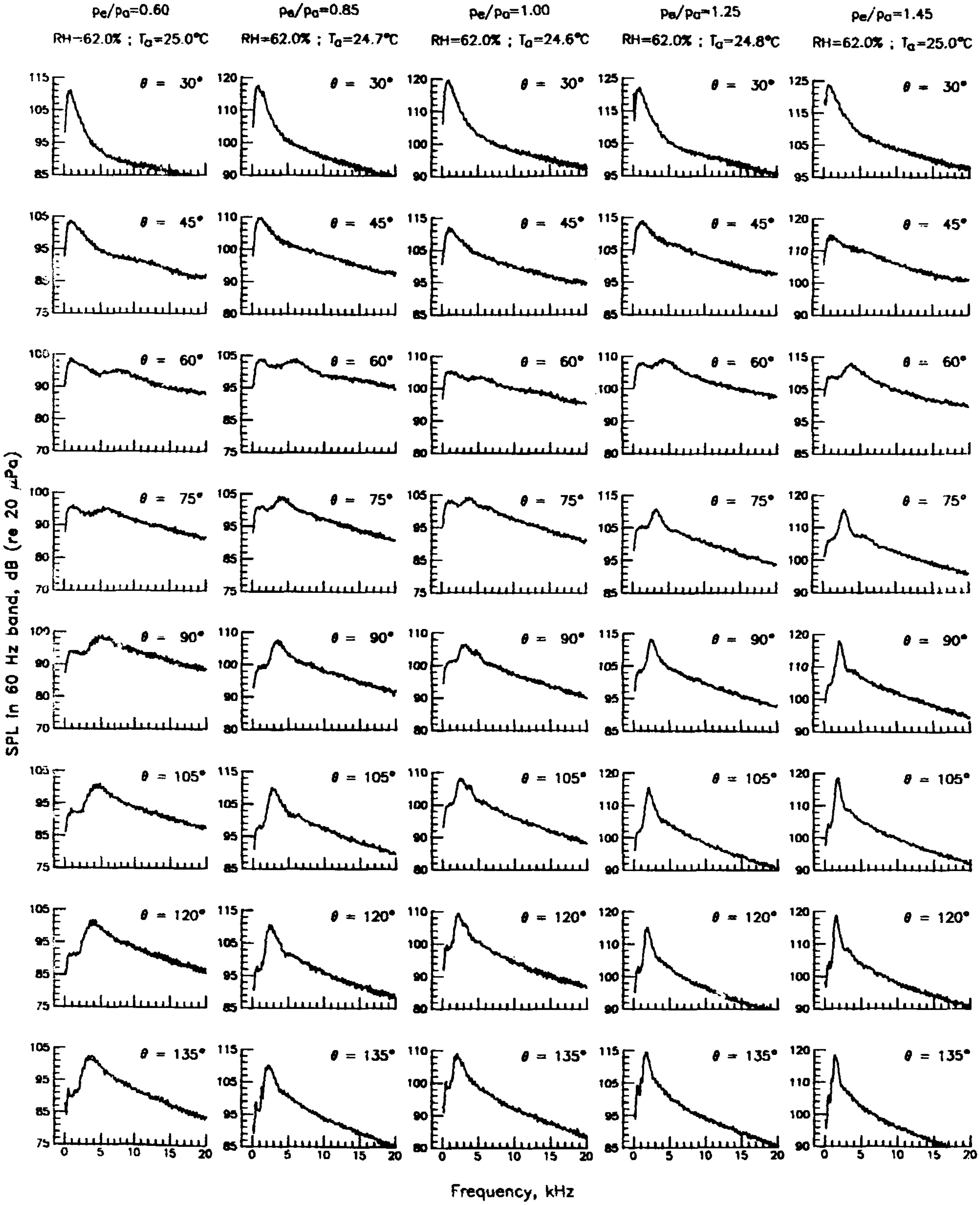

(a) $\phi = 0°$.

Figure 4. Spectra for rectangular nozzle with throat aspect ratio of 2.0.

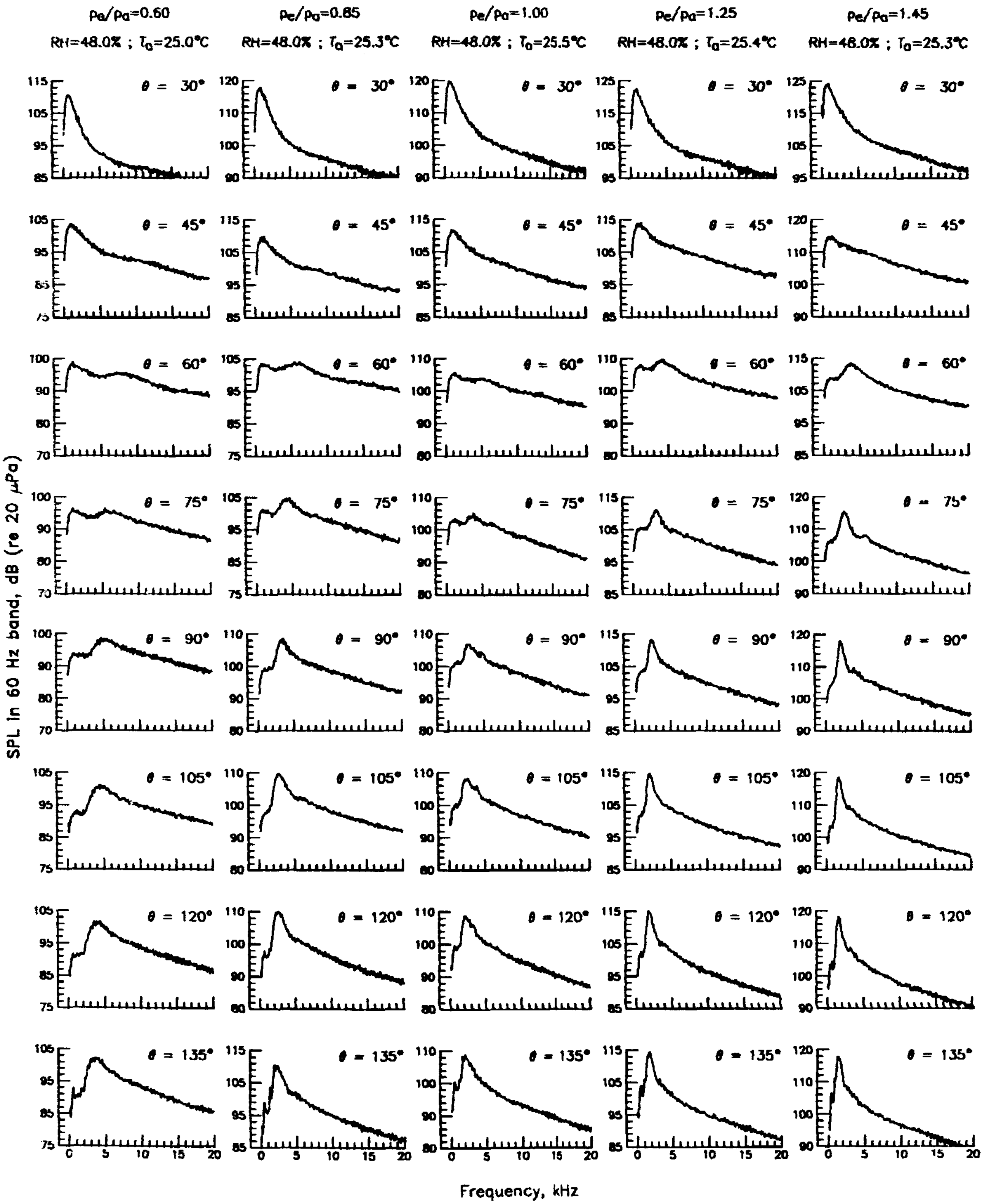

(b) $\phi = 15°$.

Figure 4. Continued.

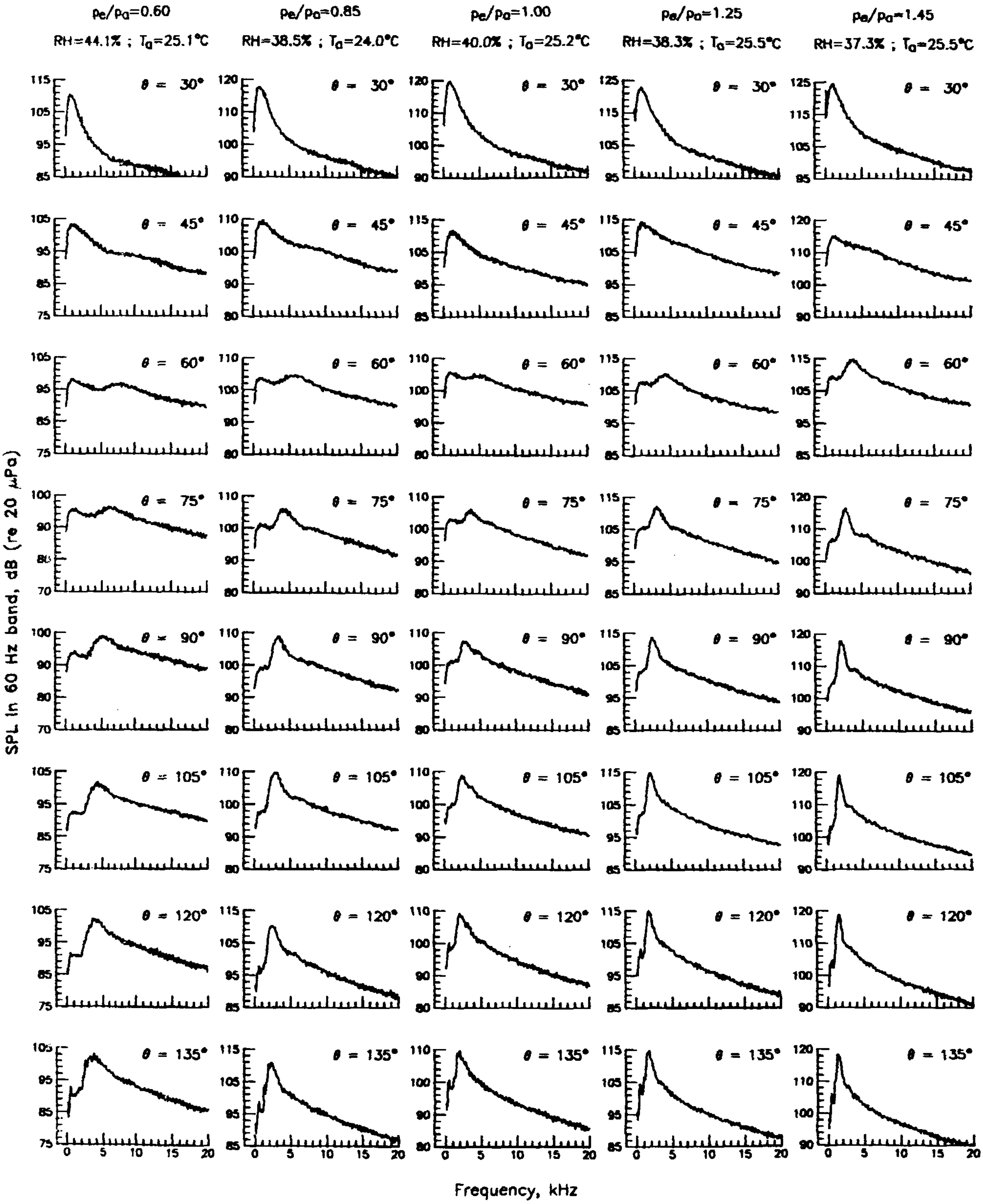

(c) $\phi = 30°$.

Figure 4. Continued.

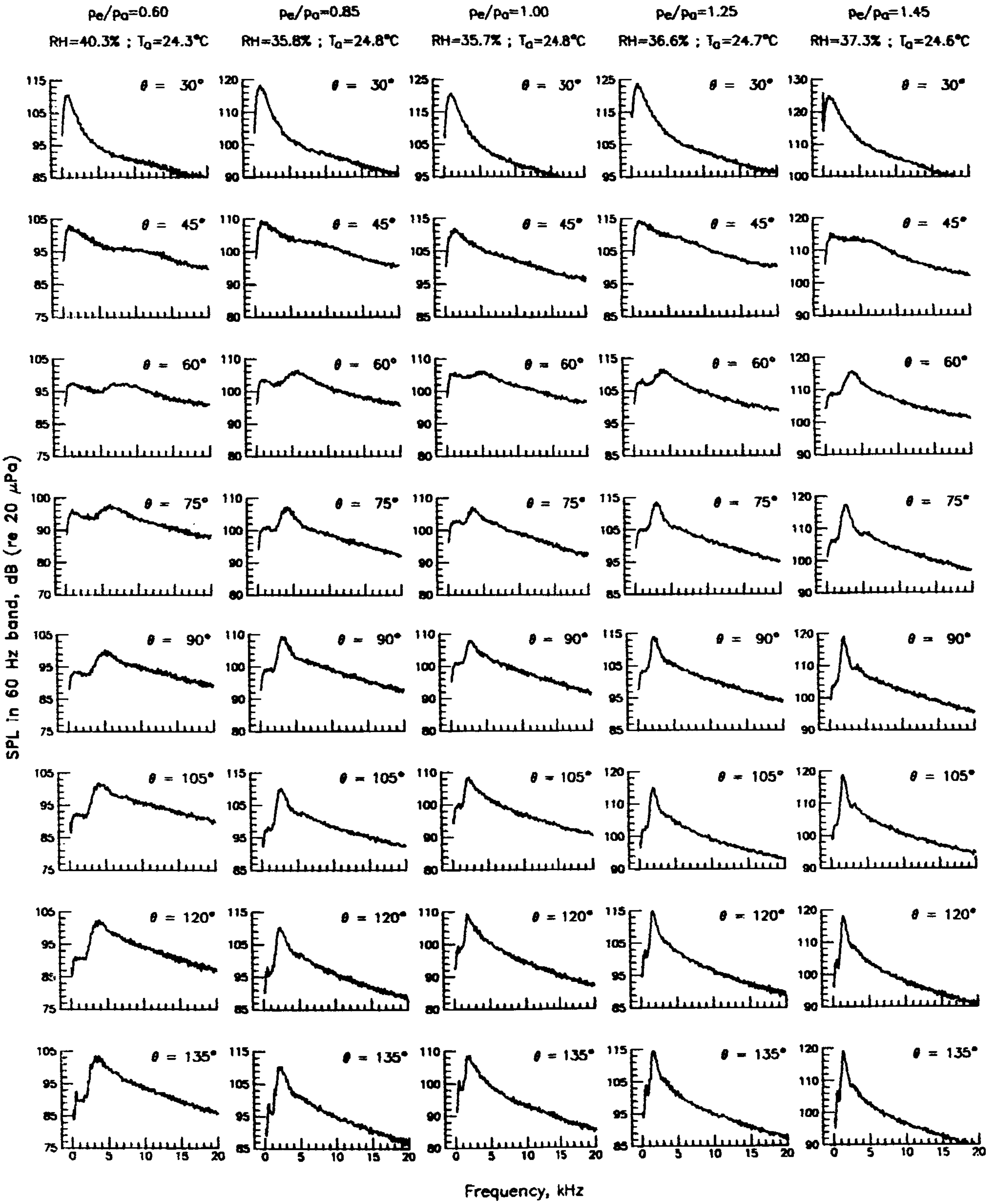

(d) $\phi = 45°$.

Figure 4. Continued.

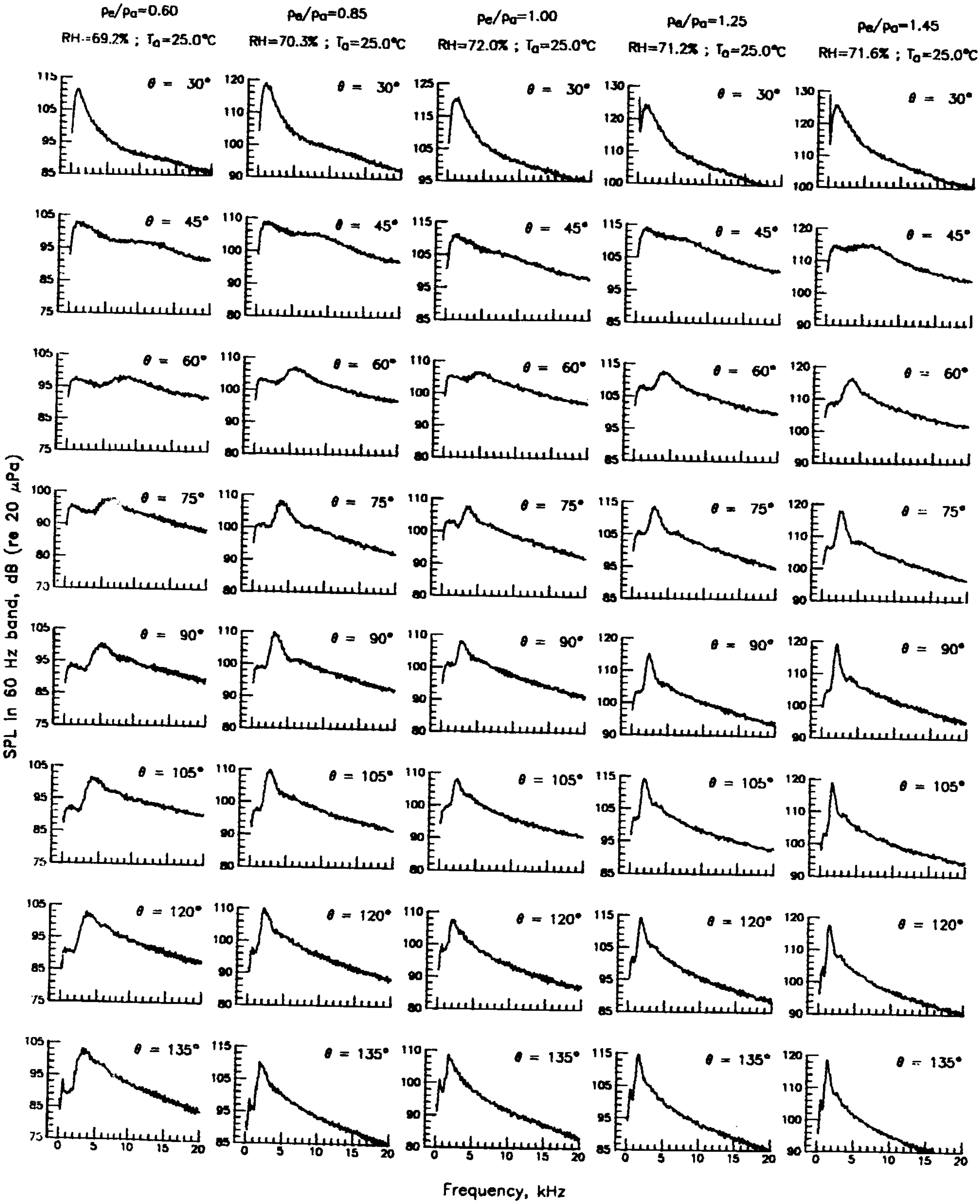

(e) $\phi = 60°$

Figure 4. Continued.

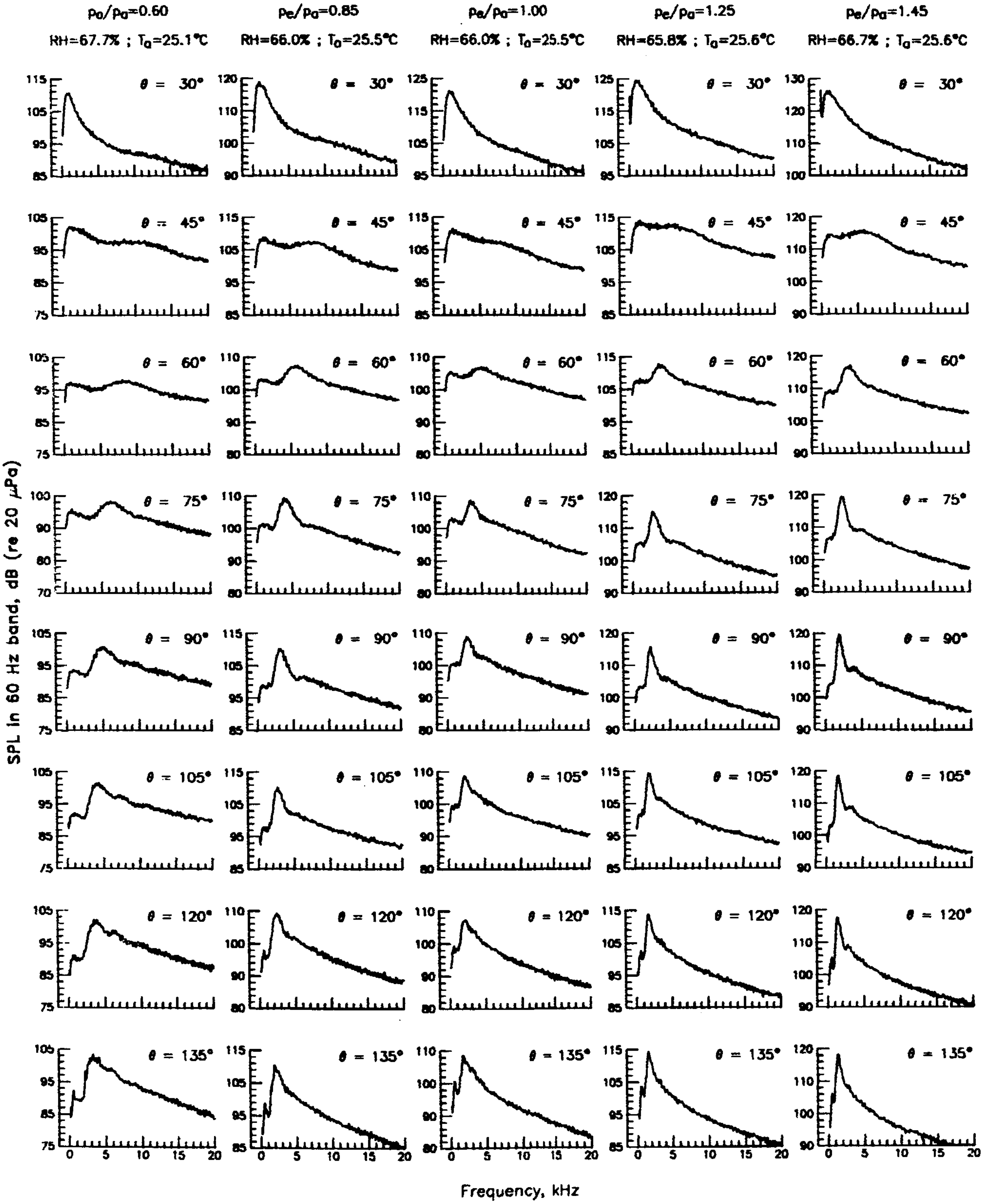

(f) $\phi = 75°$.

Figure 4. Continued.

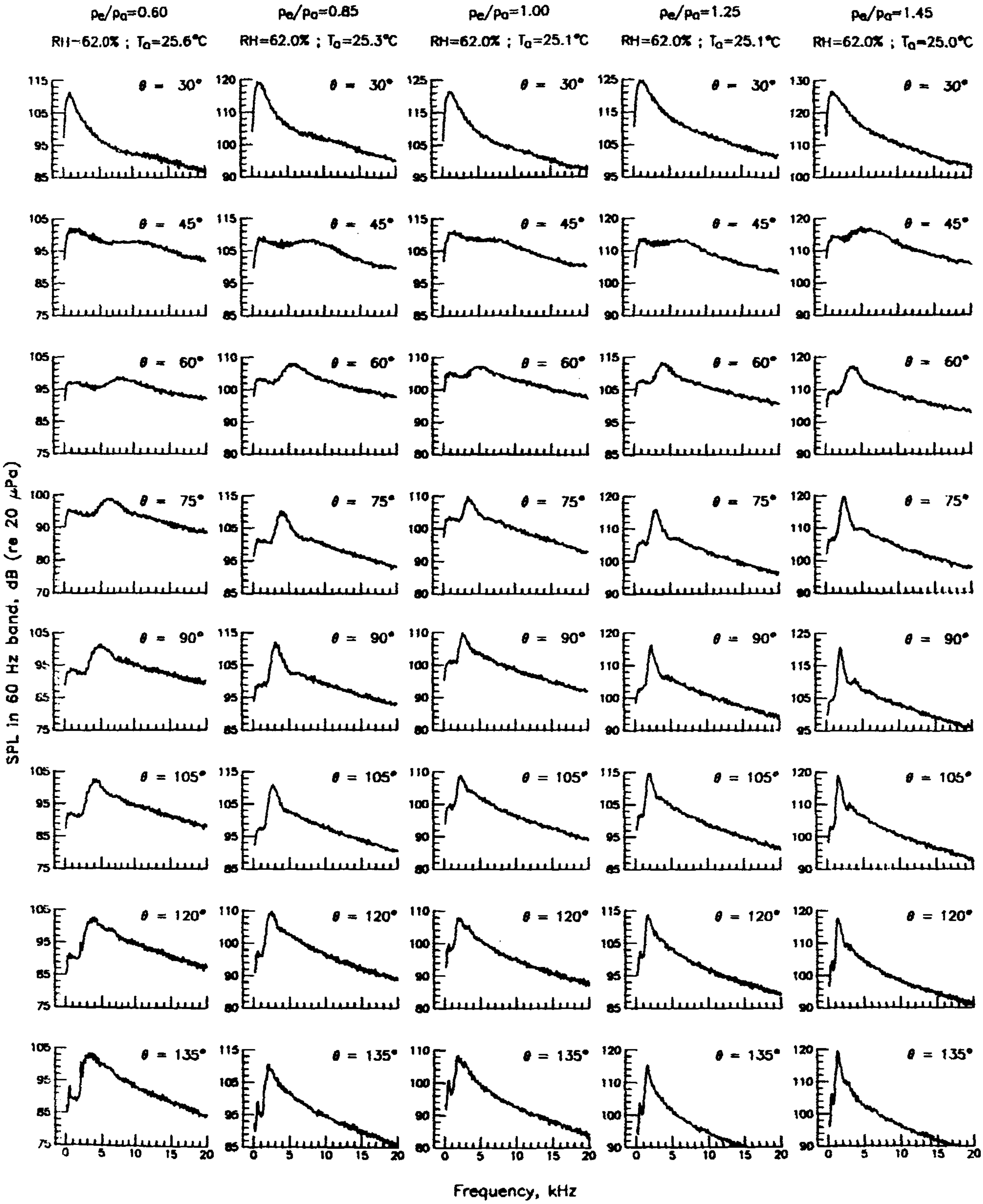

(g) $\phi = 90°$.

Figure 4. Continued.

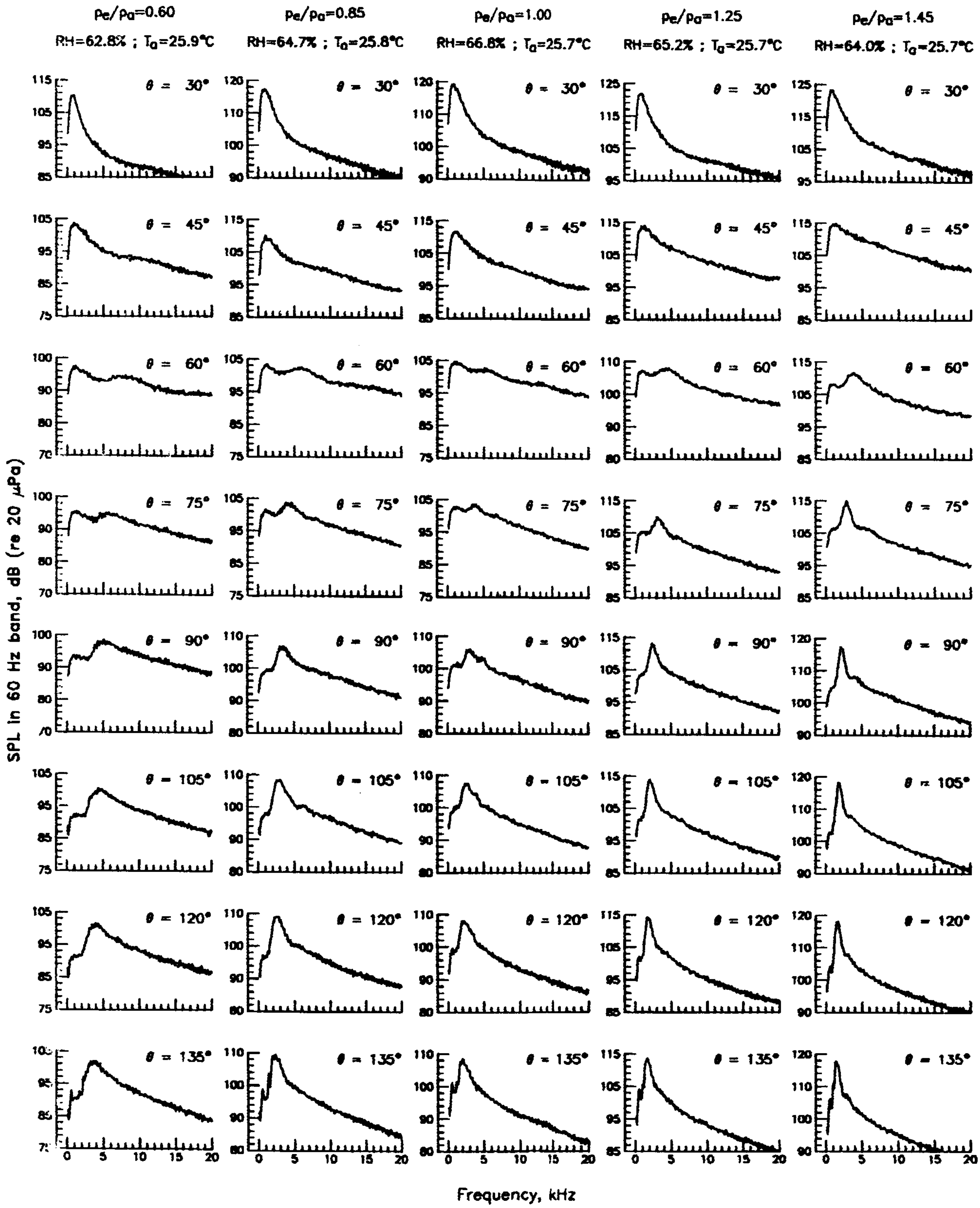

(h) $\phi = 180°$.

Figure 4. Continued.

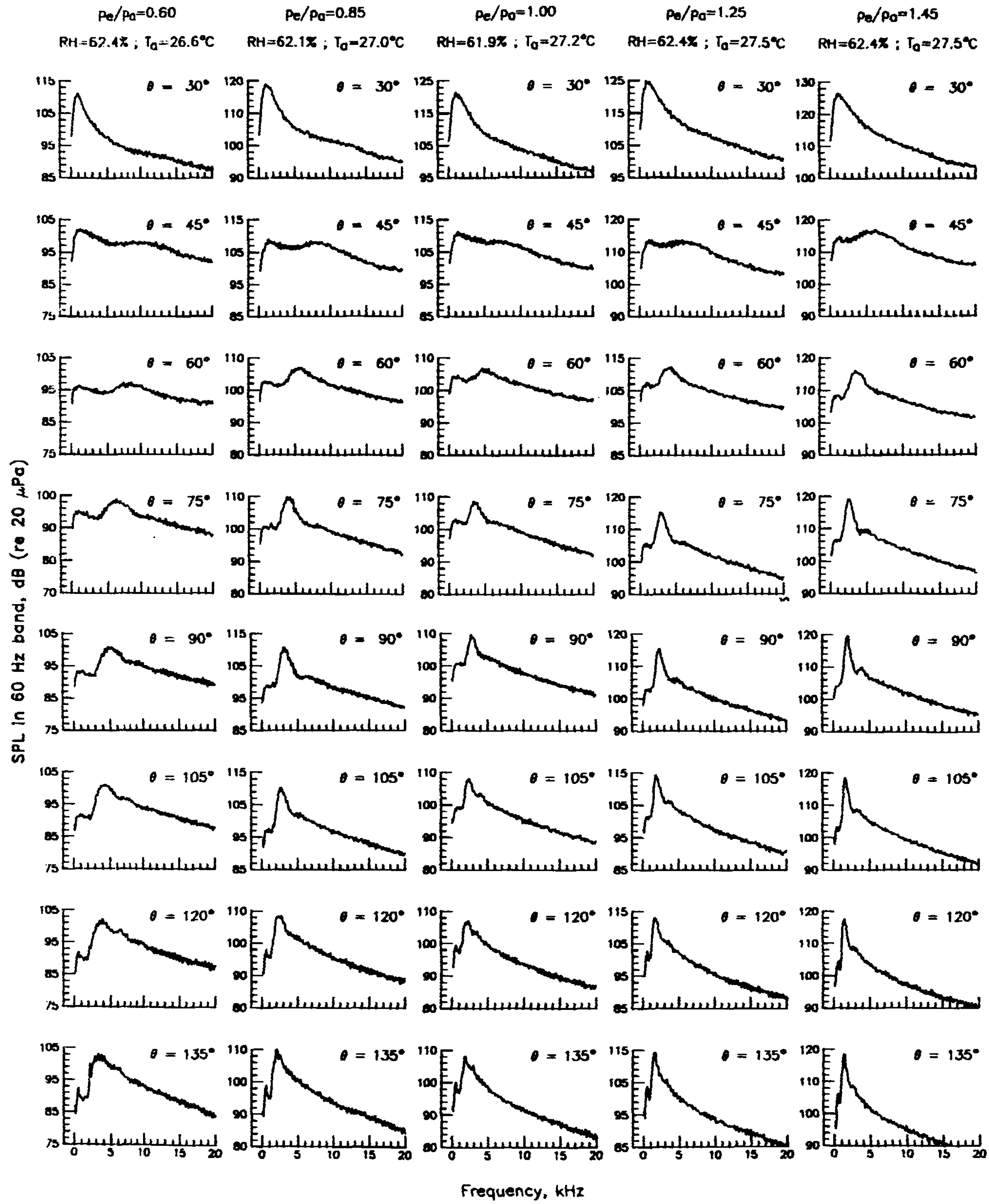

(i) $\phi = 270°$.

Figure 4. Concluded.

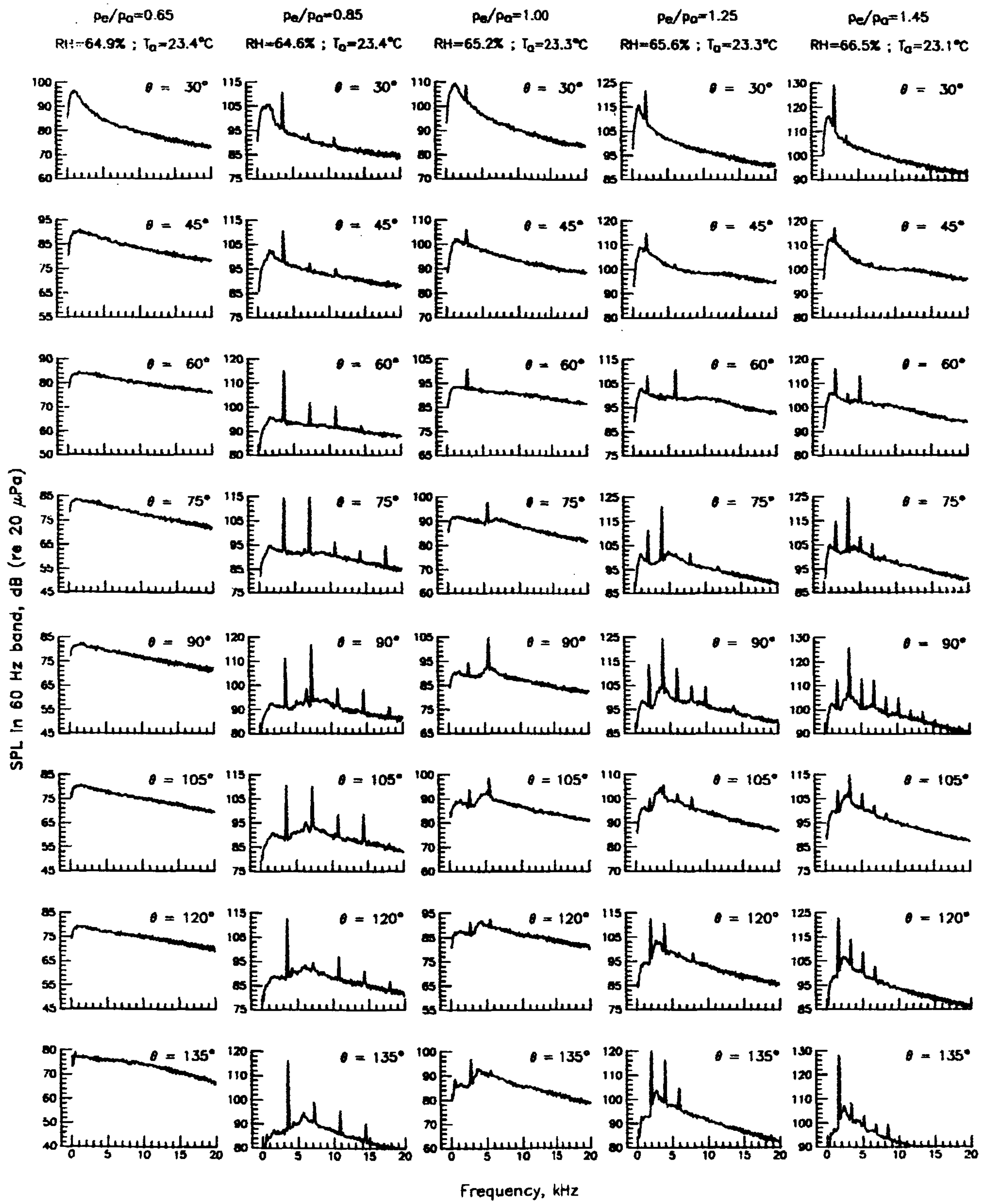

(a) $\phi = 0°$.

Figure 5. Spectra for rectangular nozzle with throat aspect ratio of 3.7.

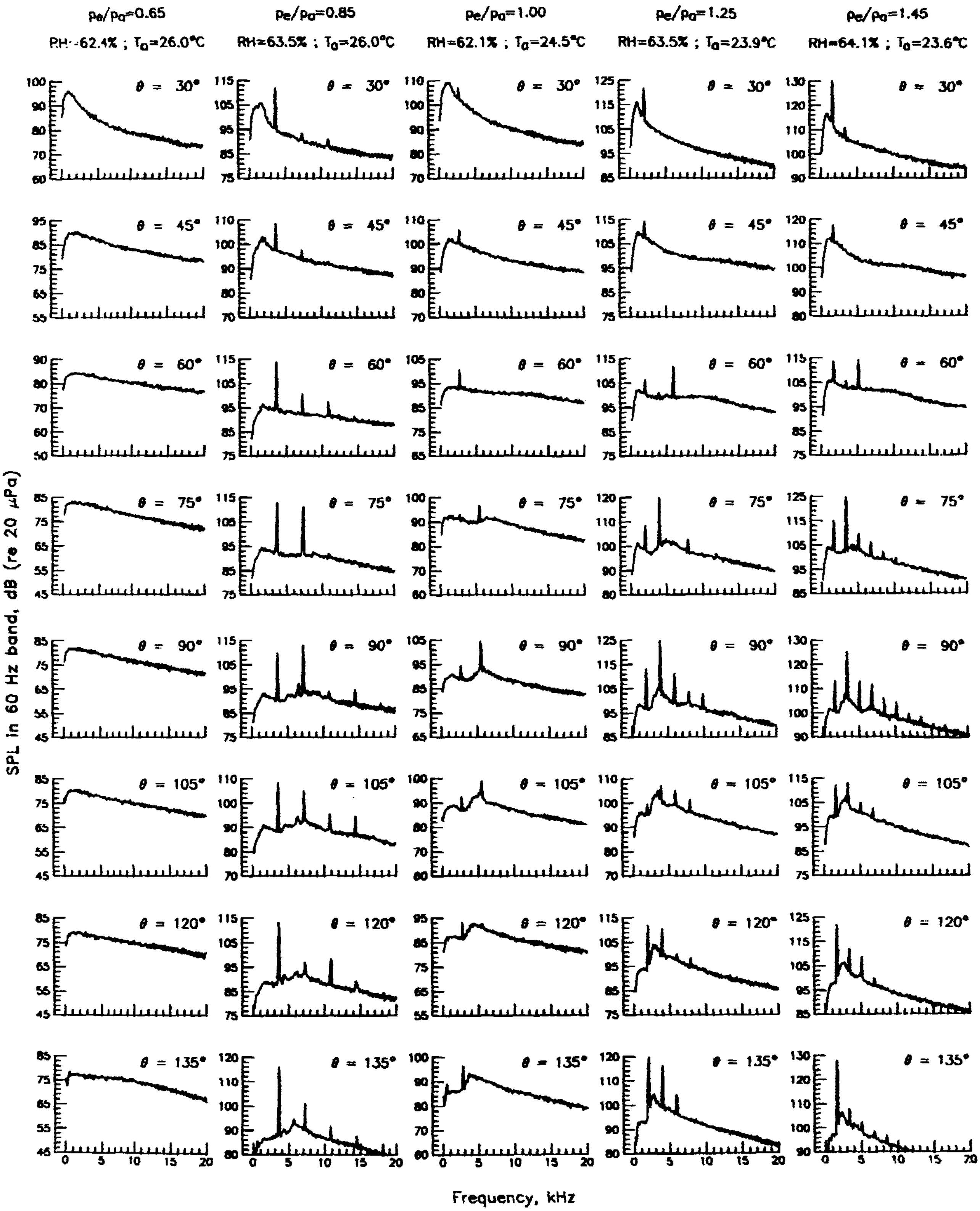

(b) $\phi = 15°$.

Figure 5. Continued.

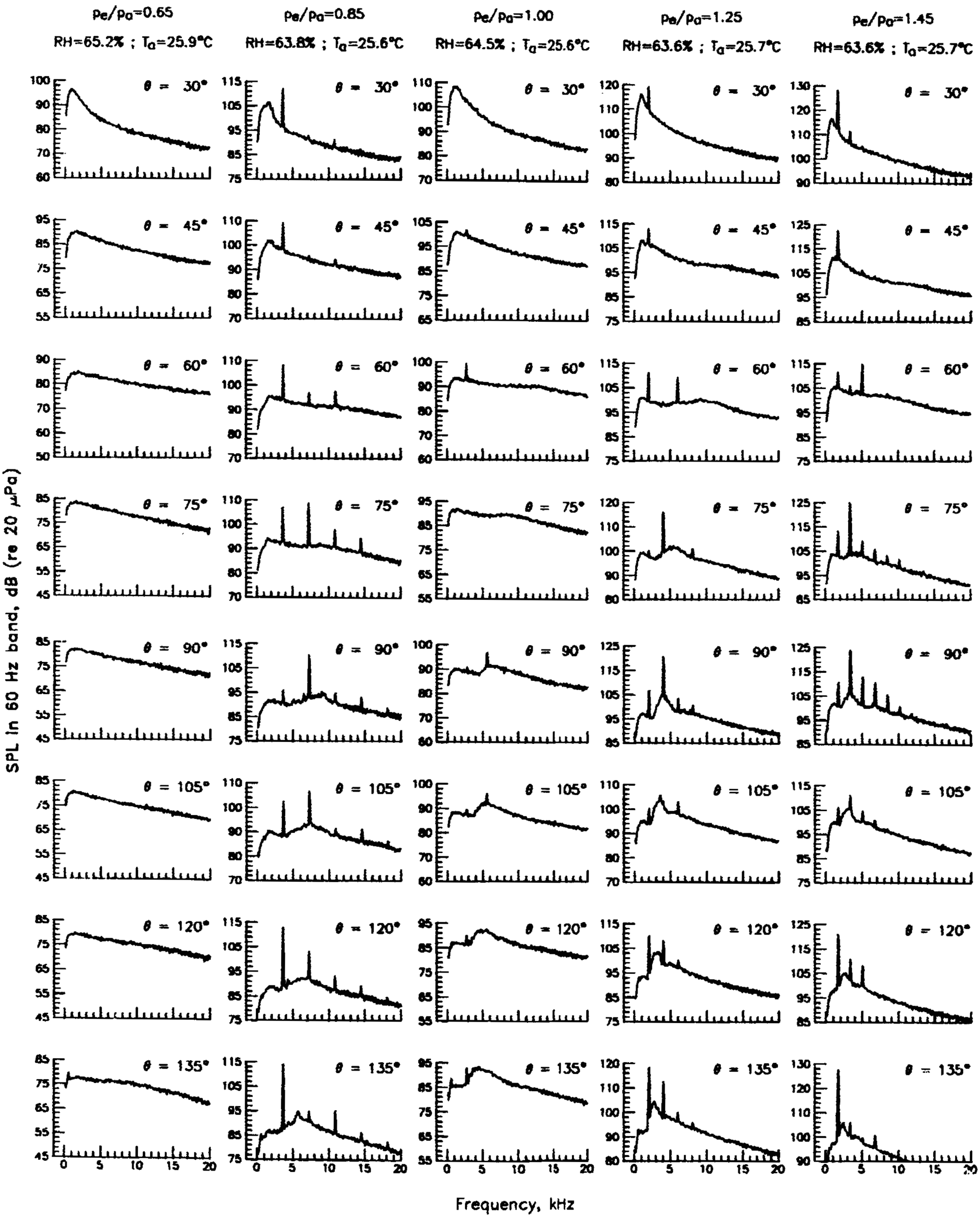

(c) $\phi = 30°$.

Figure 5. Continued.

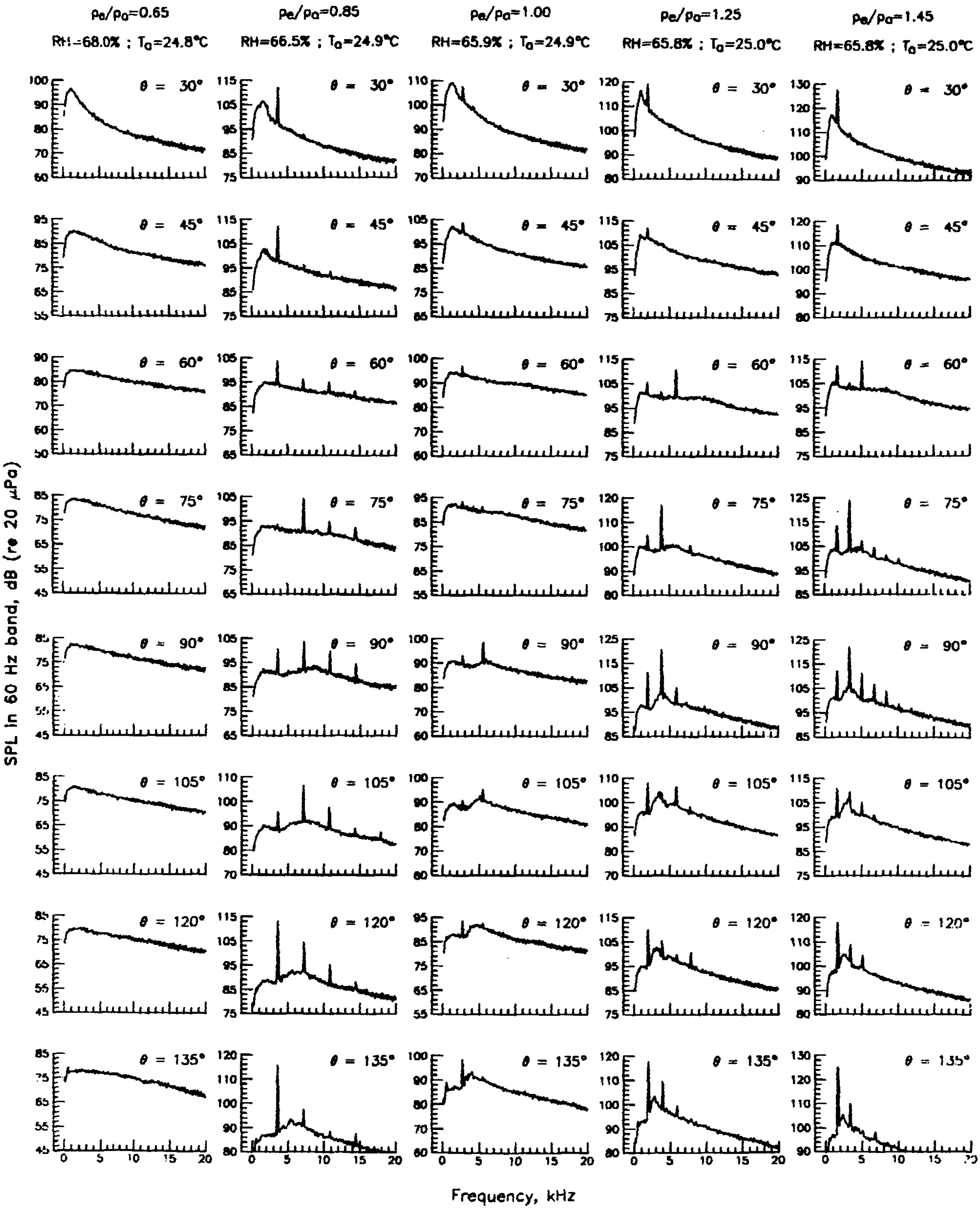

(d) $\phi = 45^{\circ}$.

Figure 5. Continued.

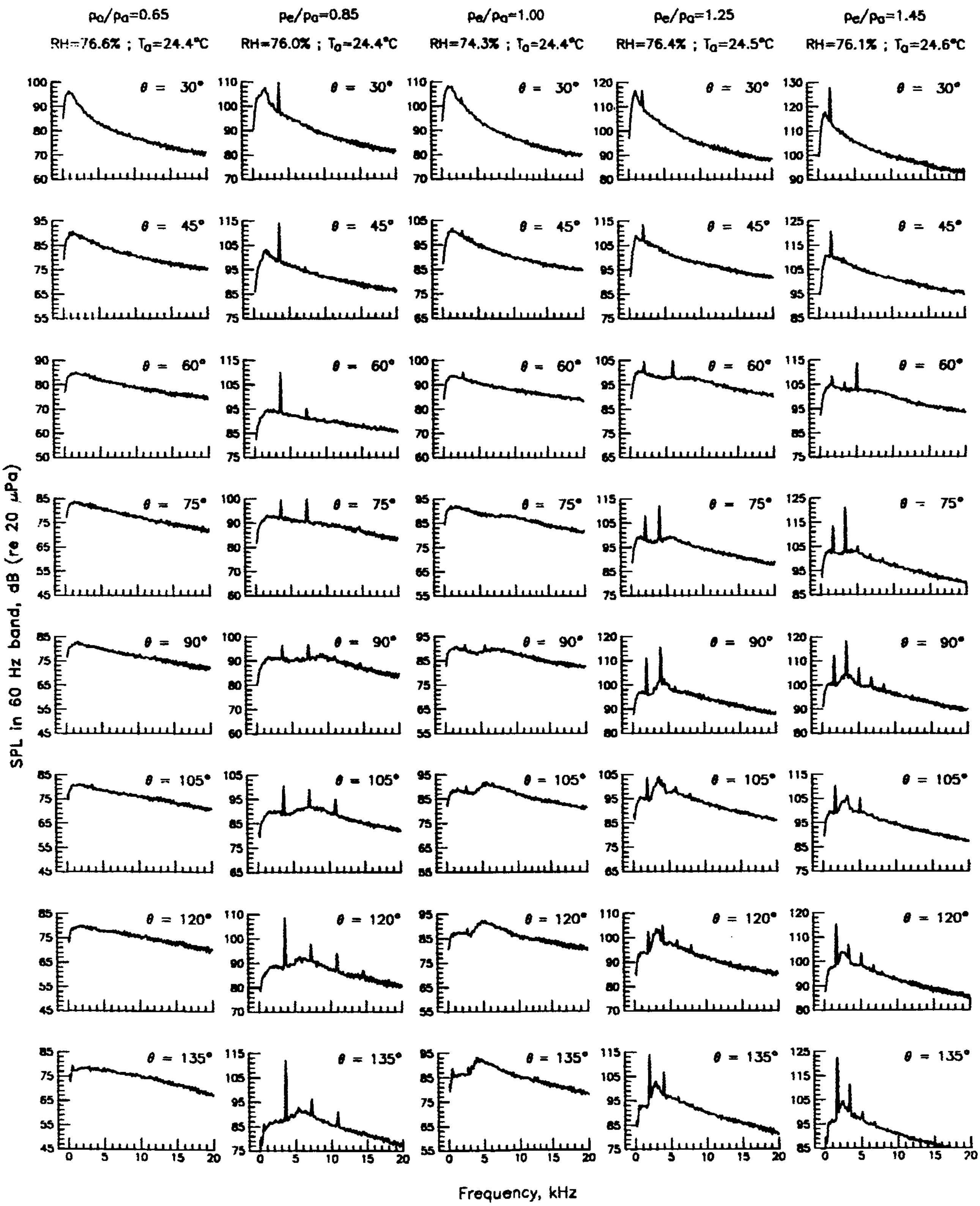

(e) $\phi = 60°$.

Figure 5. Continued.

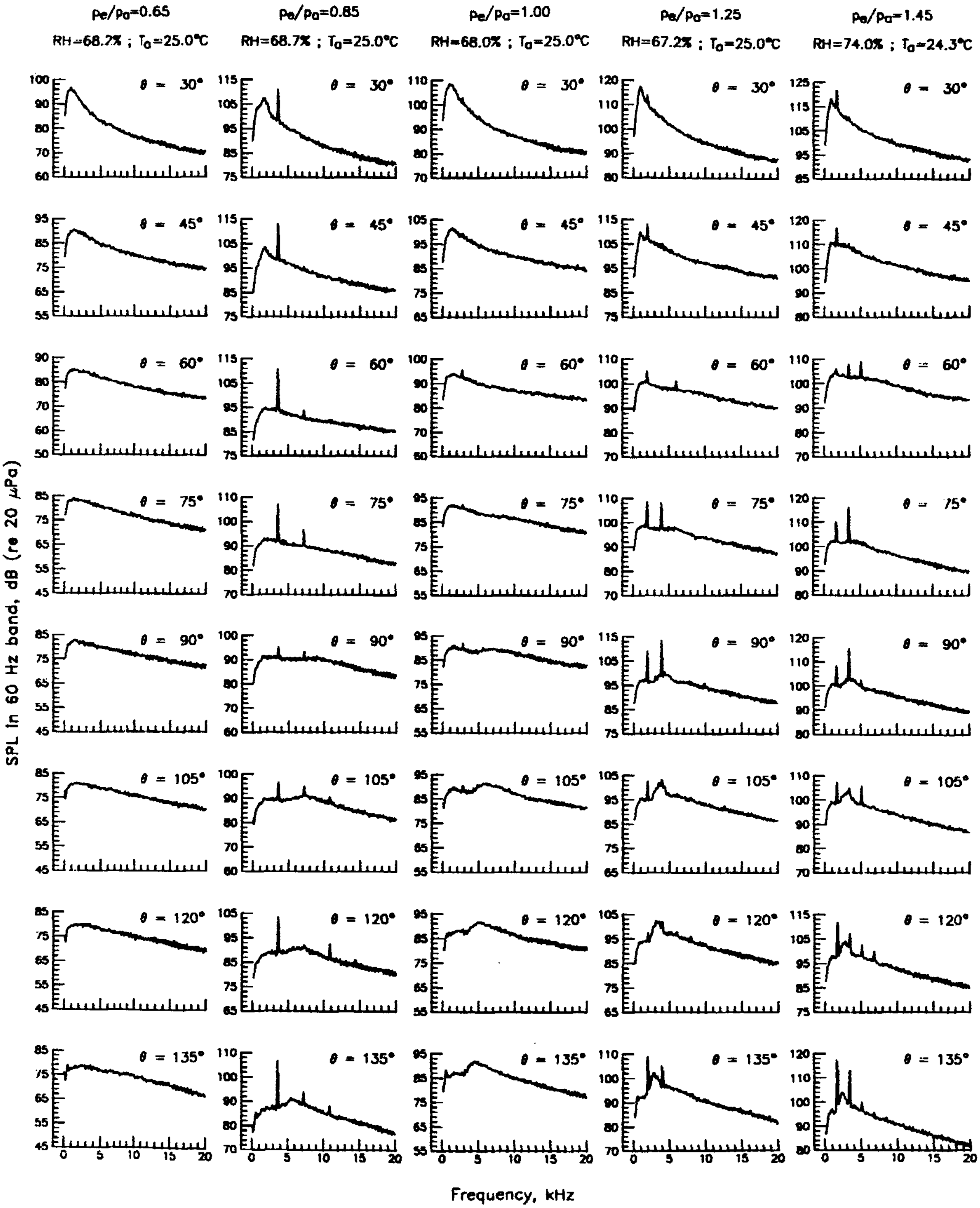

(f) $\phi = 75°$.

Figure 5. Continued.

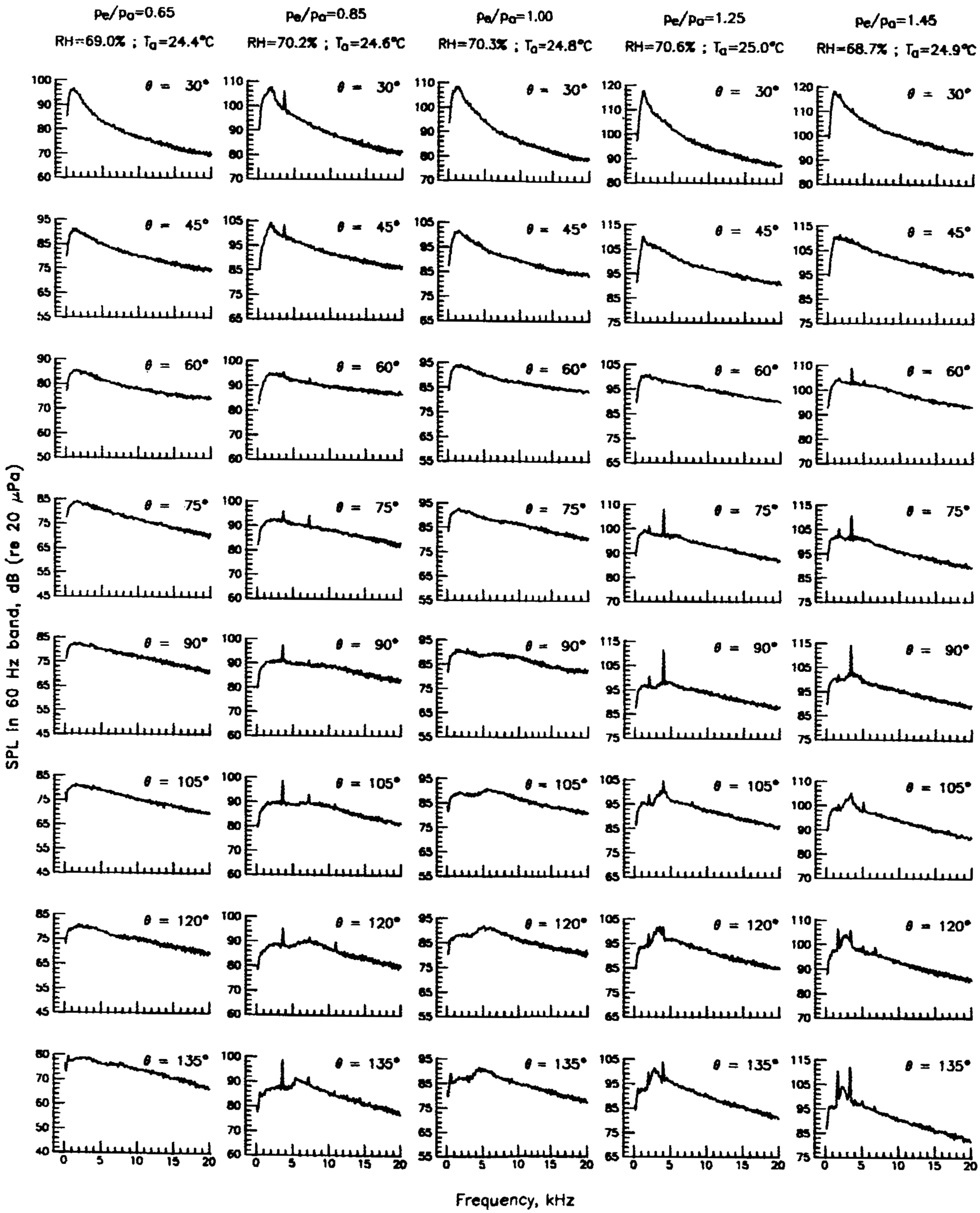

(g) $\phi = 90°$.

Figure 5. Continued.

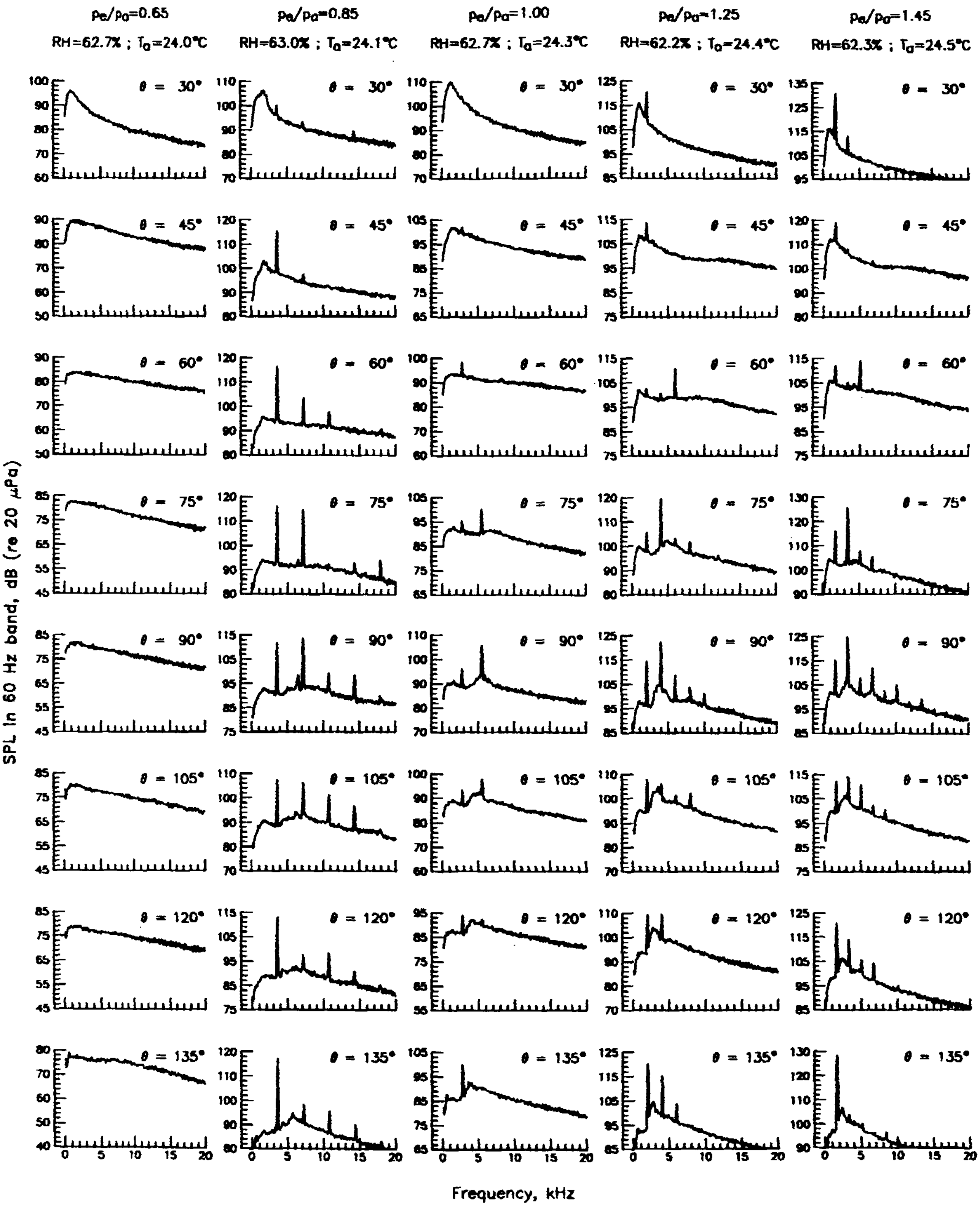

(h) $\phi = 180°$.

Figure 5. Continued.

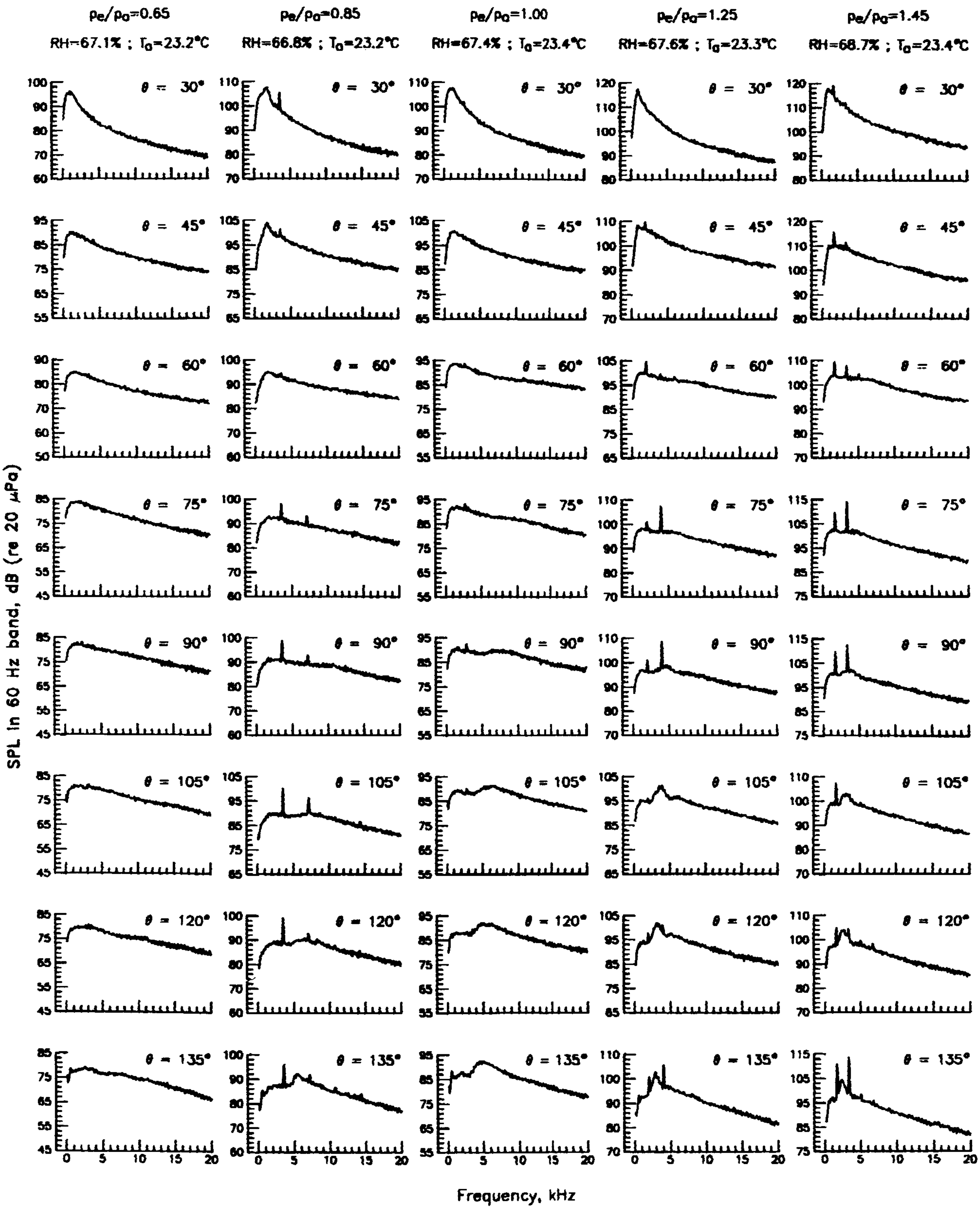

(i) $\phi = 270°$.

Figure 5. Concluded.

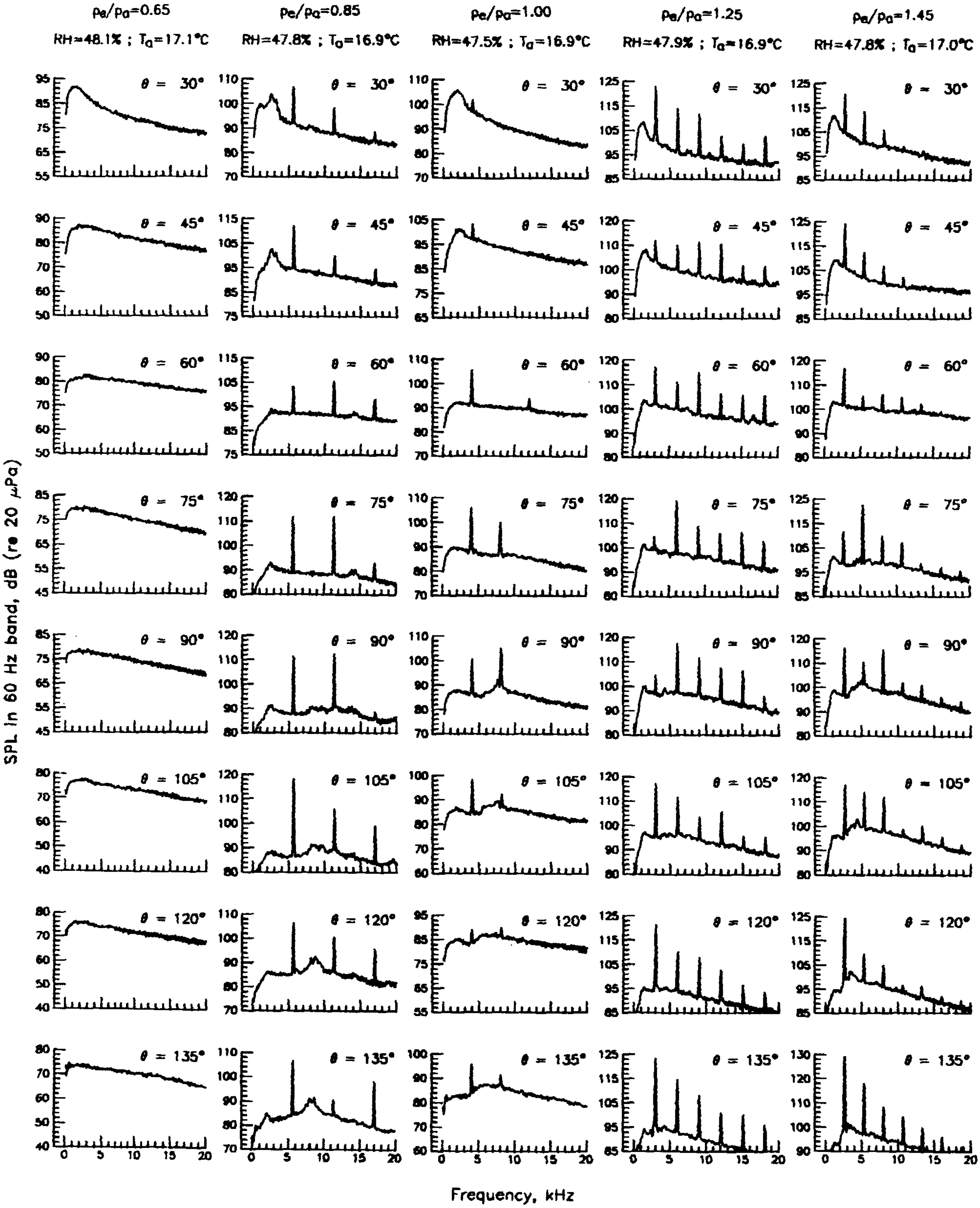

(a) $\phi = 0°$.

Figure 6. Spectra for rectangular nozzle with throat aspect ratio of 5.8.

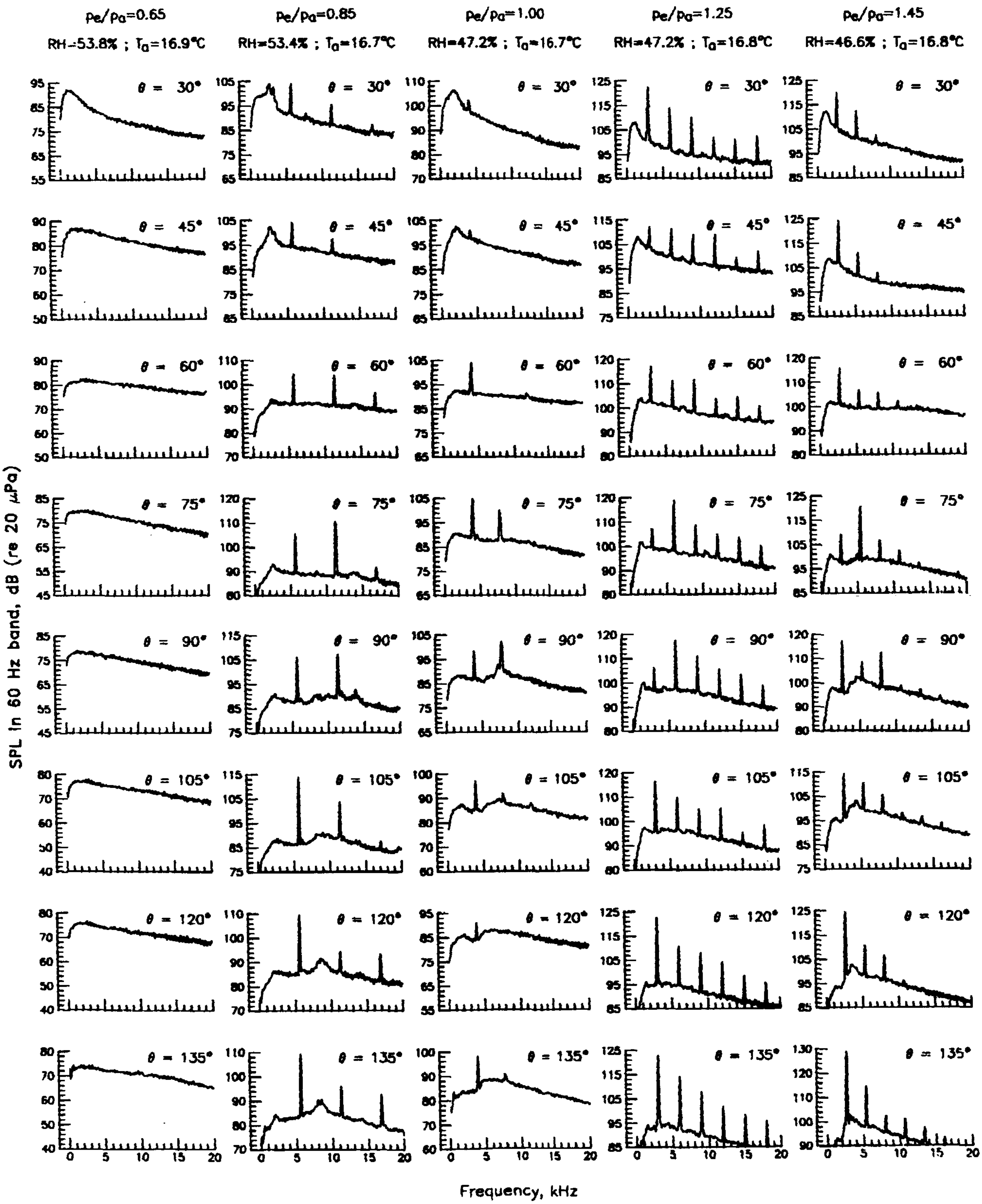

(b) $\phi = 15°$.

Figure 6. Continued.

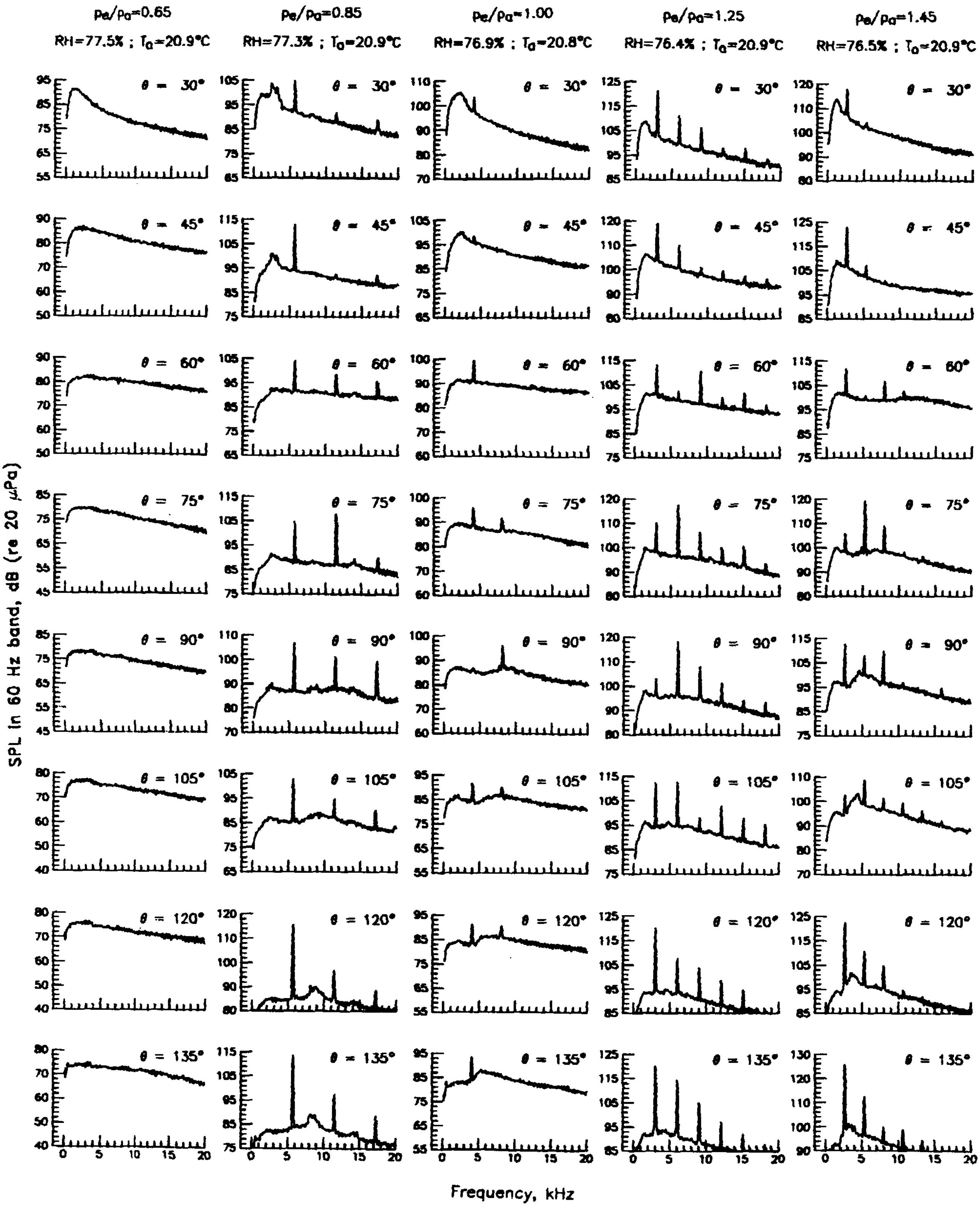

(c) $\phi = 30°$.

Figure 6. Continued.

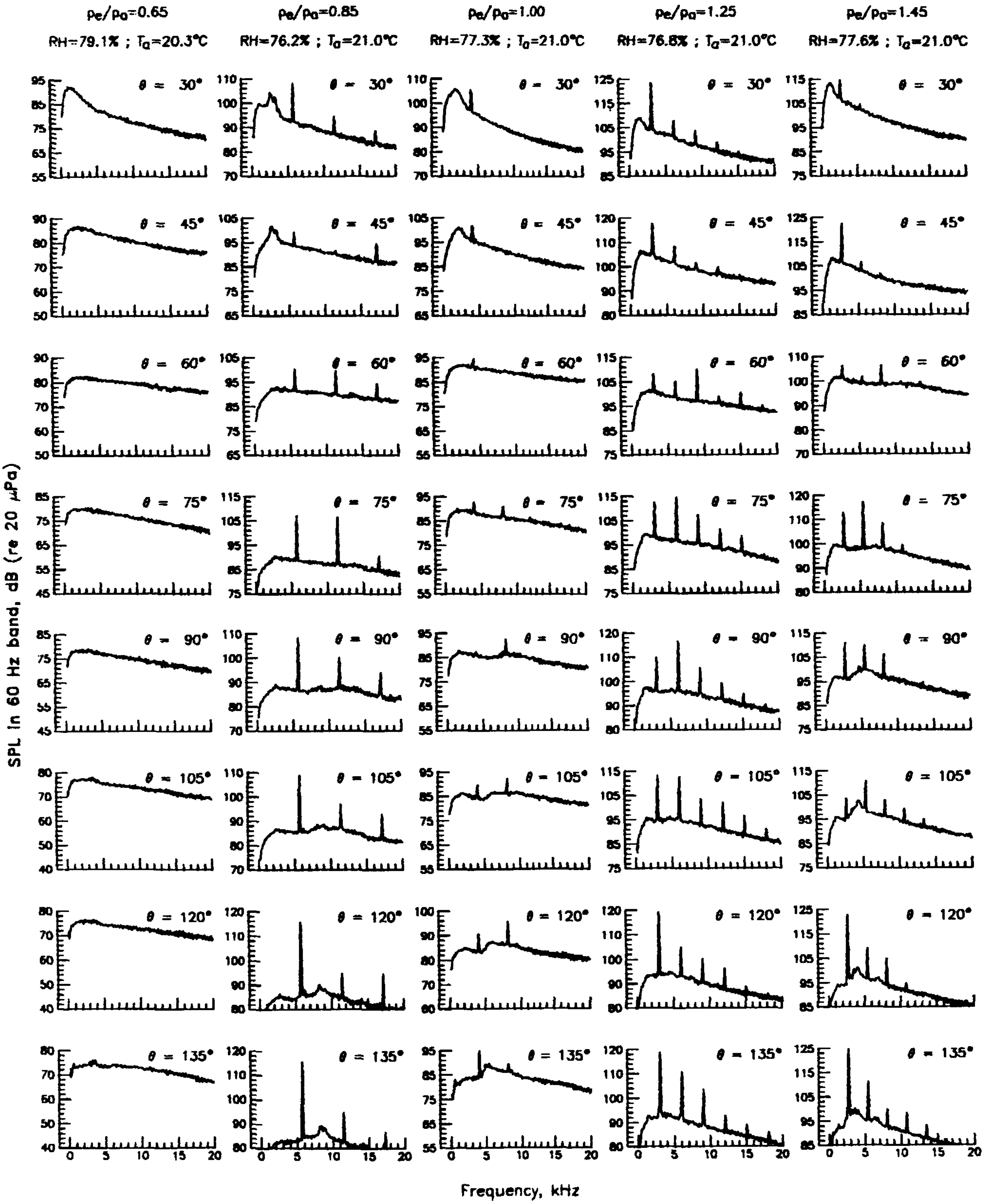

(d) $\phi = 45°$.

Figure 6. Continued.

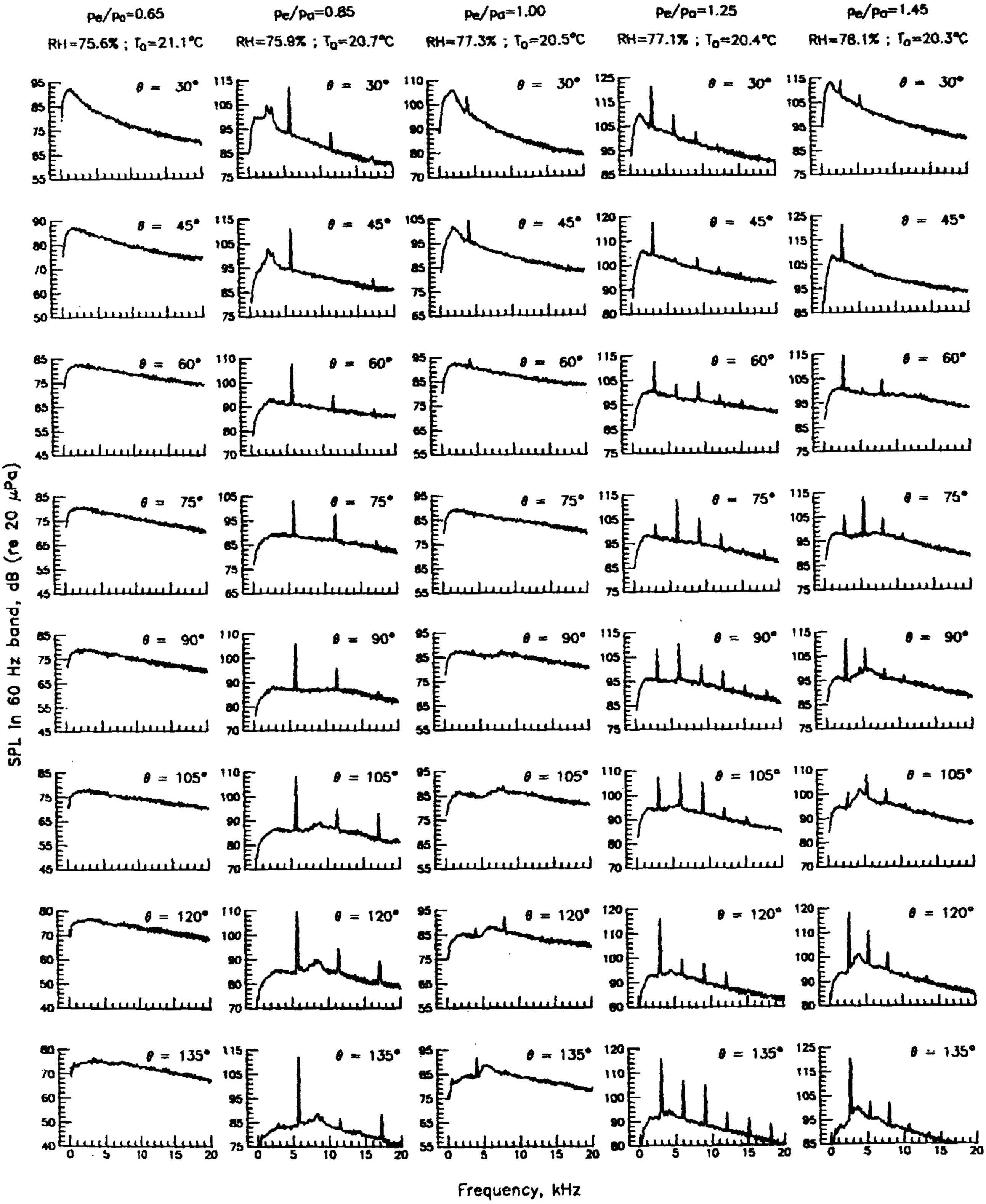

(e) $\phi = 60°$.

Figure 6. Continued.

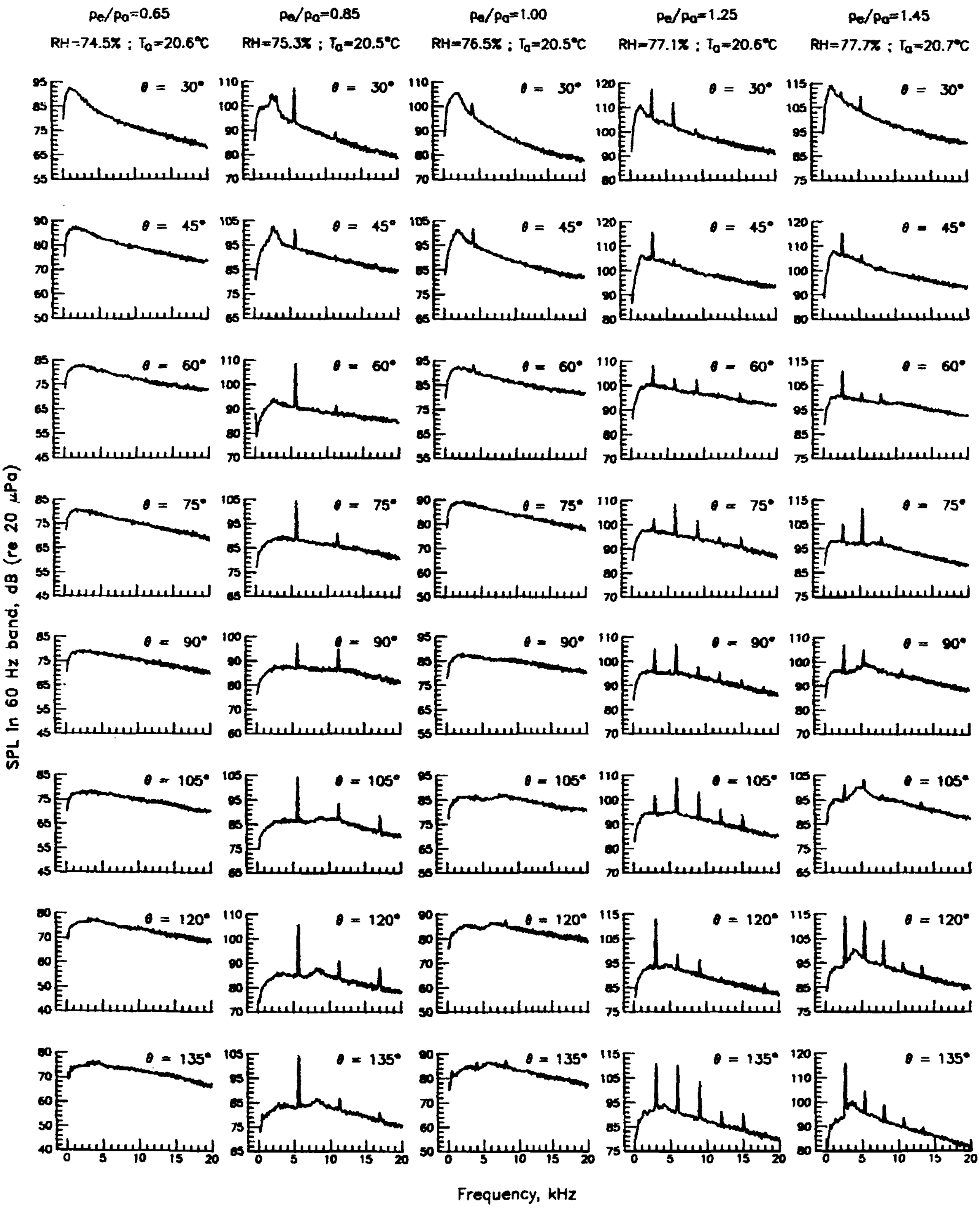

(f) $\phi = 75°$.

Figure 6. Continued.

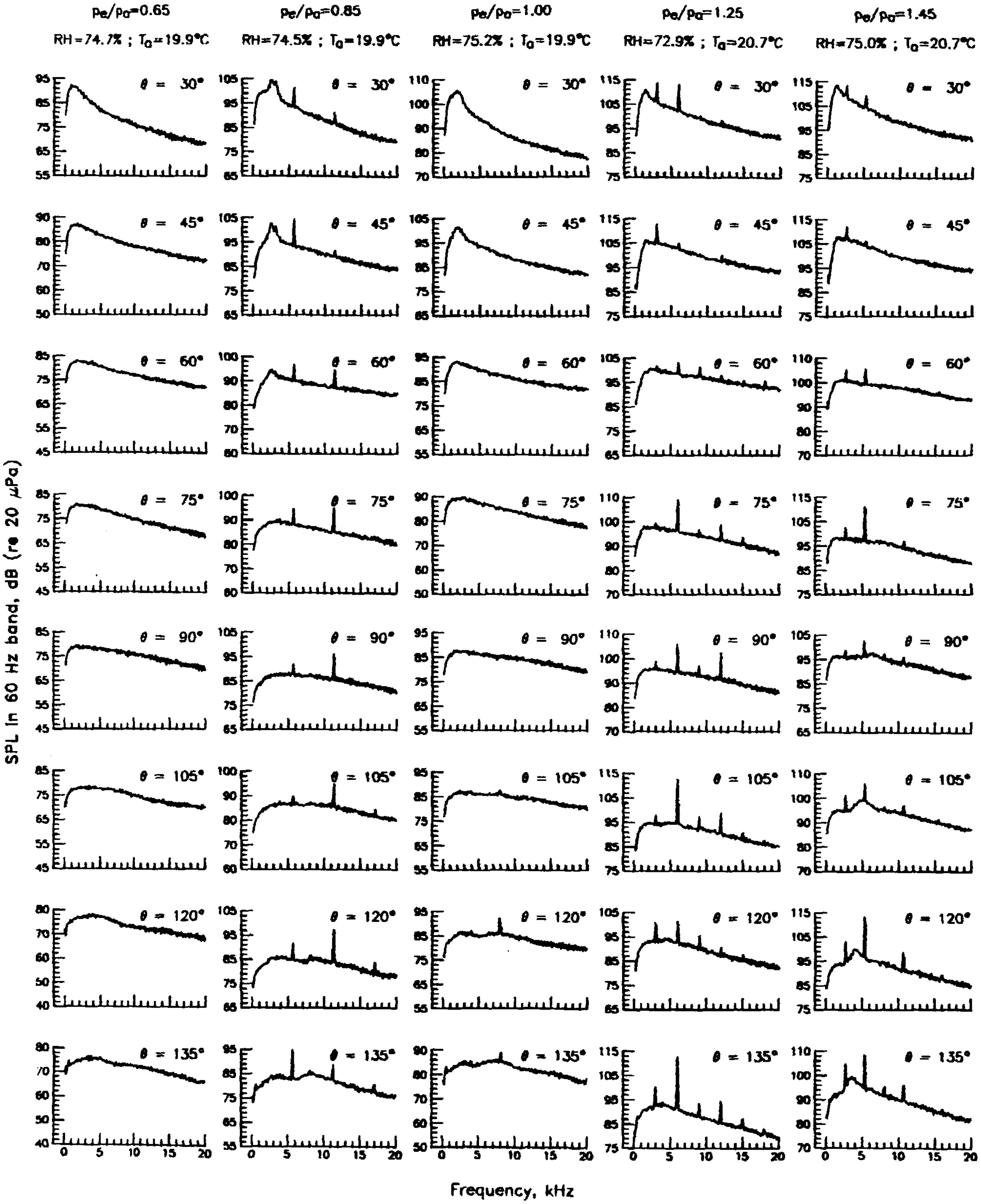

(g) $\phi = 90°$.

Figure 6. Continued.

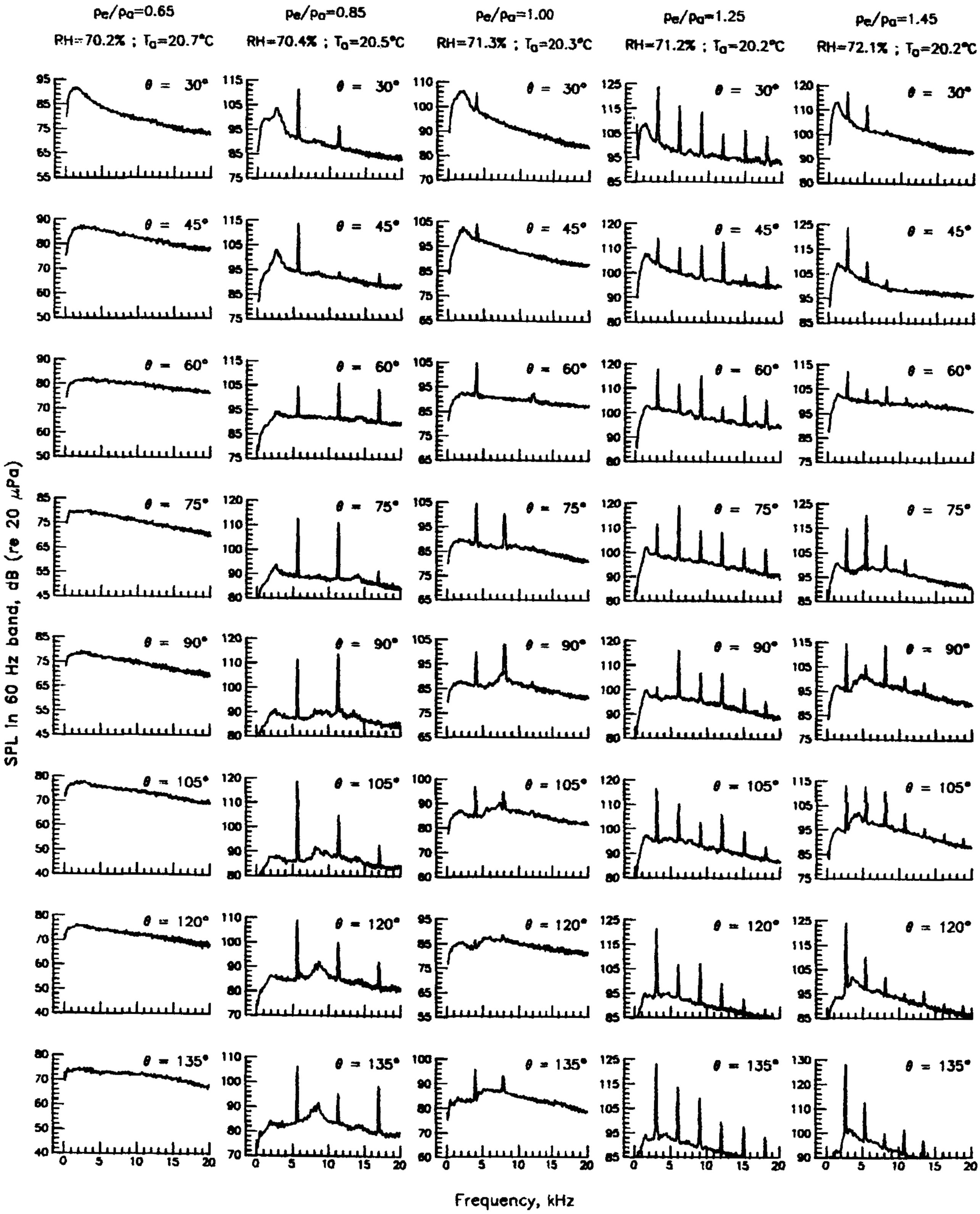

(h) $\phi = 180°$.

Figure 6. Continued.

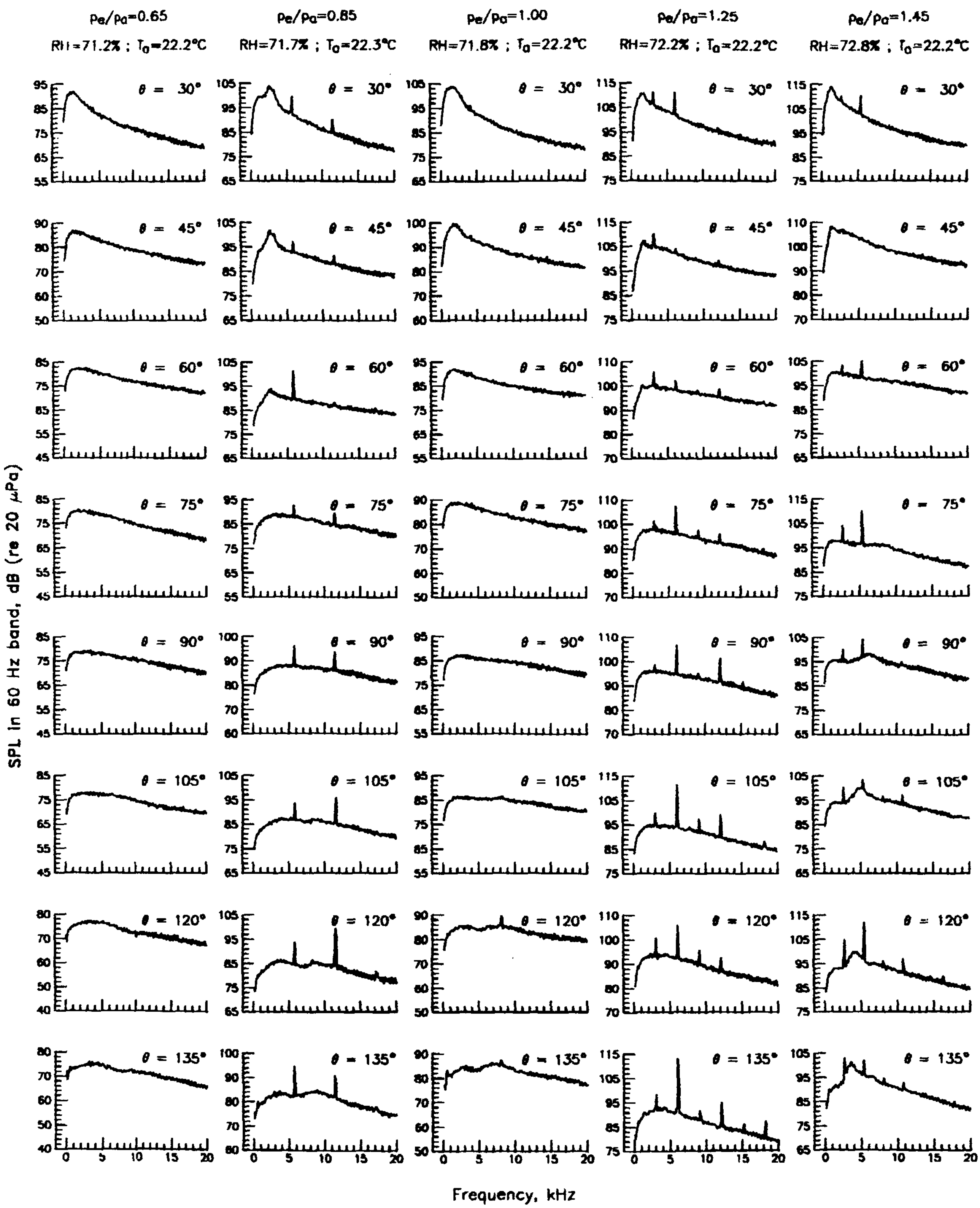

(i) $\phi = 270°$.

Figure 6. Concluded.

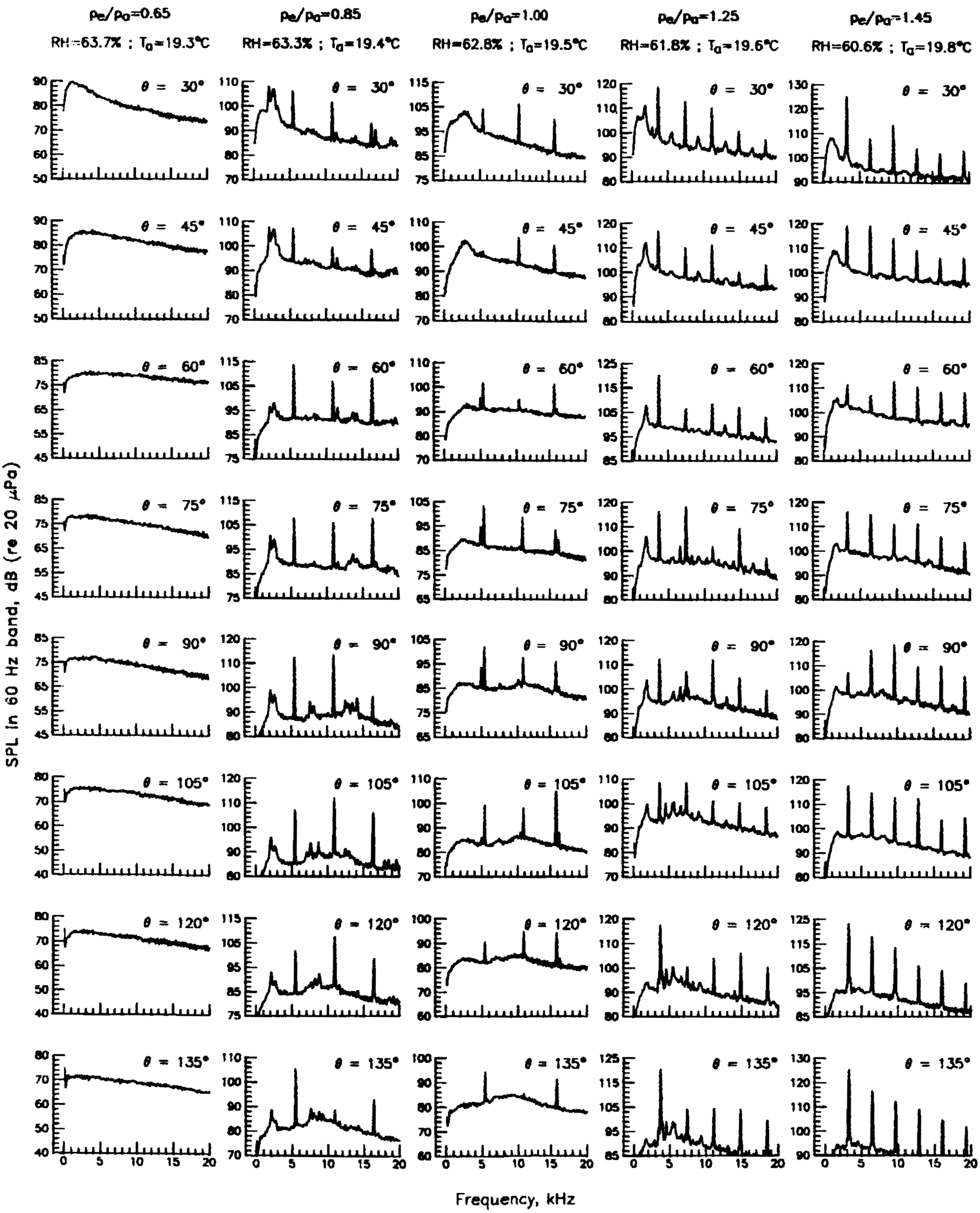

(a) $\phi = 0°$.

Figure 7. Spectra for rectangular nozzle with throat aspect ratio of 7.6.

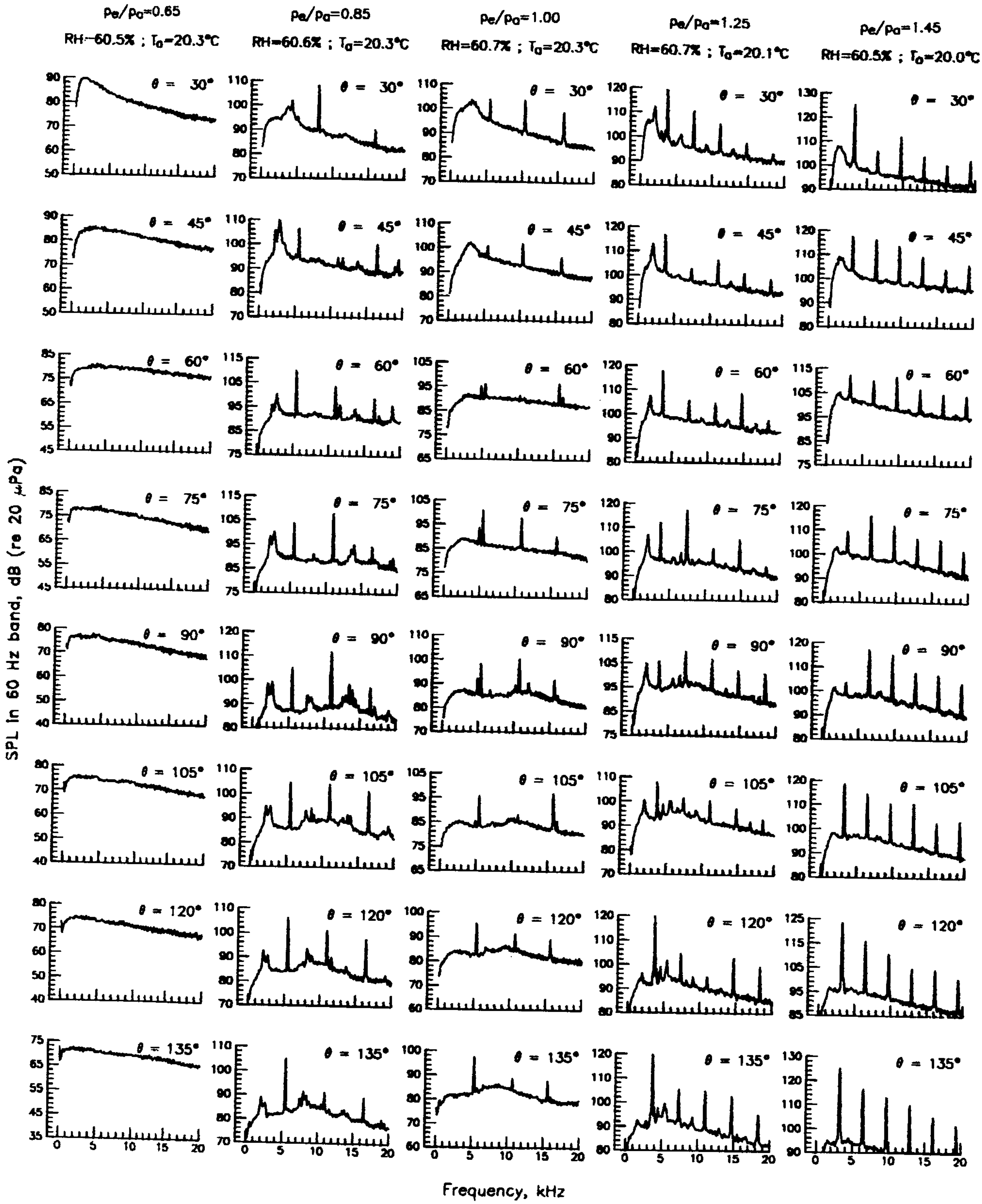

(b) $\phi = 15°$.

Figure 7. Continued.

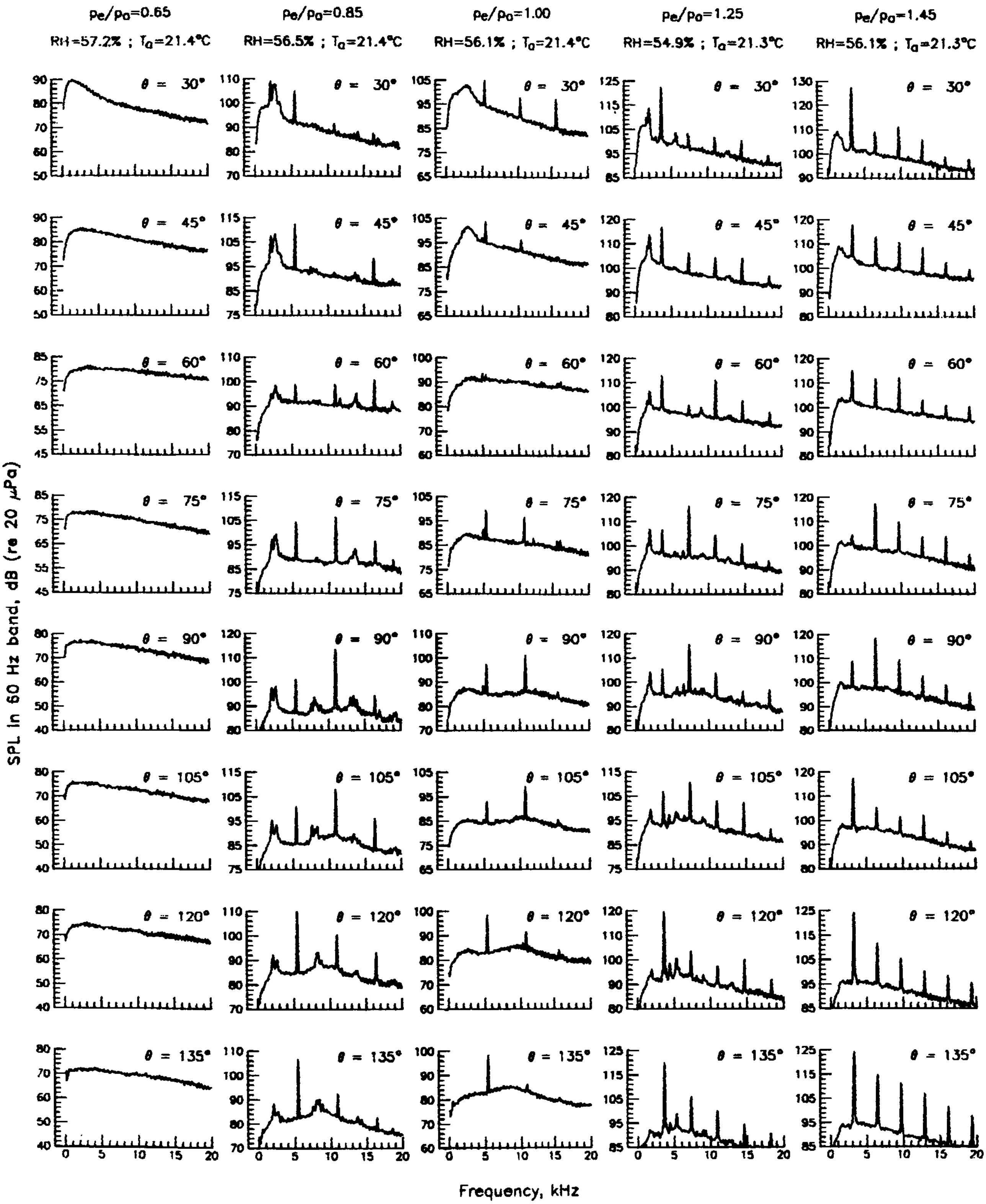

(c) $\phi = 30°$.

Figure 7. Continued.

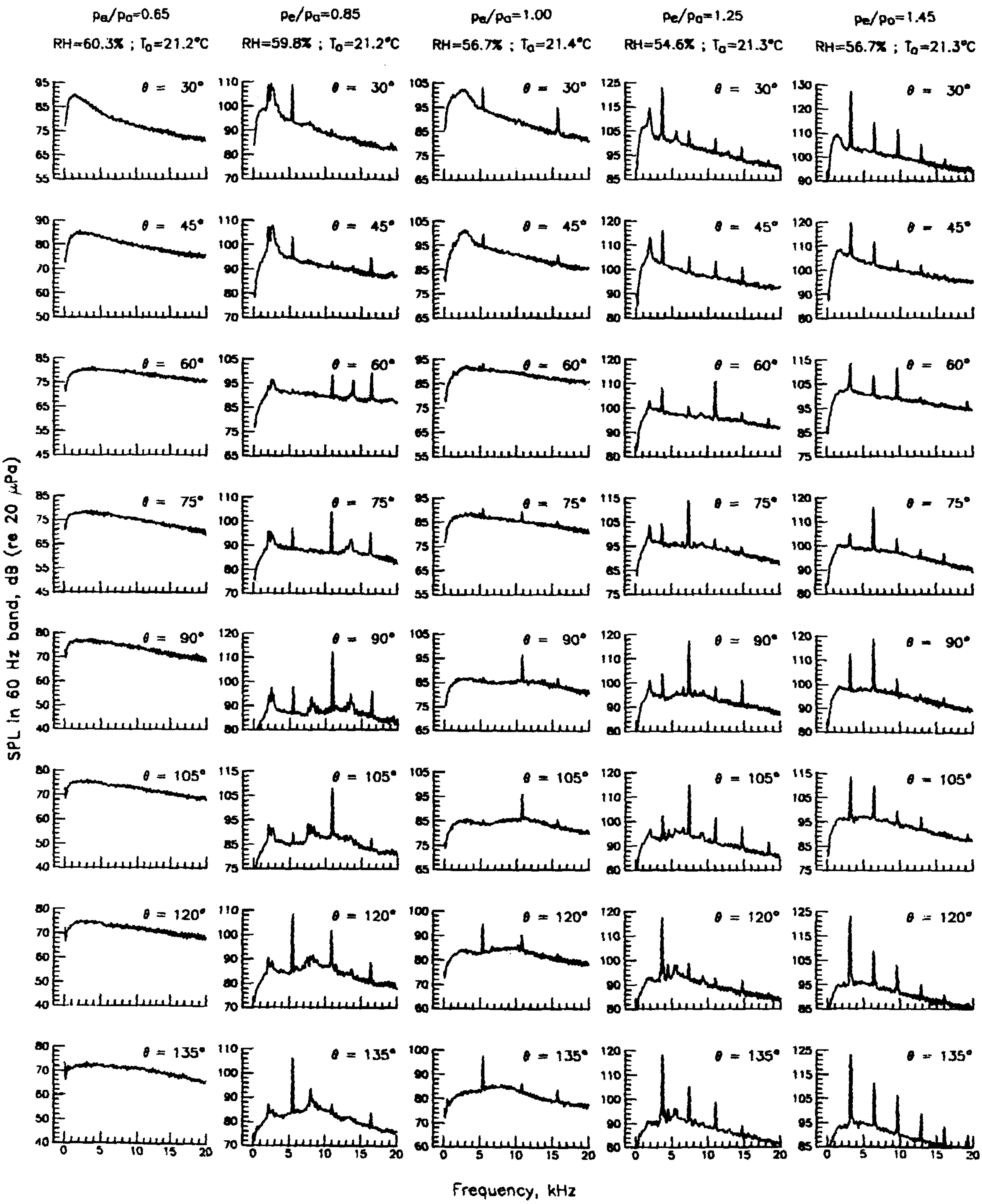

(d) $\phi = 45°$.

Figure 7. Continued.

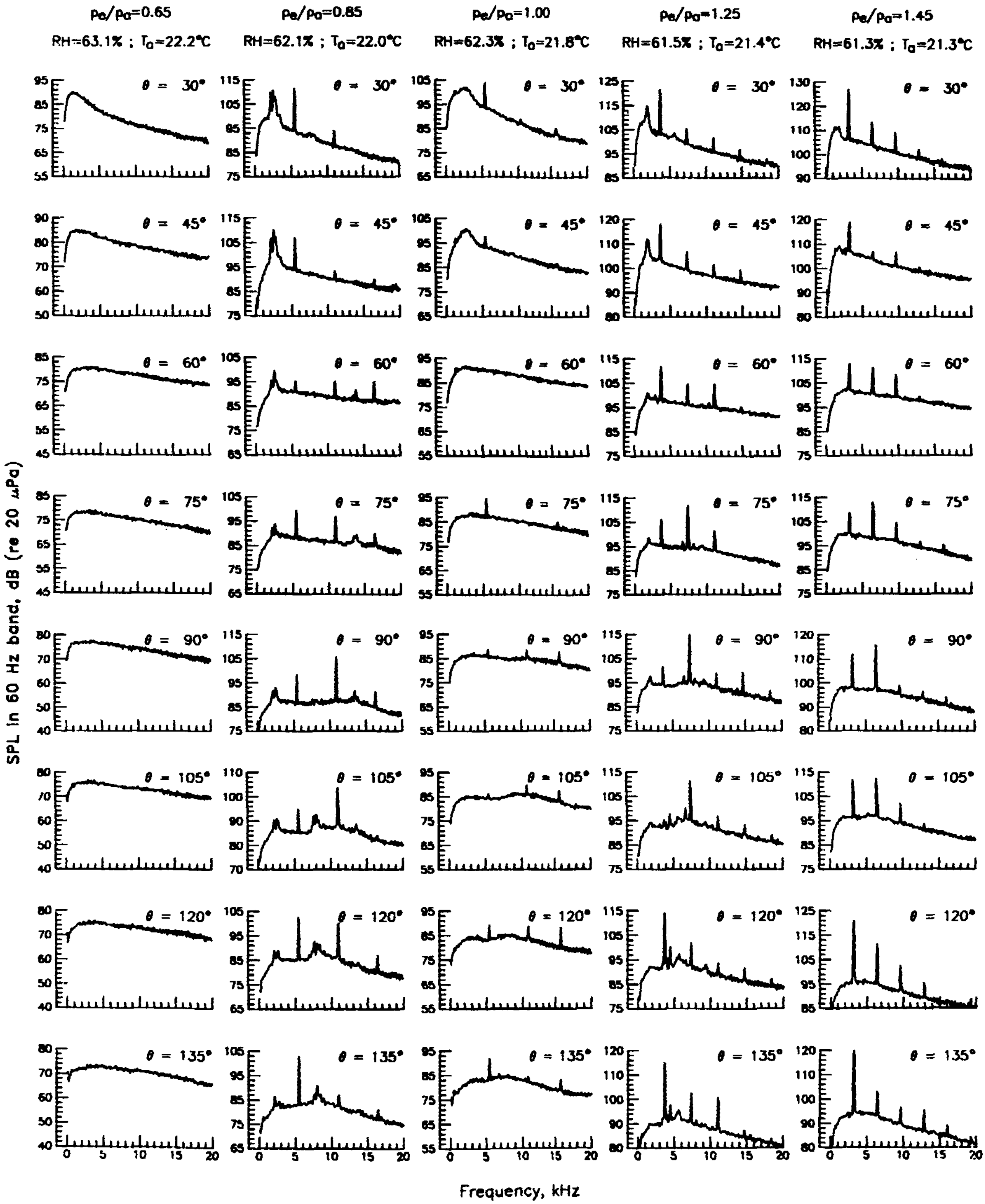

(e) $\phi = 60°$.

Figure 7. Continued.

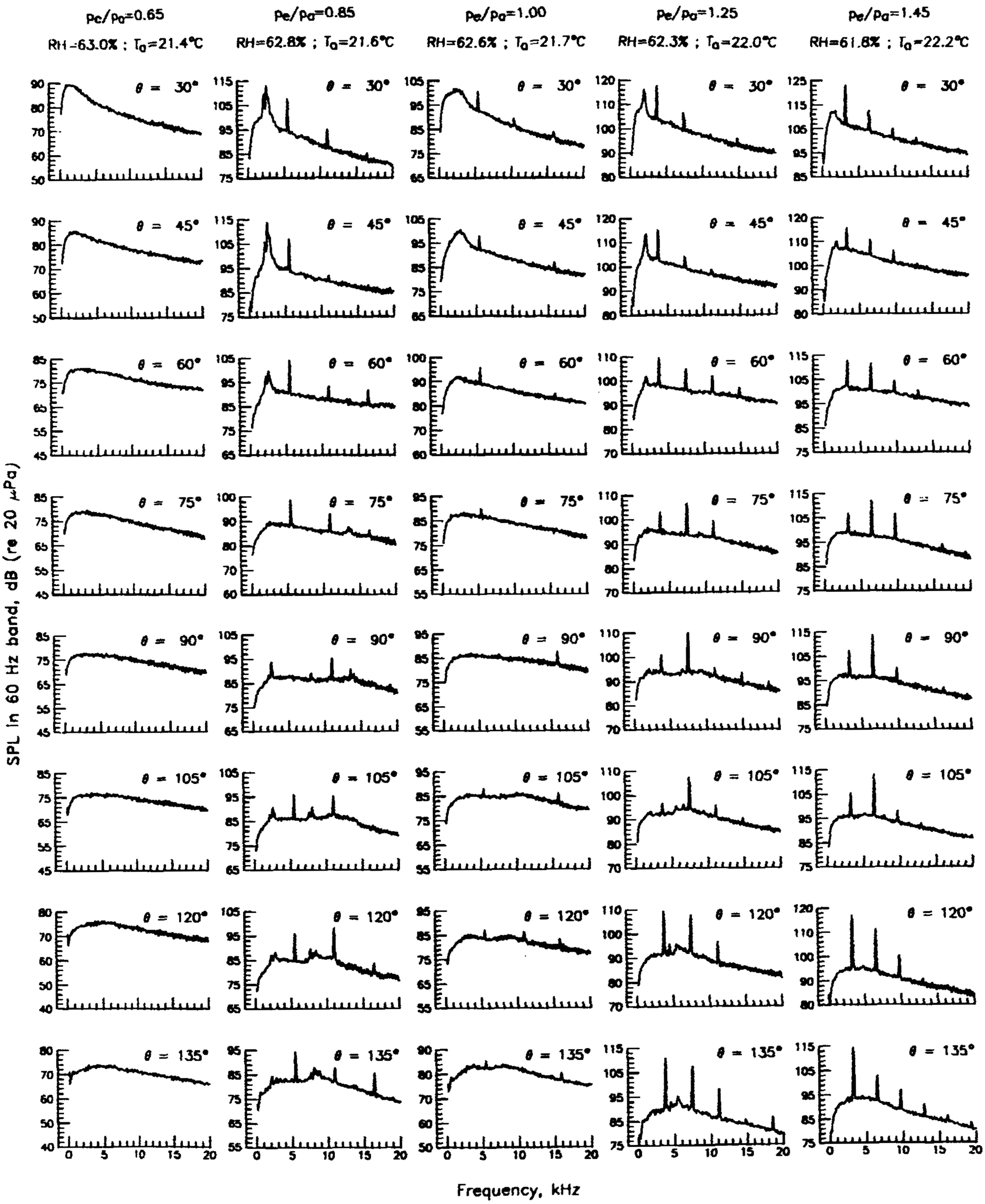

(f) $\phi = 75°$.

Figure 7. Continued.

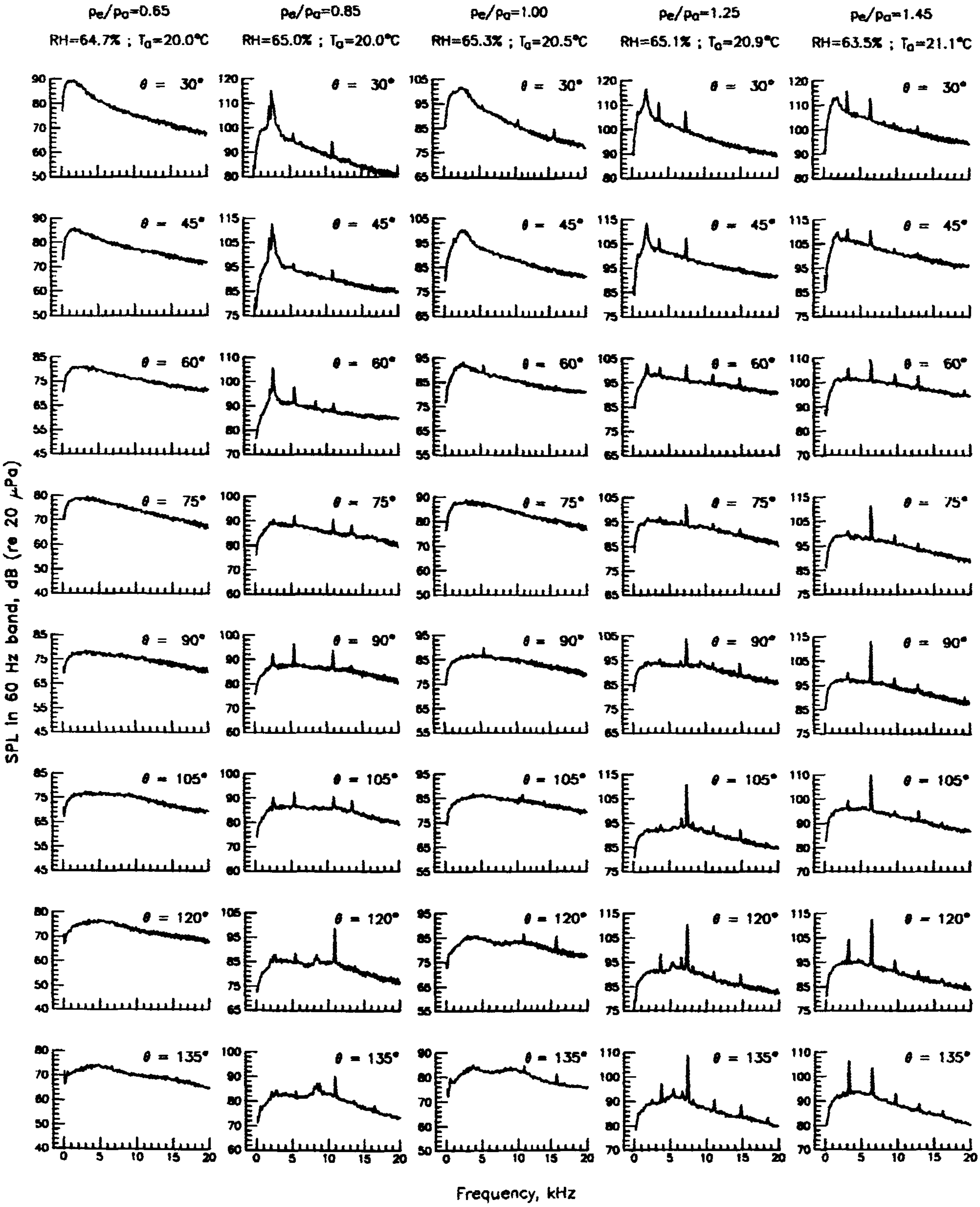

(g) $\phi = 90°$.

Figure 7. Continued.

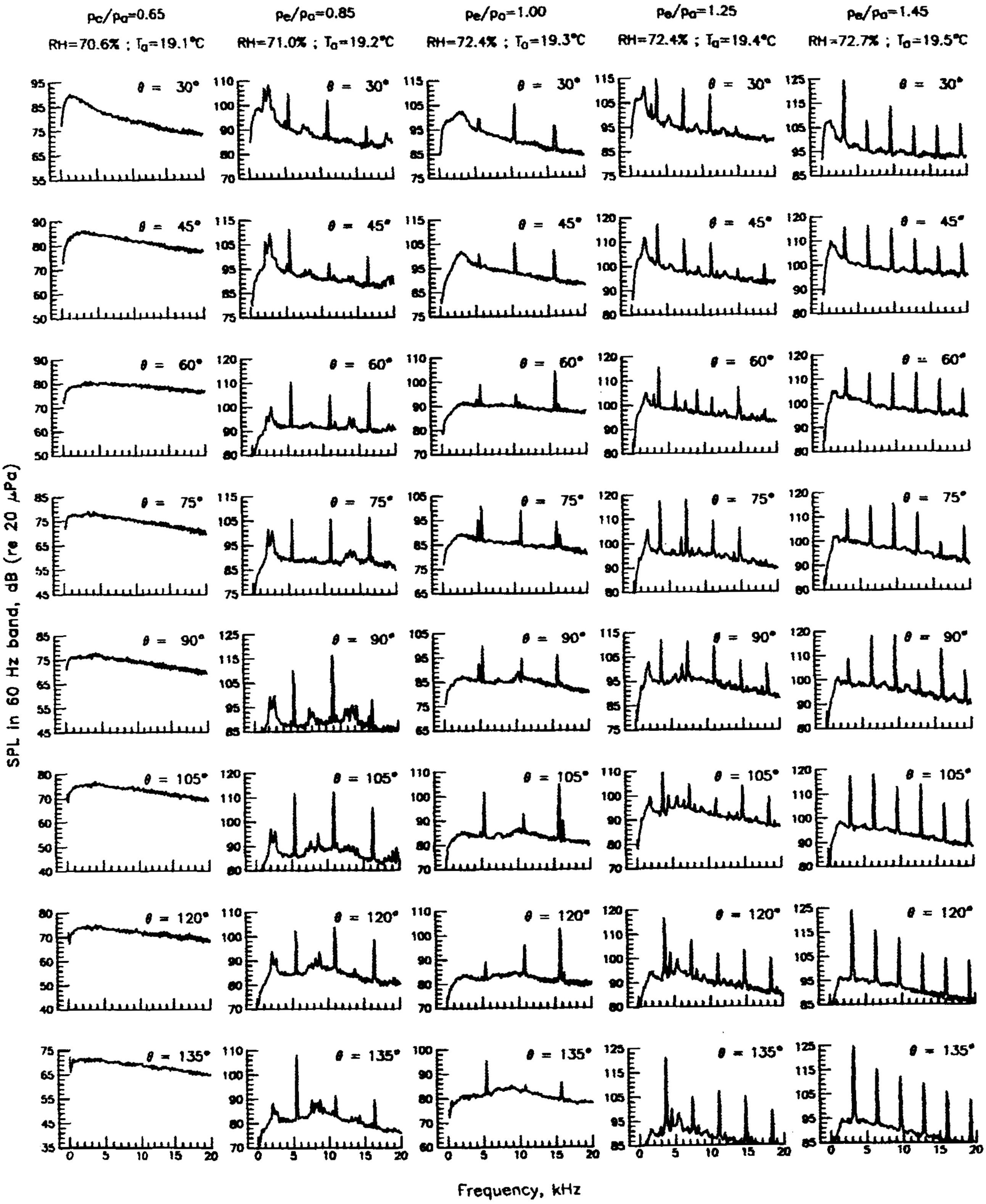

(h) $\phi = 180°$.

Figure 7. Continued.

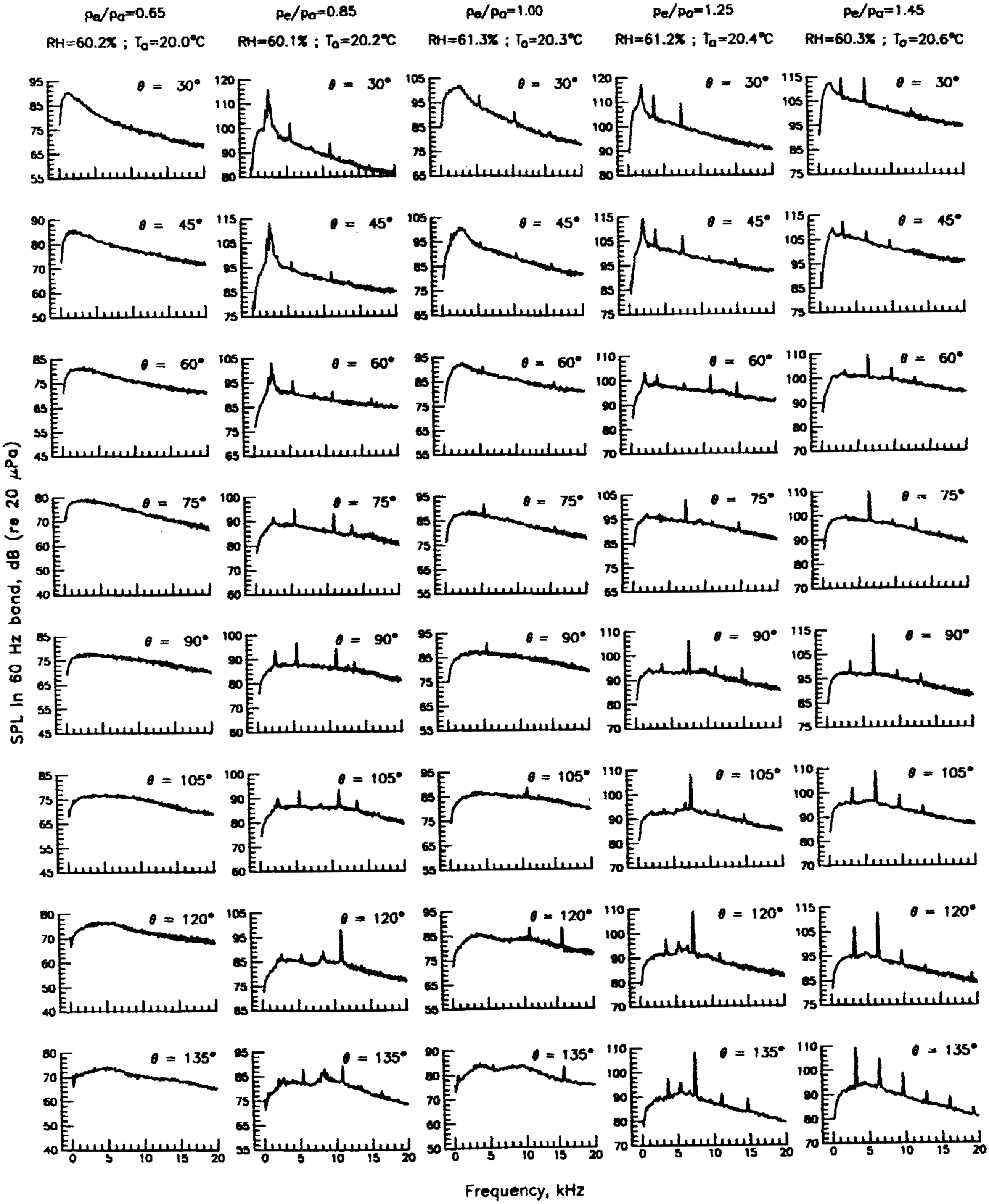

(i) $\phi = 270°$.

Figure 7. Concluded.

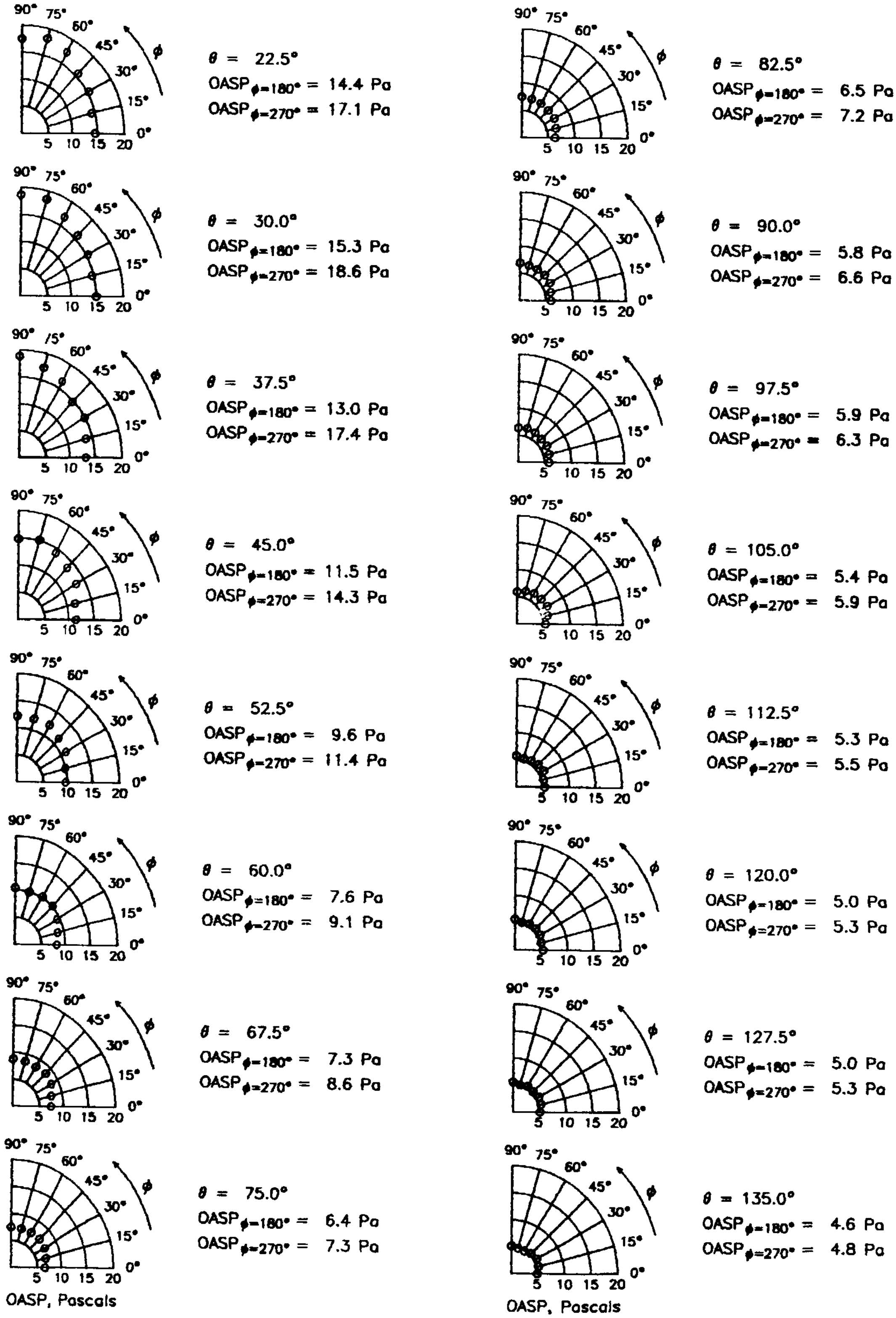

(a) $p_e/p_a = 0.50$.

Figure 8. Directivity plots for rectangular nozzle with throat aspect ratio of 2.0.

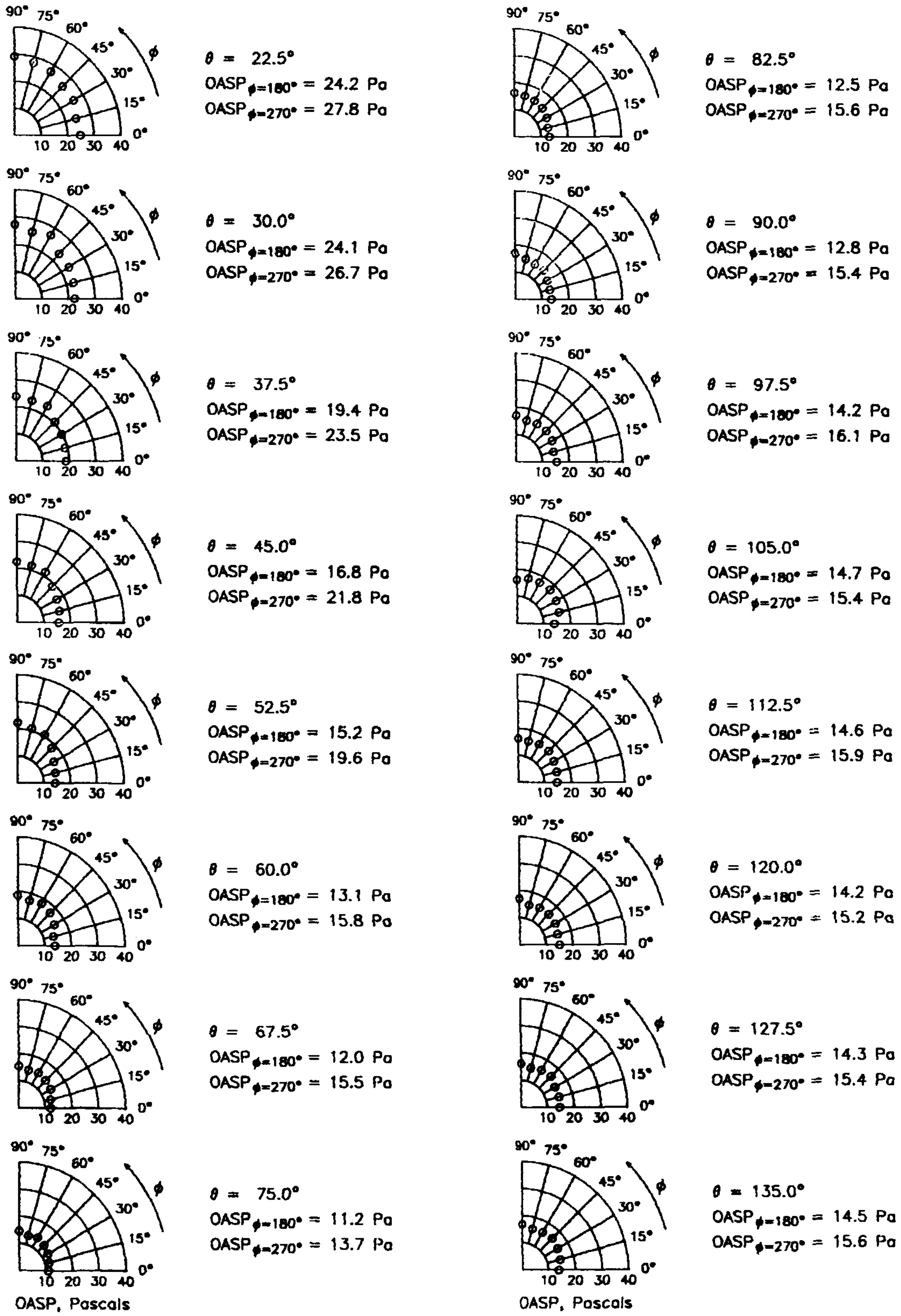

(b) $p_e/p_a = 0.60$.

Figure 8. Continued.

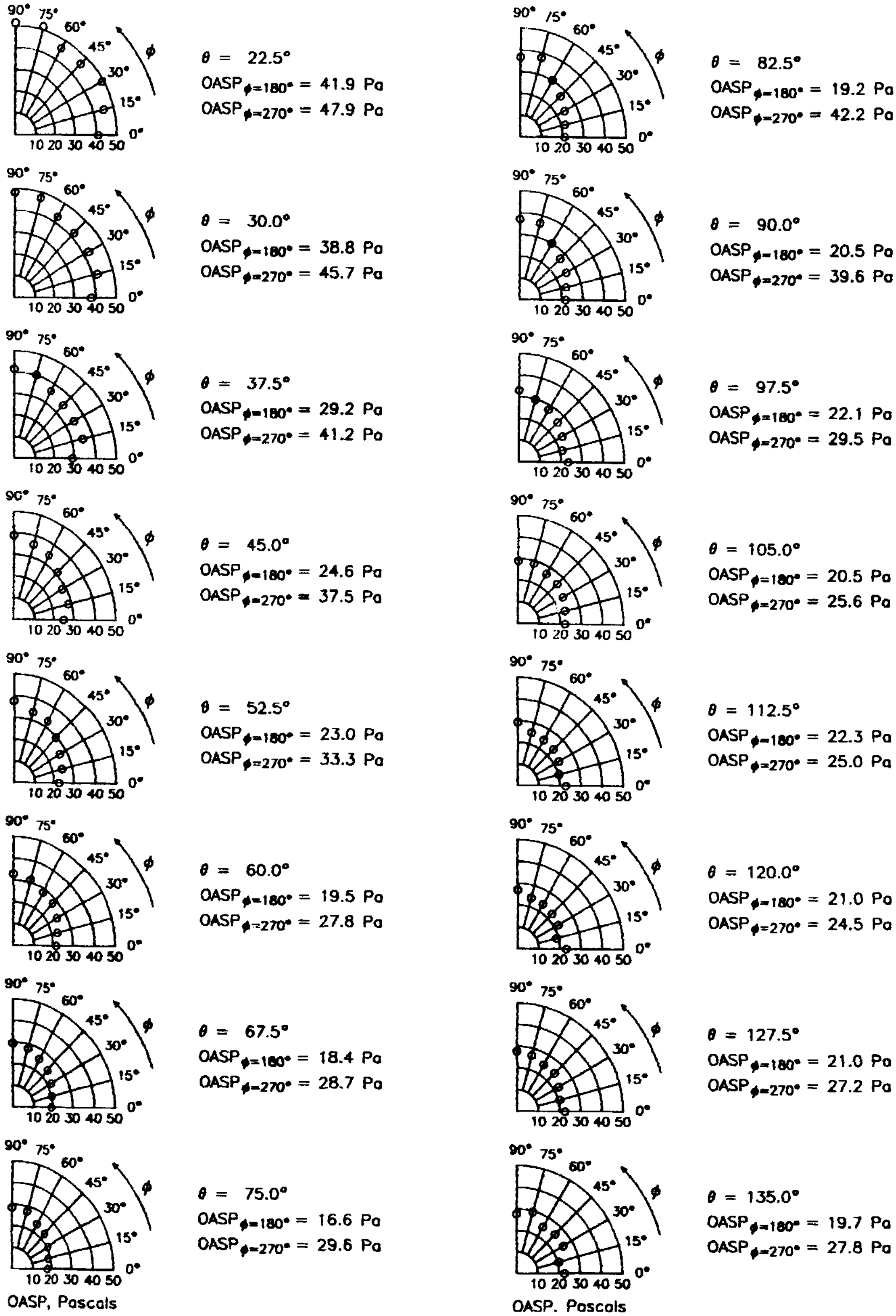

(c) $p_e/p_a = 0.70$.

Figure 8. Continued.

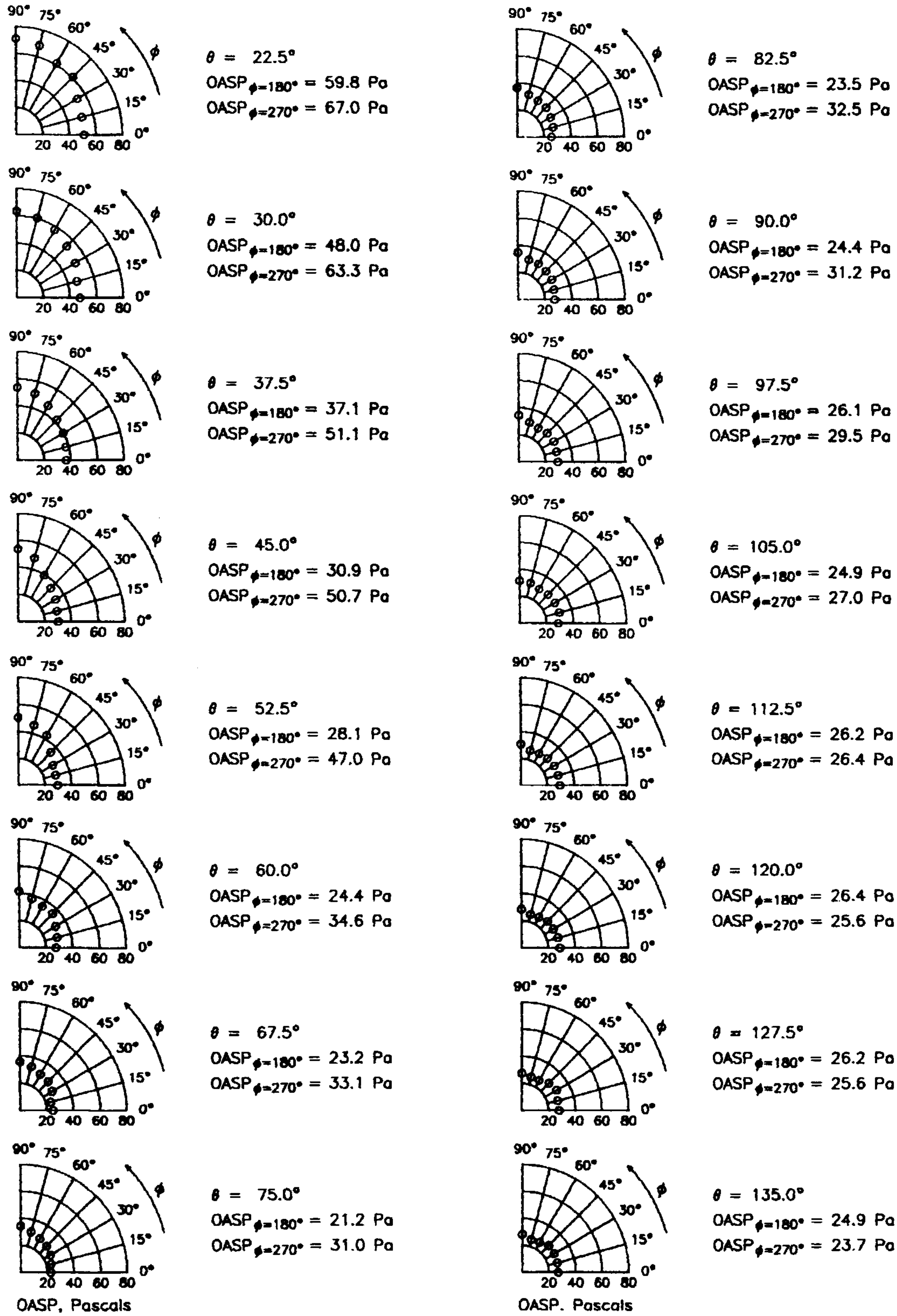

(d) $p_e/p_a = 0.80$.

Figure 8. Continued.

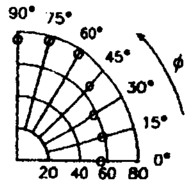

θ = 22.5°
$OASP_{\phi=180°}$ = 57.7 Pa
$OASP_{\phi=270°}$ = 76.2 Pa

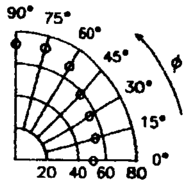

θ = 30.0°
$OASP_{\phi=180°}$ = 57.1 Pa
$OASP_{\phi=270°}$ = 72.8 Pa

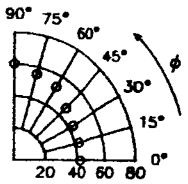

θ = 37.5°
$OASP_{\phi=180°}$ = 42.2 Pa
$OASP_{\phi=270°}$ = 57.5 Pa

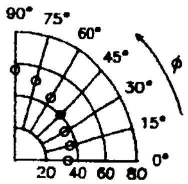

θ = 45.0°
$OASP_{\phi=180°}$ = 33.4 Pa
$OASP_{\phi=270°}$ = 54.0 Pa

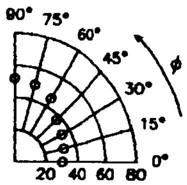

θ = 52.5°
$OASP_{\phi=180°}$ = 31.8 Pa
$OASP_{\phi=270°}$ = 49.8 Pa

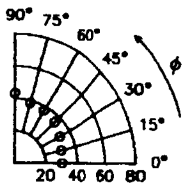

θ = 60.0°
$OASP_{\phi=180°}$ = 26.8 Pa
$OASP_{\phi=270°}$ = 36.4 Pa

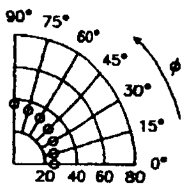

θ = 67.5°
$OASP_{\phi=180°}$ = 24.5 Pa
$OASP_{\phi=270°}$ = 35.3 Pa

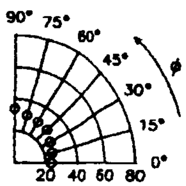

OASP, Pascals

θ = 75.0°
$OASP_{\phi=180°}$ = 22.2 Pa
$OASP_{\phi=270°}$ = 31.9 Pa

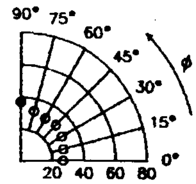

θ = 82.5°
$OASP_{\phi=180°}$ = 25.2 Pa
$OASP_{\phi=270°}$ = 32.5 Pa

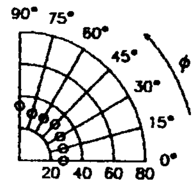

θ = 90.0°
$OASP_{\phi=180°}$ = 24.9 Pa
$OASP_{\phi=270°}$ = 31.4 Pa

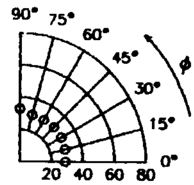

θ = 97.5°
$OASP_{\phi=180°}$ = 27.1 Pa
$OASP_{\phi=270°}$ = 30.7 Pa

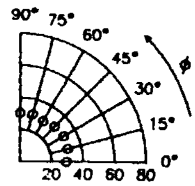

θ = 105.0°
$OASP_{\phi=180°}$ = 26.2 Pa
$OASP_{\phi=270°}$ = 26.8 Pa

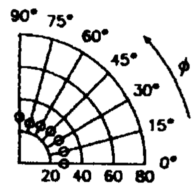

θ = 112.5°
$OASP_{\phi=180°}$ = 27.0 Pa
$OASP_{\phi=270°}$ = 26.5 Pa

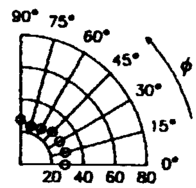

θ = 120.0°
$OASP_{\phi=180°}$ = 25.5 Pa
$OASP_{\phi=270°}$ = 25.4 Pa

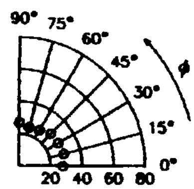

θ = 127.5°
$OASP_{\phi=180°}$ = 24.7 Pa
$OASP_{\phi=270°}$ = 24.9 Pa

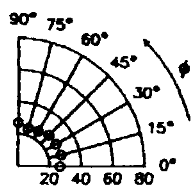

OASP, Pascals

θ = 135.0°
$OASP_{\phi=180°}$ = 23.7 Pa
$OASP_{\phi=270°}$ = 24.3 Pa

(e) $p_e/p_a = 0.85$.

Figure 8. Continued.

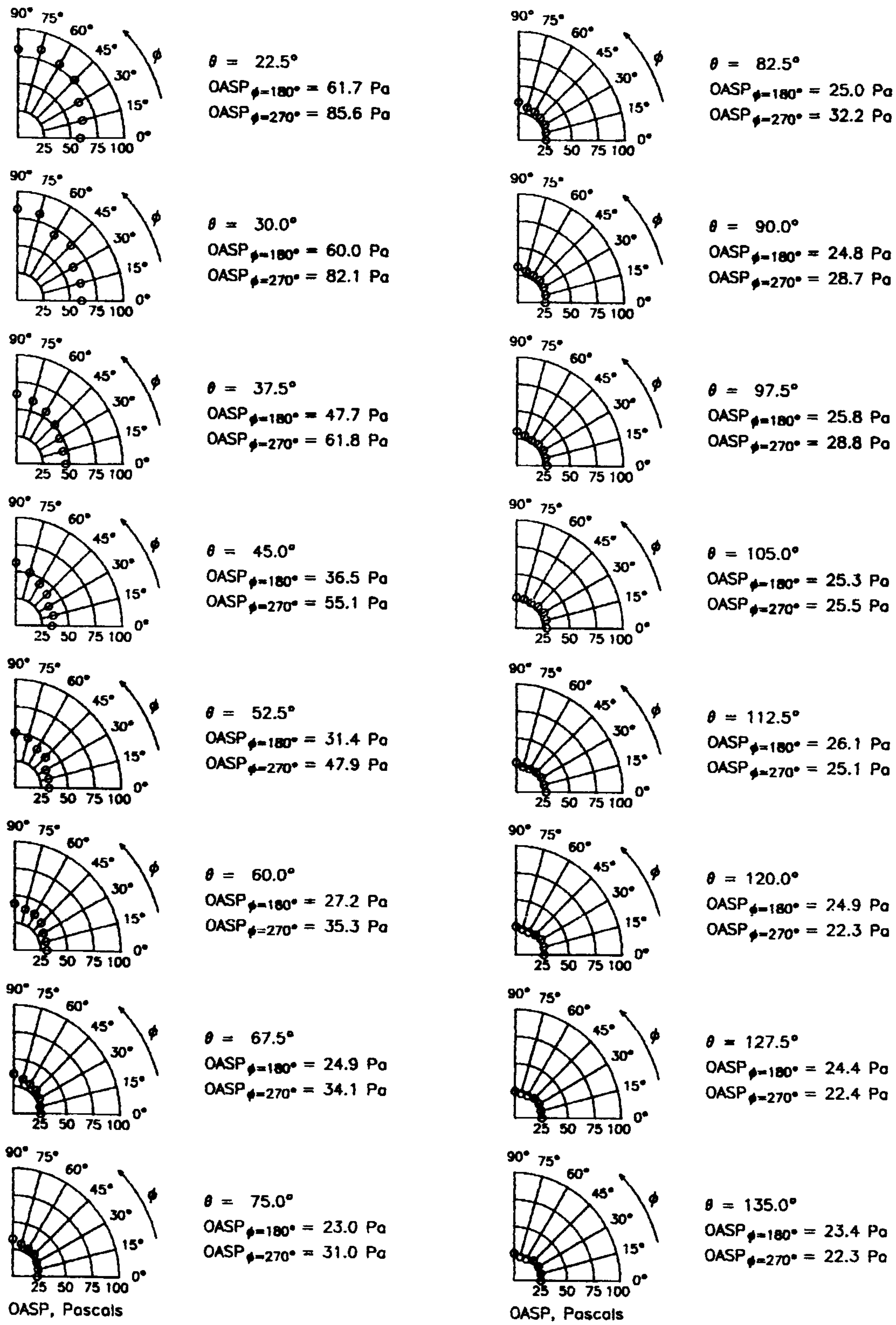

(f) $p_e/p_a = 0.90$.

Figure 8. Continued.

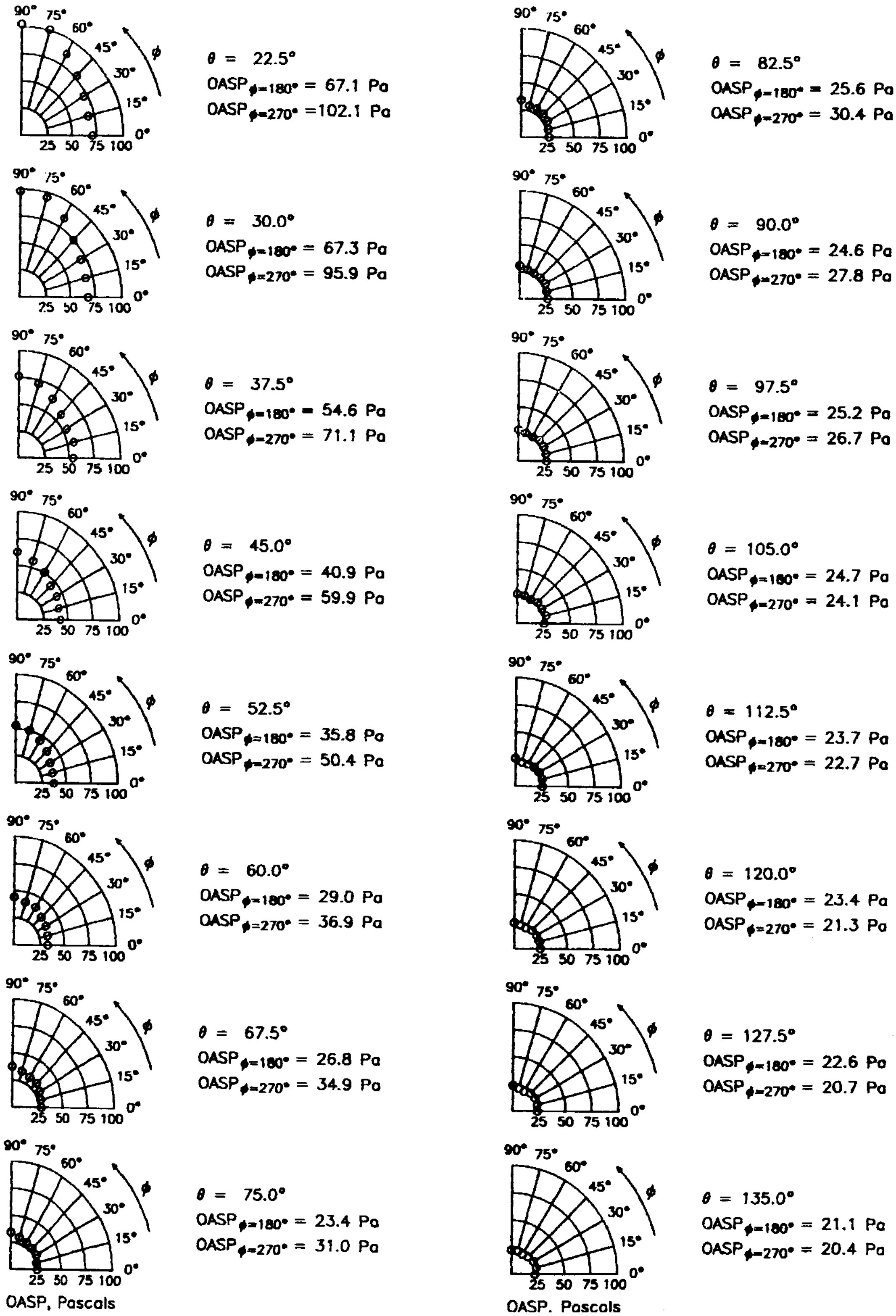

(g) $p_e/p_a = 1.00$.

Figure 8. Continued.

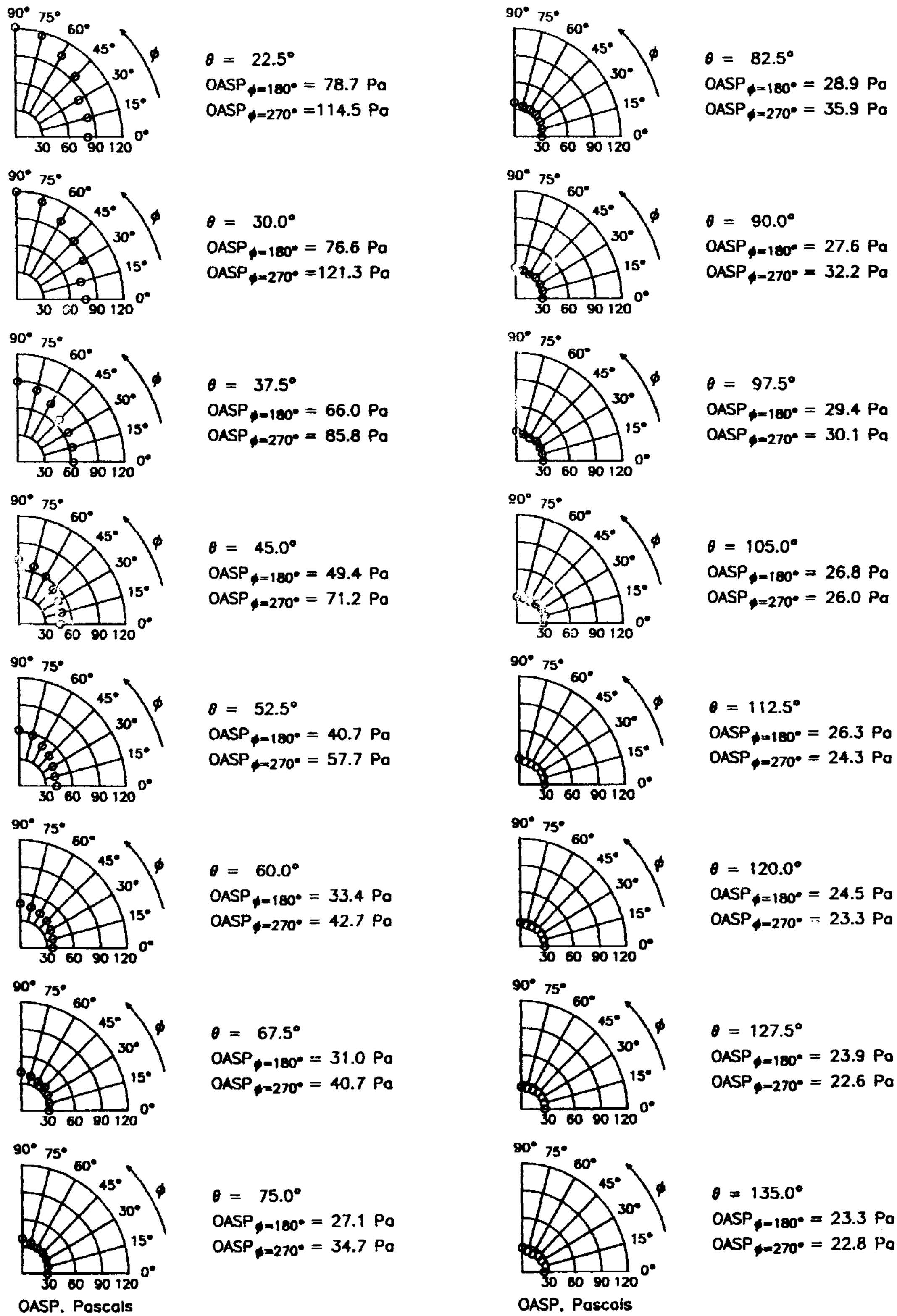

(h) $p_e/p_a = 1.10$.

Figure 8. Continued.

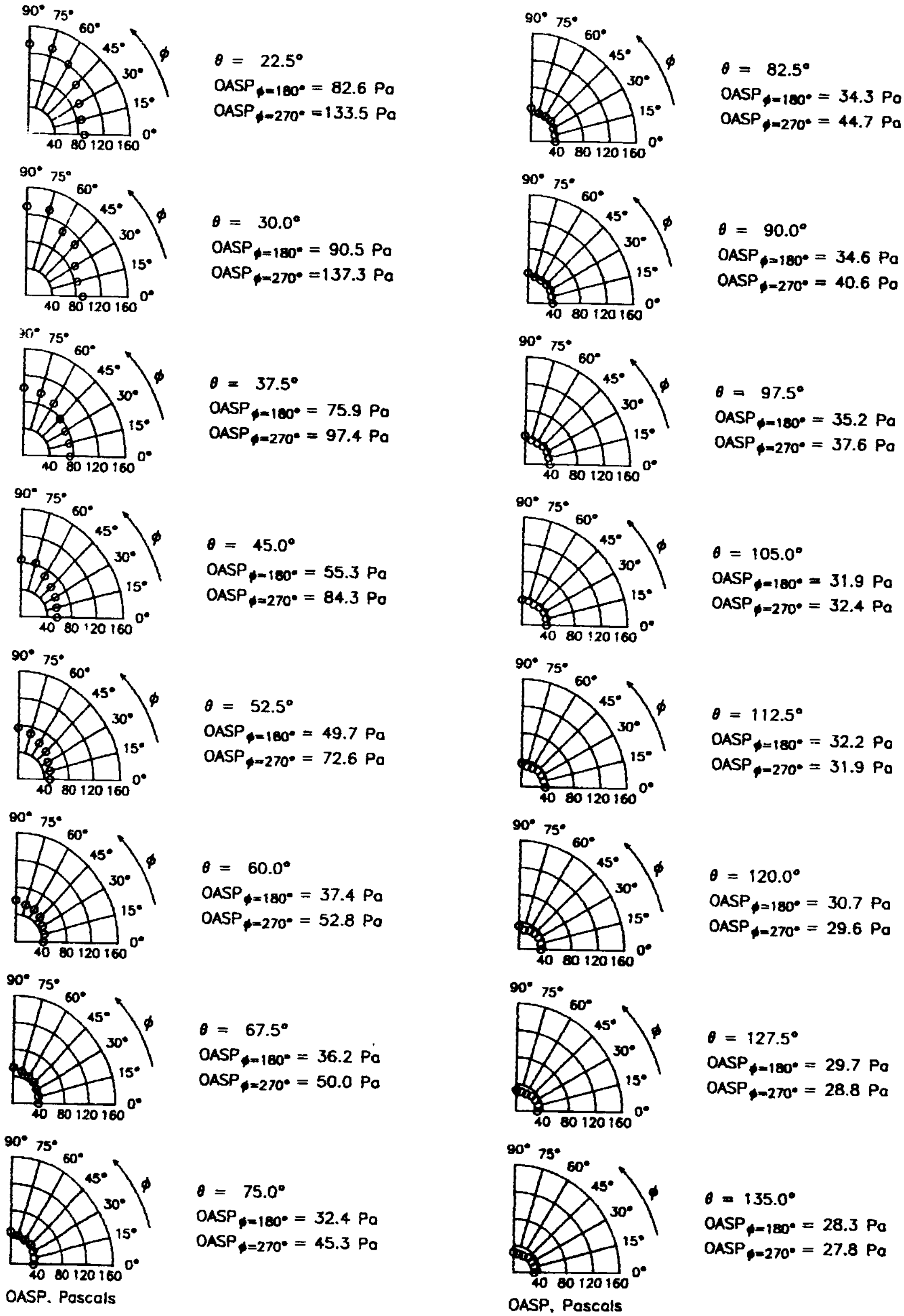

(i) $p_e/p_a = 1.20$.

Figure 8. Continued.

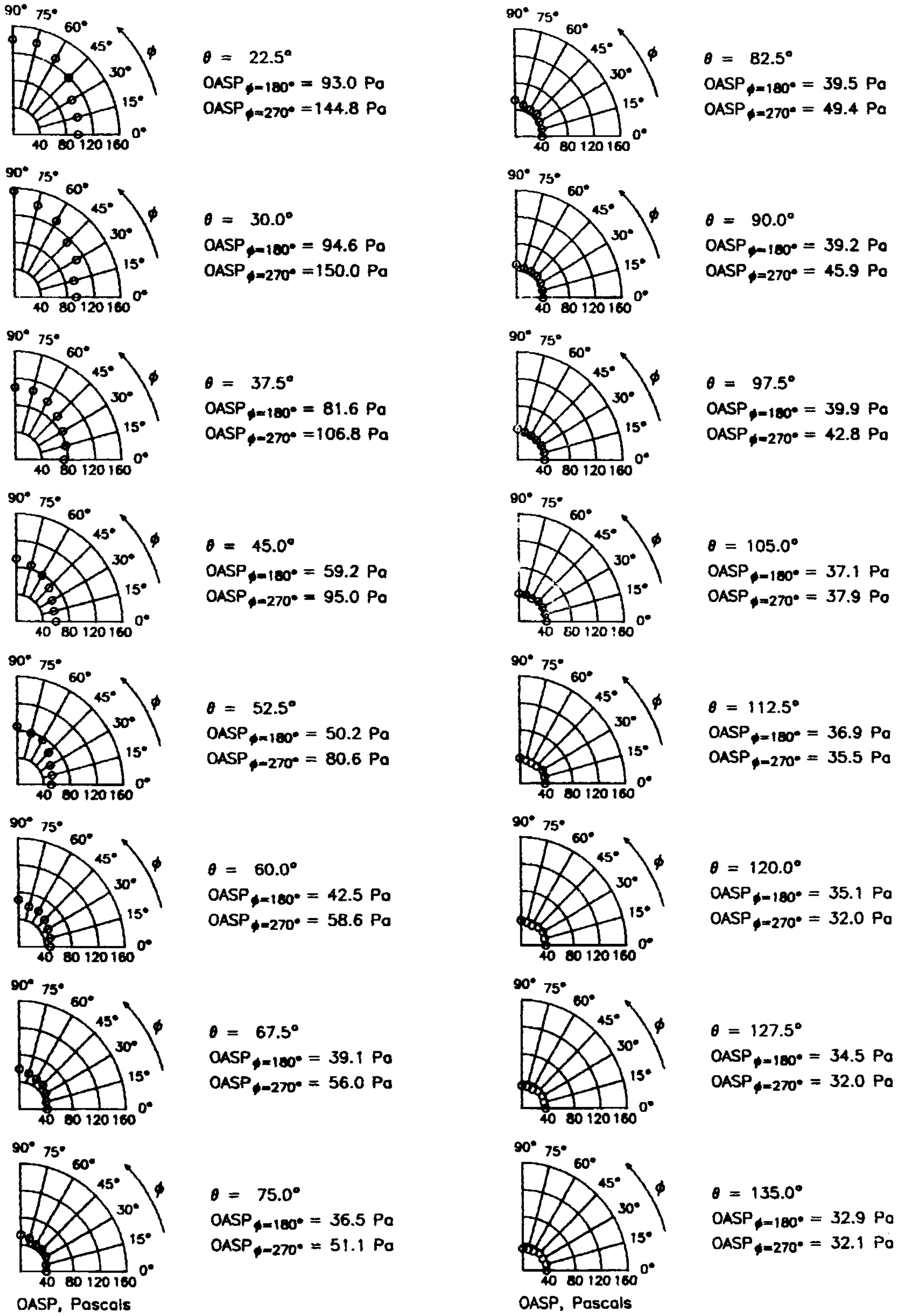

(j) $p_e/p_a = 1.25$.

Figure 8. Continued.

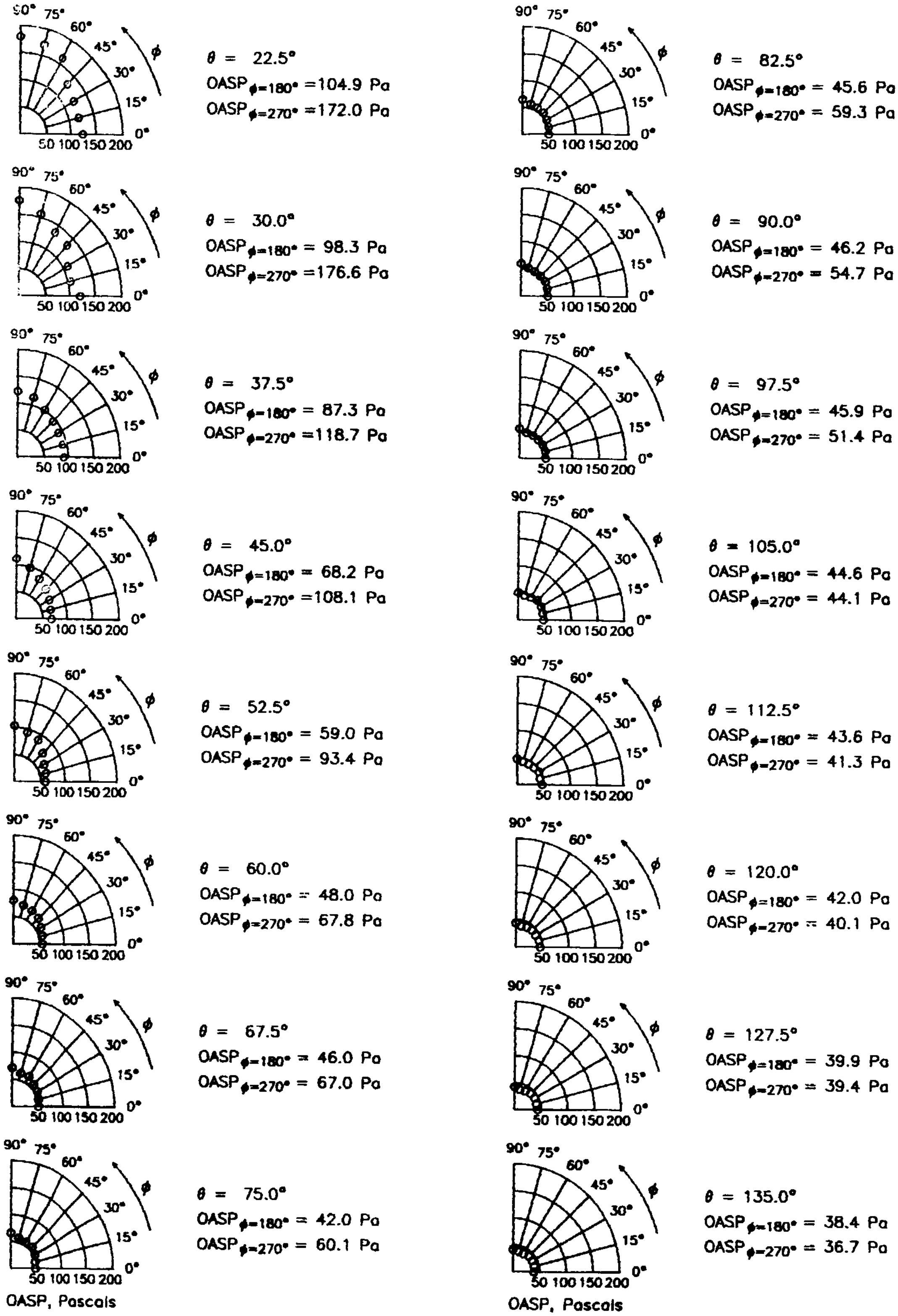

(k) $p_e/p_a = 1.35$.

Figure 8. Continued.

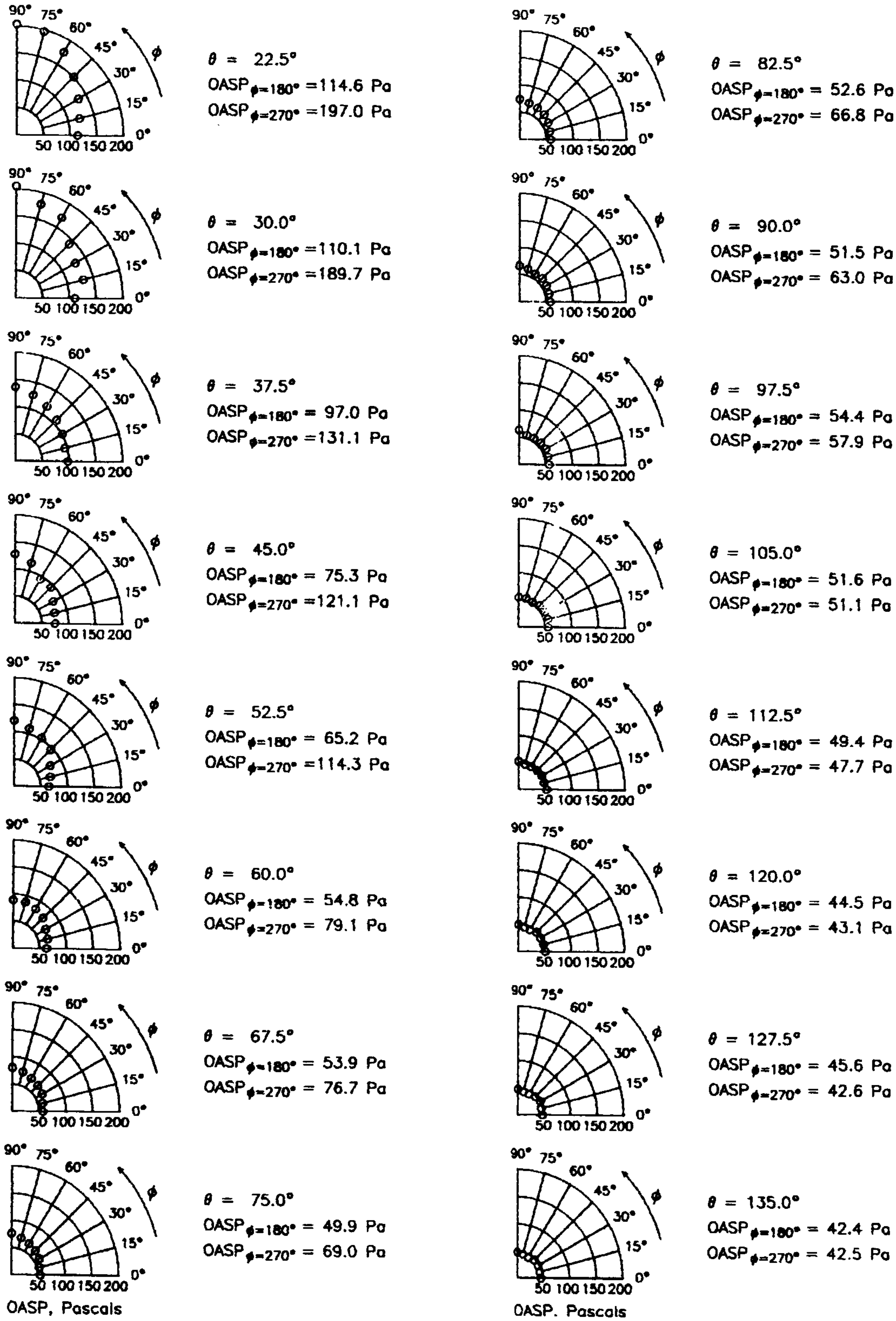

(l) $p_e/p_a = 1.45$.

Figure 8. Concluded.

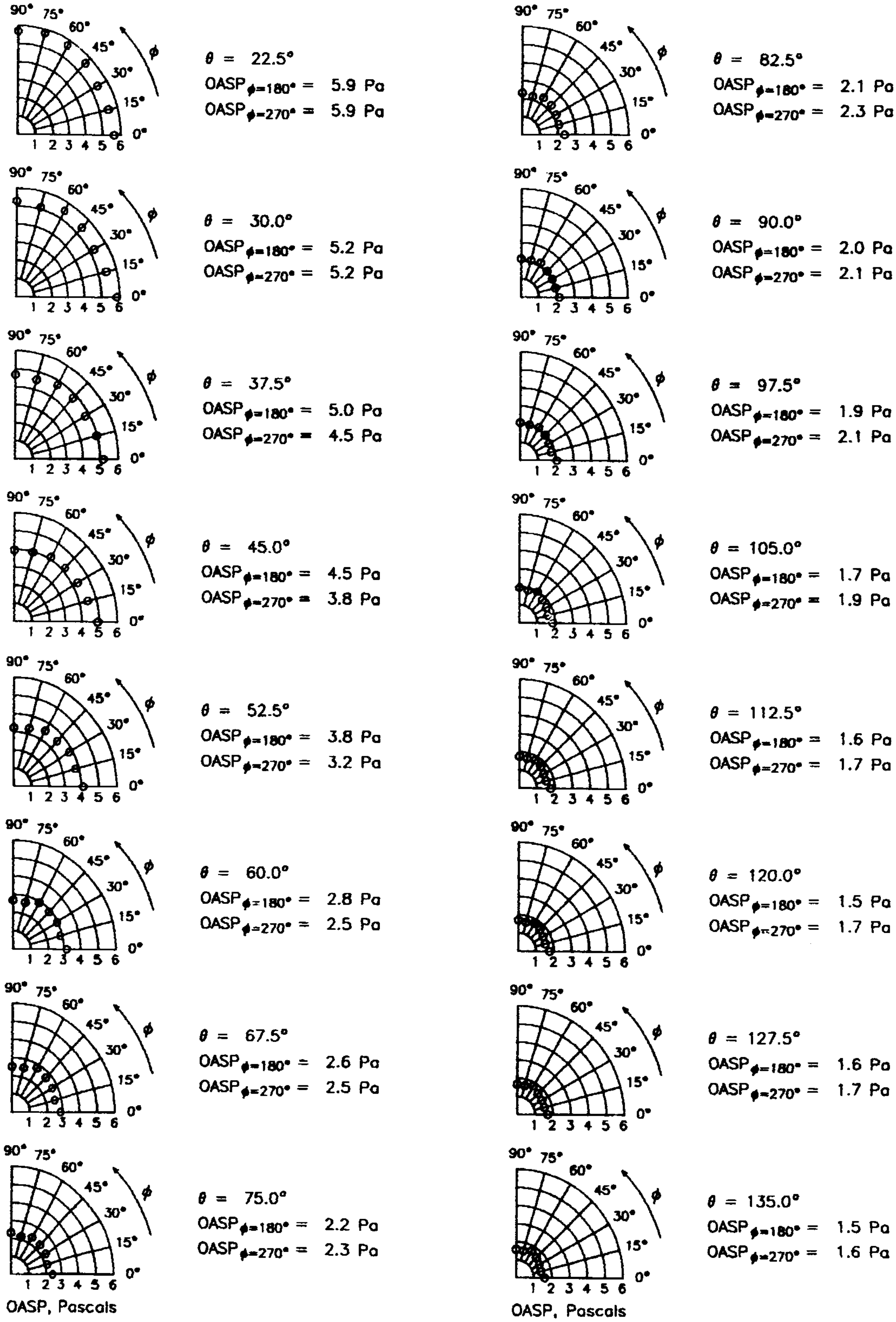

(a) $p_e/p_a = 0.65$.

Figure 9. Directivity plots for rectangular nozzle with throat aspect ratio of 3.7.

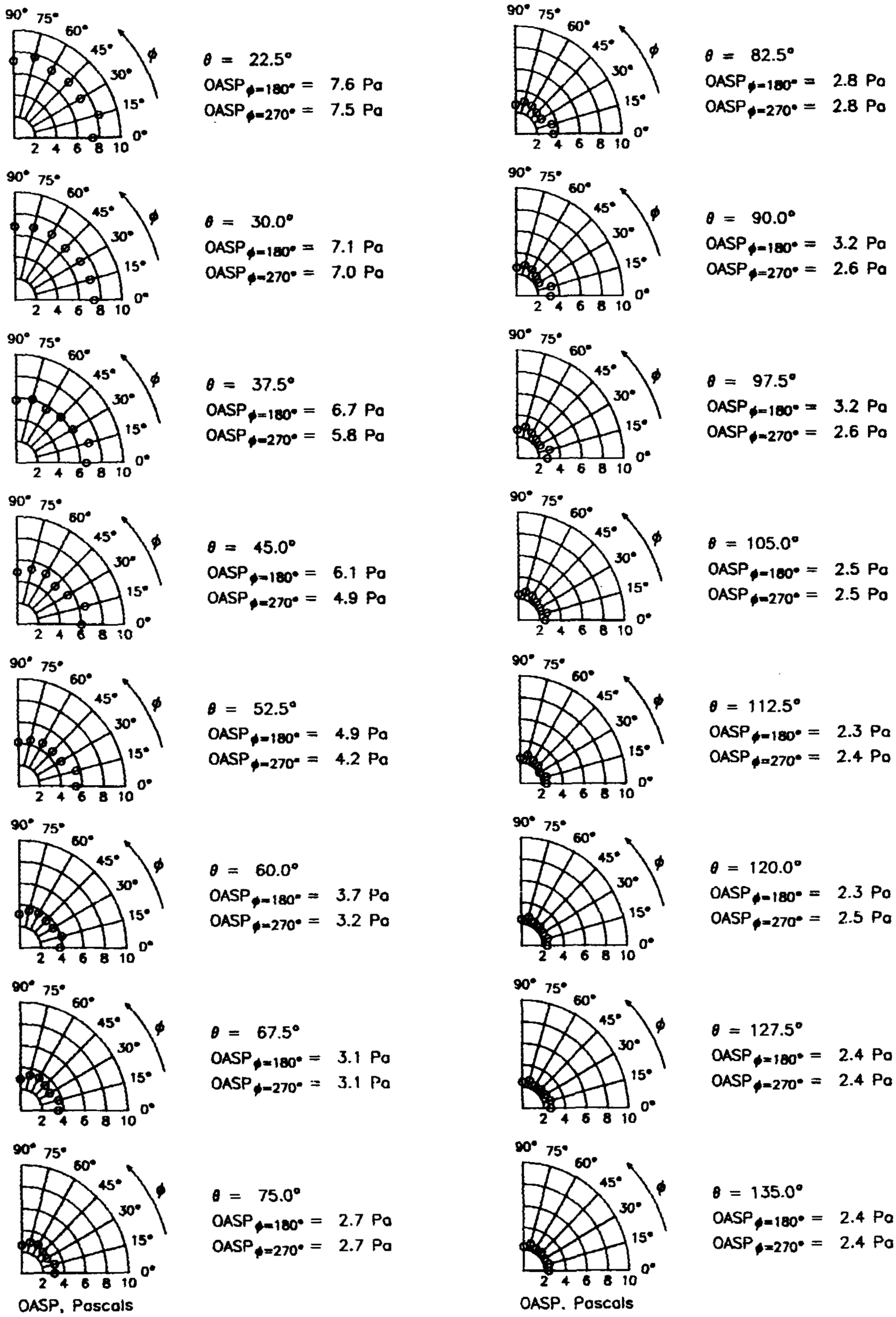

(b) $p_e/p_a = 0.70$.

Figure 9. Continued.

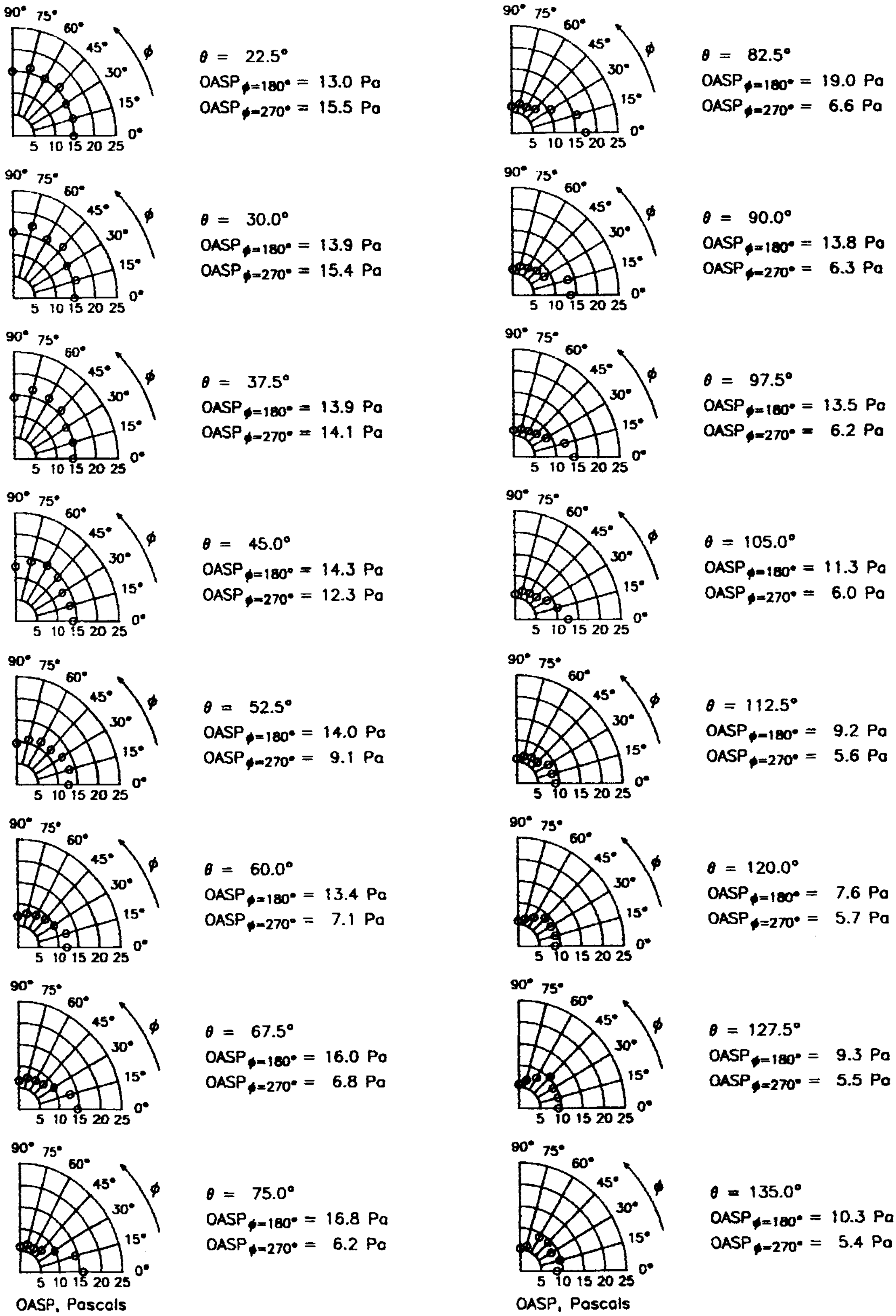

(c) $p_e/p_a = 0.80$.

Figure 9. Continued.

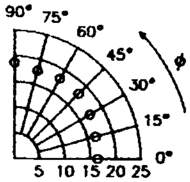

θ = 22.5°
OASP$_{\phi=180°}$ = 15.0 Pa
OASP$_{\phi=270°}$ = 18.1 Pa

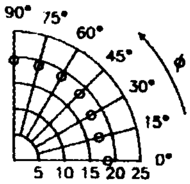

θ = 30.0°
OASP$_{\phi=180°}$ = 16.1 Pa
OASP$_{\phi=270°}$ = 18.4 Pa

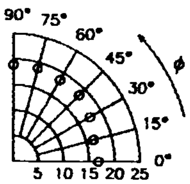

θ = 37.5°
OASP$_{\phi=180°}$ = 16.9 Pa
OASP$_{\phi=270°}$ = 17.4 Pa

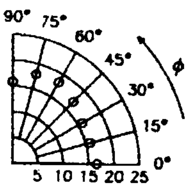

θ = 45.0°
OASP$_{\phi=180°}$ = 19.1 Pa
OASP$_{\phi=270°}$ = 14.5 Pa

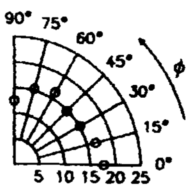

θ = 52.5°
OASP$_{\phi=180°}$ = 20.5 Pa
OASP$_{\phi=270°}$ = 11.6 Pa

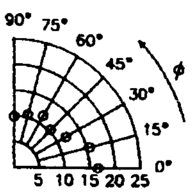

θ = 60.0°
OASP$_{\phi=180°}$ = 17.9 Pa
OASP$_{\phi=270°}$ = 8.6 Pa

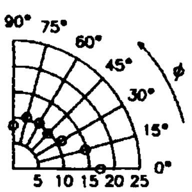

θ = 67.5°
OASP$_{\phi=180°}$ = 19.1 Pa
OASP$_{\phi=270°}$ = 8.0 Pa

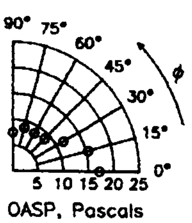

θ = 75.0°
OASP$_{\phi=180°}$ = 19.8 Pa
OASP$_{\phi=270°}$ = 7.4 Pa

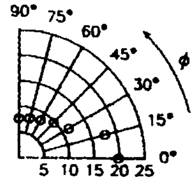

θ = 82.5°
OASP$_{\phi=180°}$ = 19.0 Pa
OASP$_{\phi=270°}$ = 7.8 Pa

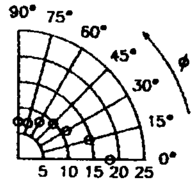

θ = 90.0°
OASP$_{\phi=180°}$ = 15.8 Pa
OASP$_{\phi=270°}$ = 7.3 Pa

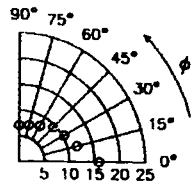

θ = 97.5°
OASP$_{\phi=180°}$ = 13.0 Pa
OASP$_{\phi=270°}$ = 7.0 Pa

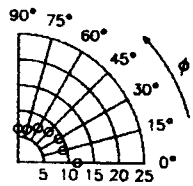

θ = 105.0°
OASP$_{\phi=180°}$ = 10.6 Pa
OASP$_{\phi=270°}$ = 6.9 Pa

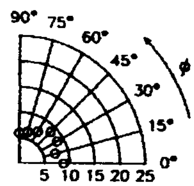

θ = 112.5°
OASP$_{\phi=180°}$ = 8.1 Pa
OASP$_{\phi=270°}$ = 6.2 Pa

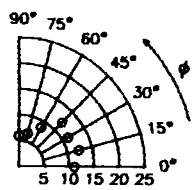

θ = 120.0°
OASP$_{\phi=180°}$ = 12.3 Pa
OASP$_{\phi=270°}$ = 6.0 Pa

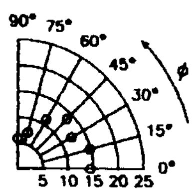

θ = 127.5°
OASP$_{\phi=180°}$ = 15.9 Pa
OASP$_{\phi=270°}$ = 6.0 Pa

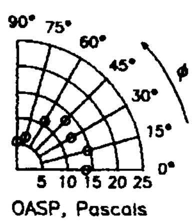

θ = 135.0°
OASP$_{\phi=180°}$ = 15.8 Pa
OASP$_{\phi=270°}$ = 5.4 Pa

(d) $p_e/p_a = 0.85$.

Figure 9. Continued.

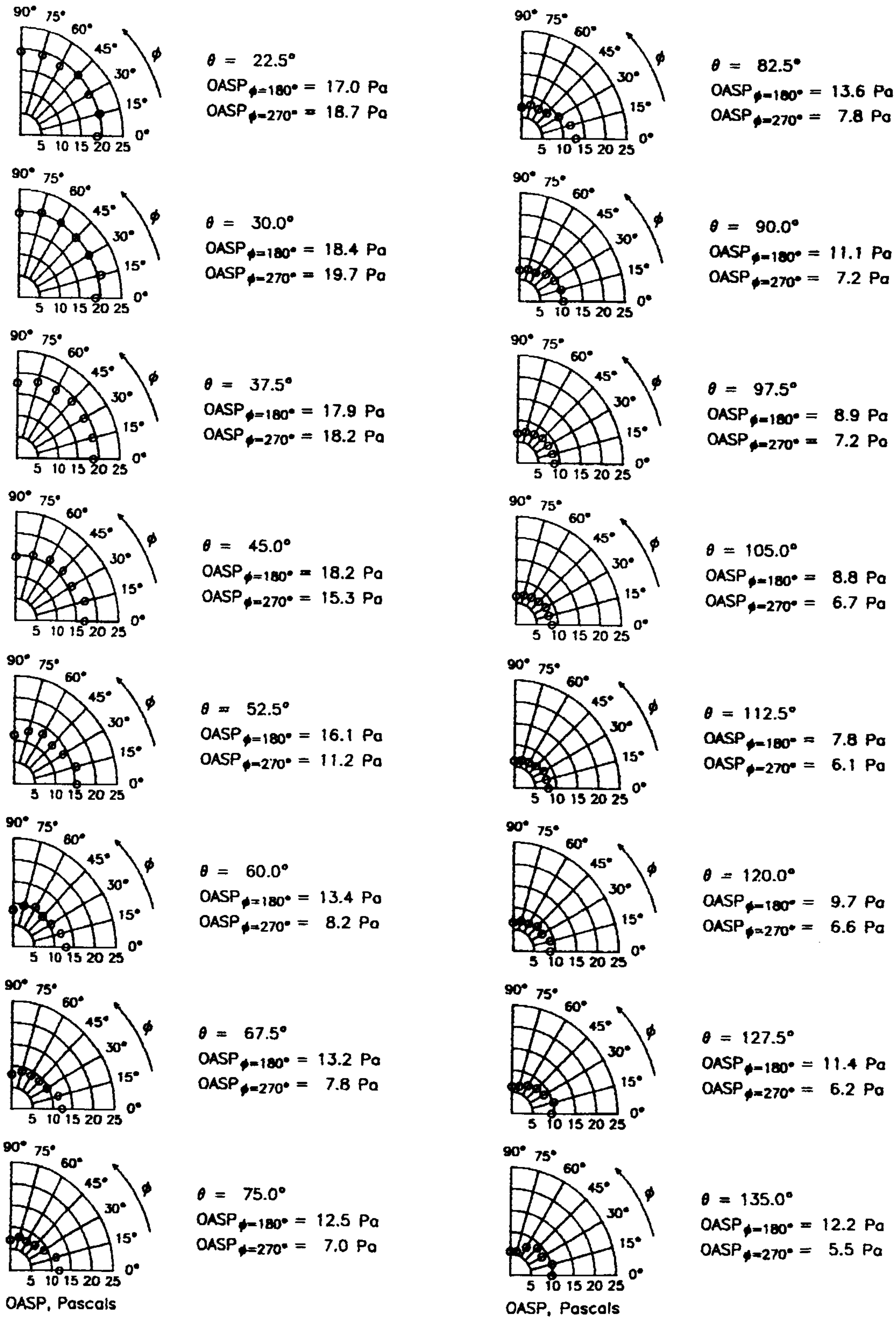

(e) $p_e/p_a = 0.90$.

Figure 9. Continued.

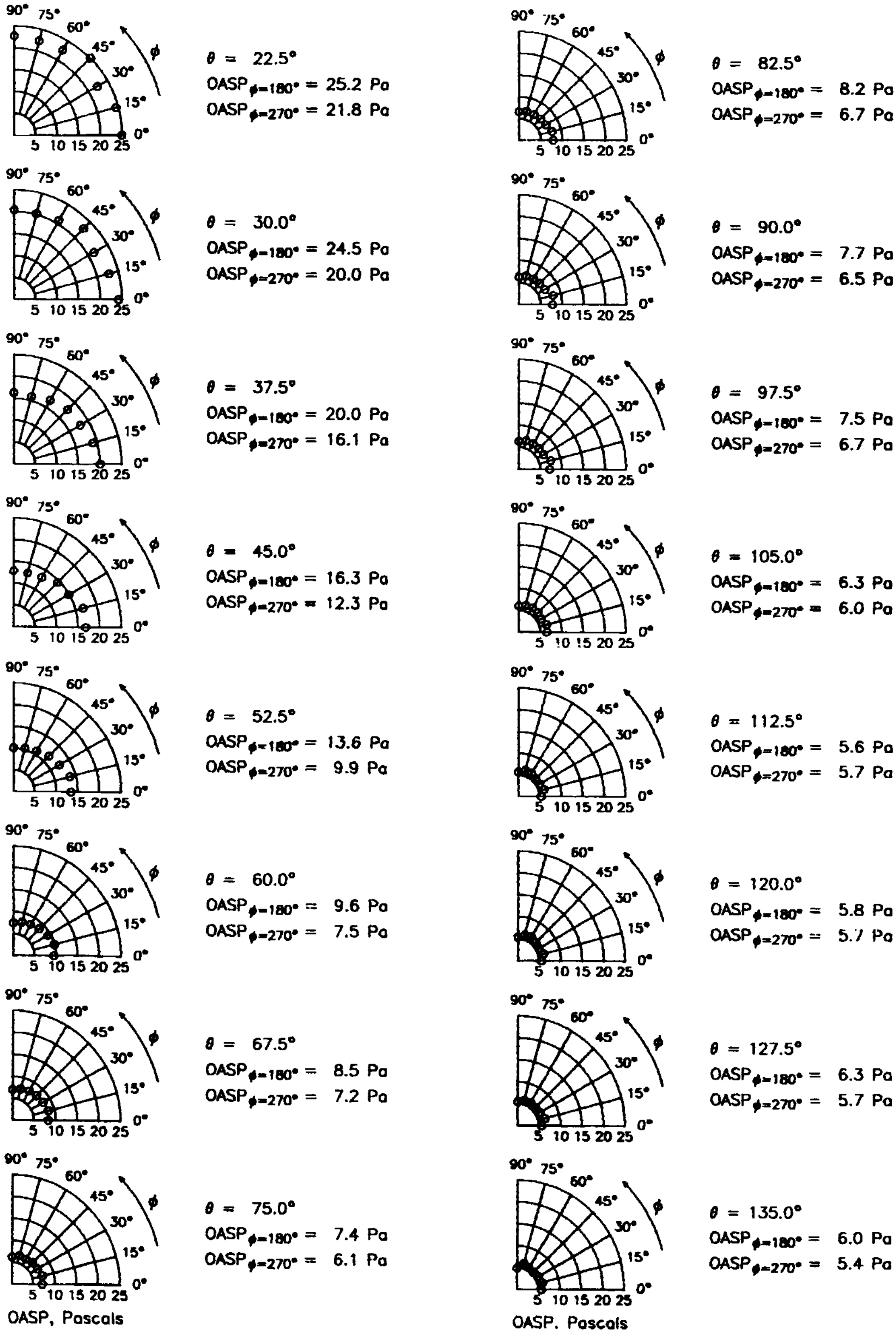

(f) $p_e/p_a = 1.00$.

Figure 9. Continued.

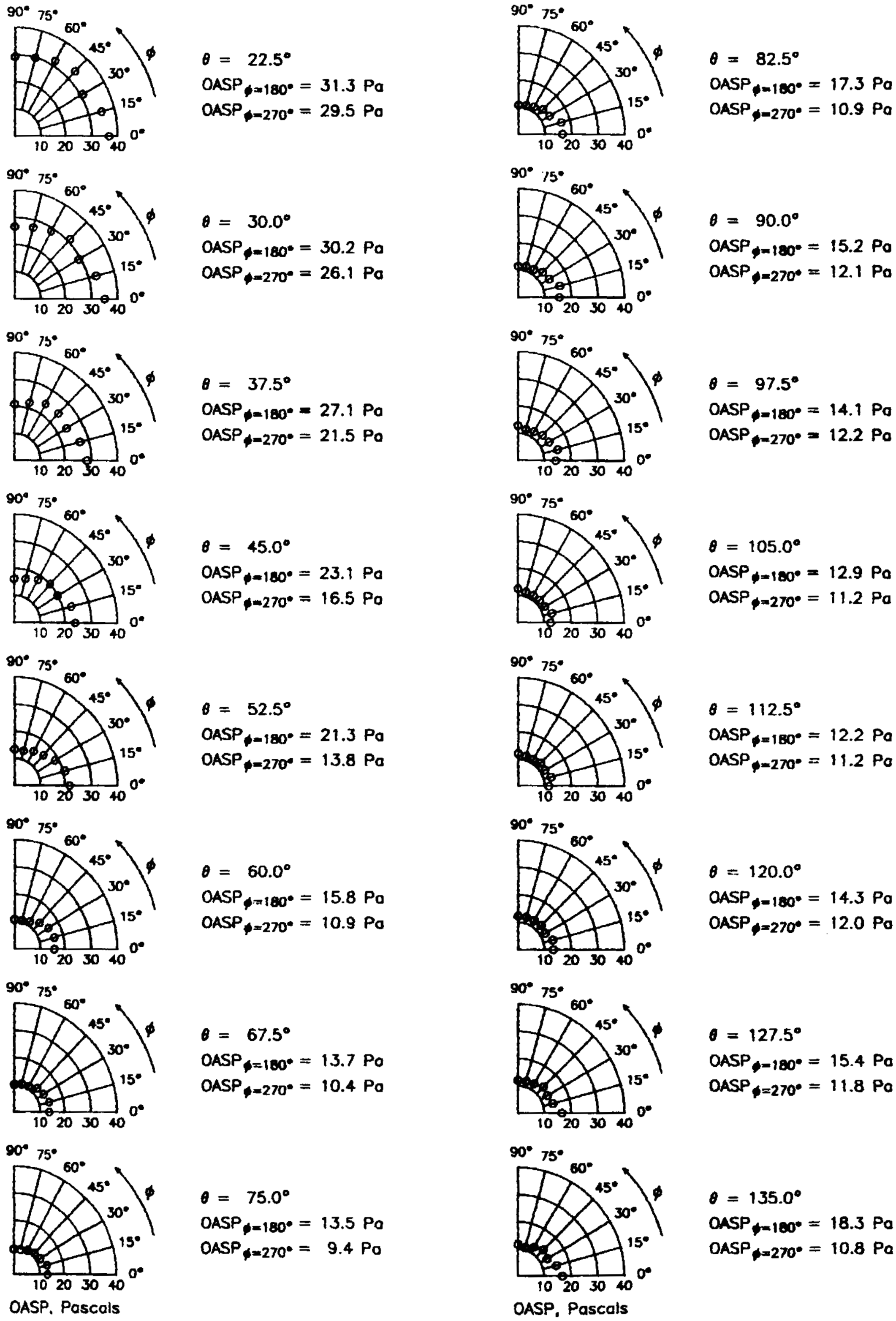

(g) $p_e/p_a = 1.10$.

Figure 9. Continued.

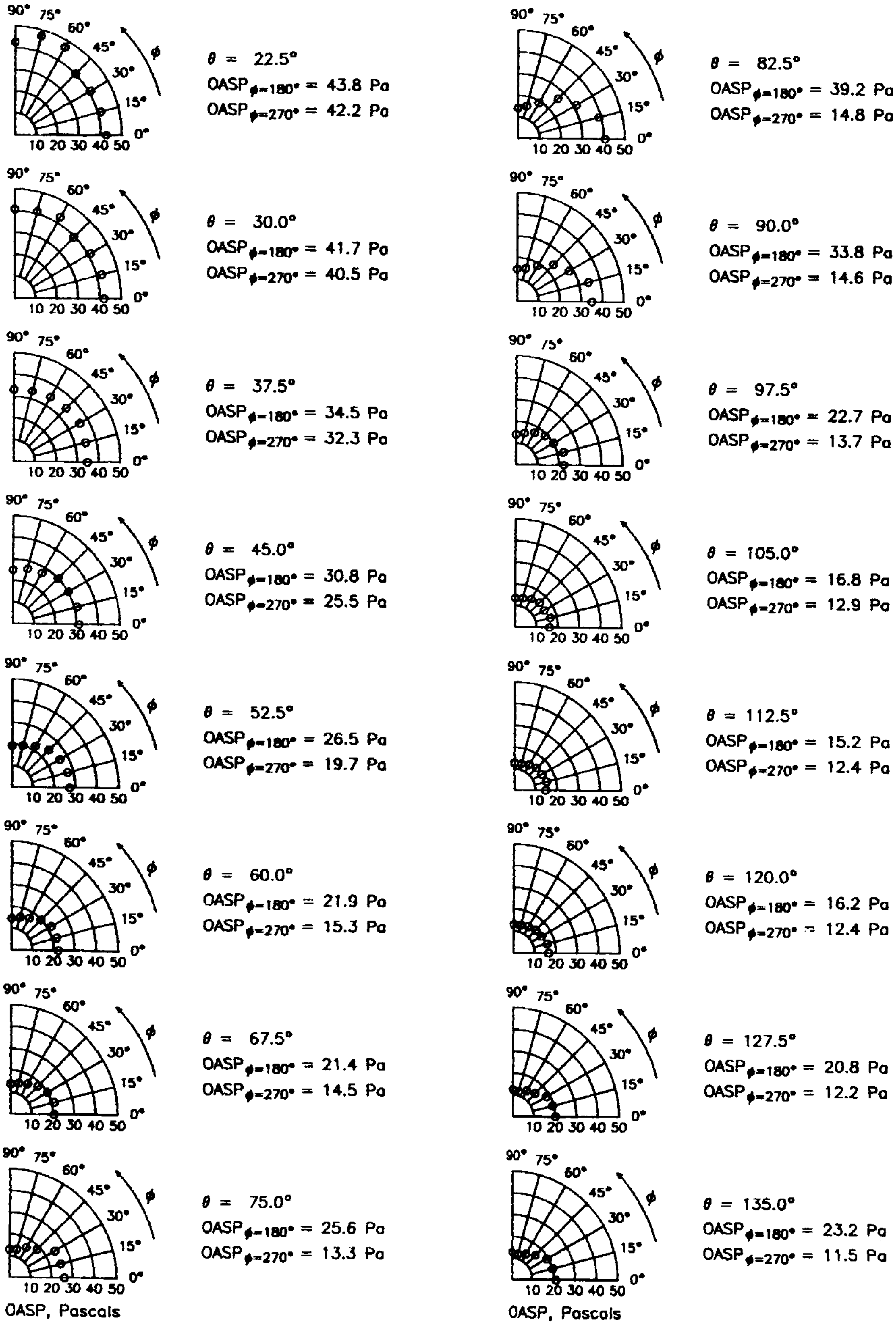

(h) $p_e/p_a = 1.20$.

Figure 9. Continued.

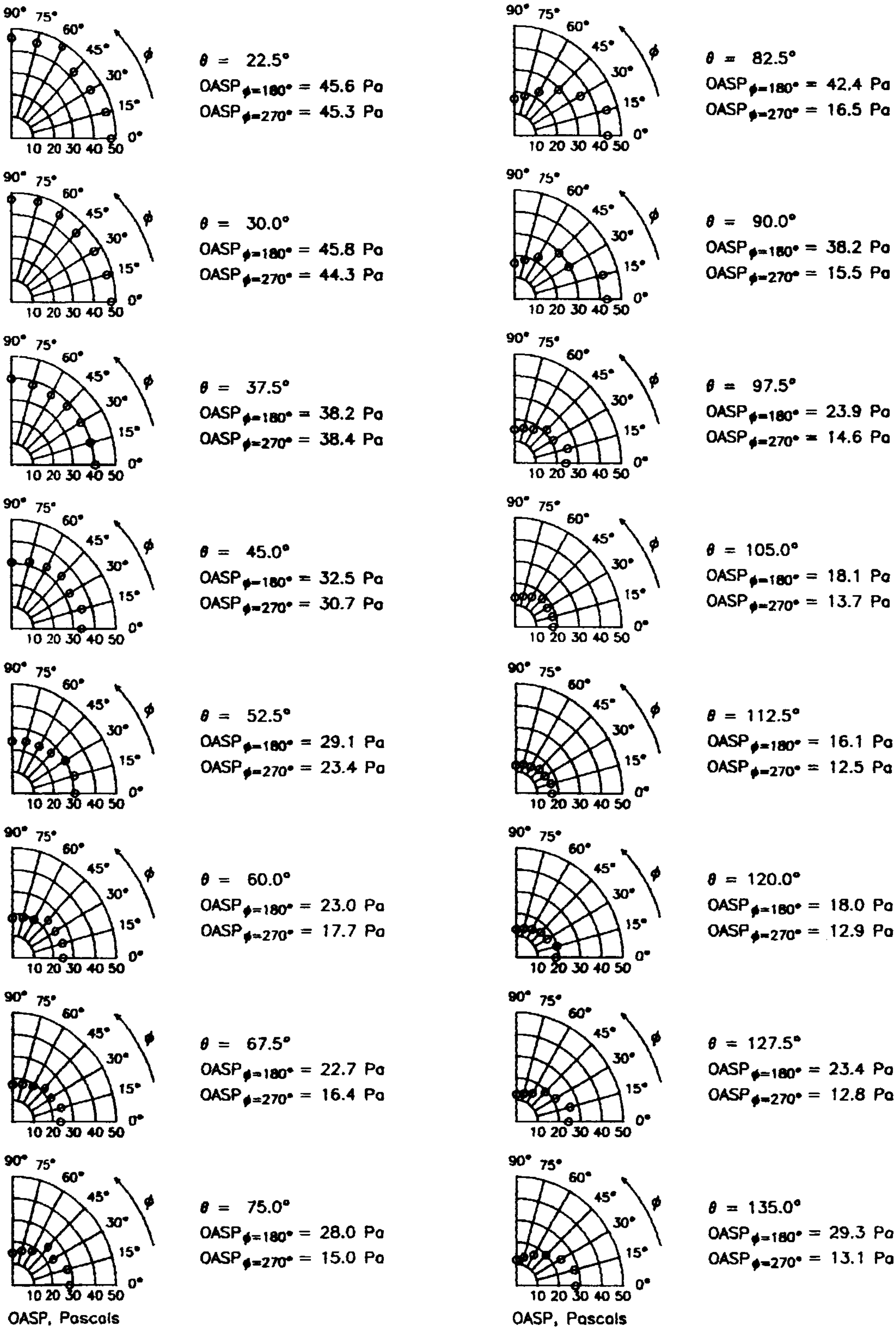

(i) $p_e/p_a = 1.25$.

Figure 9. Continued.

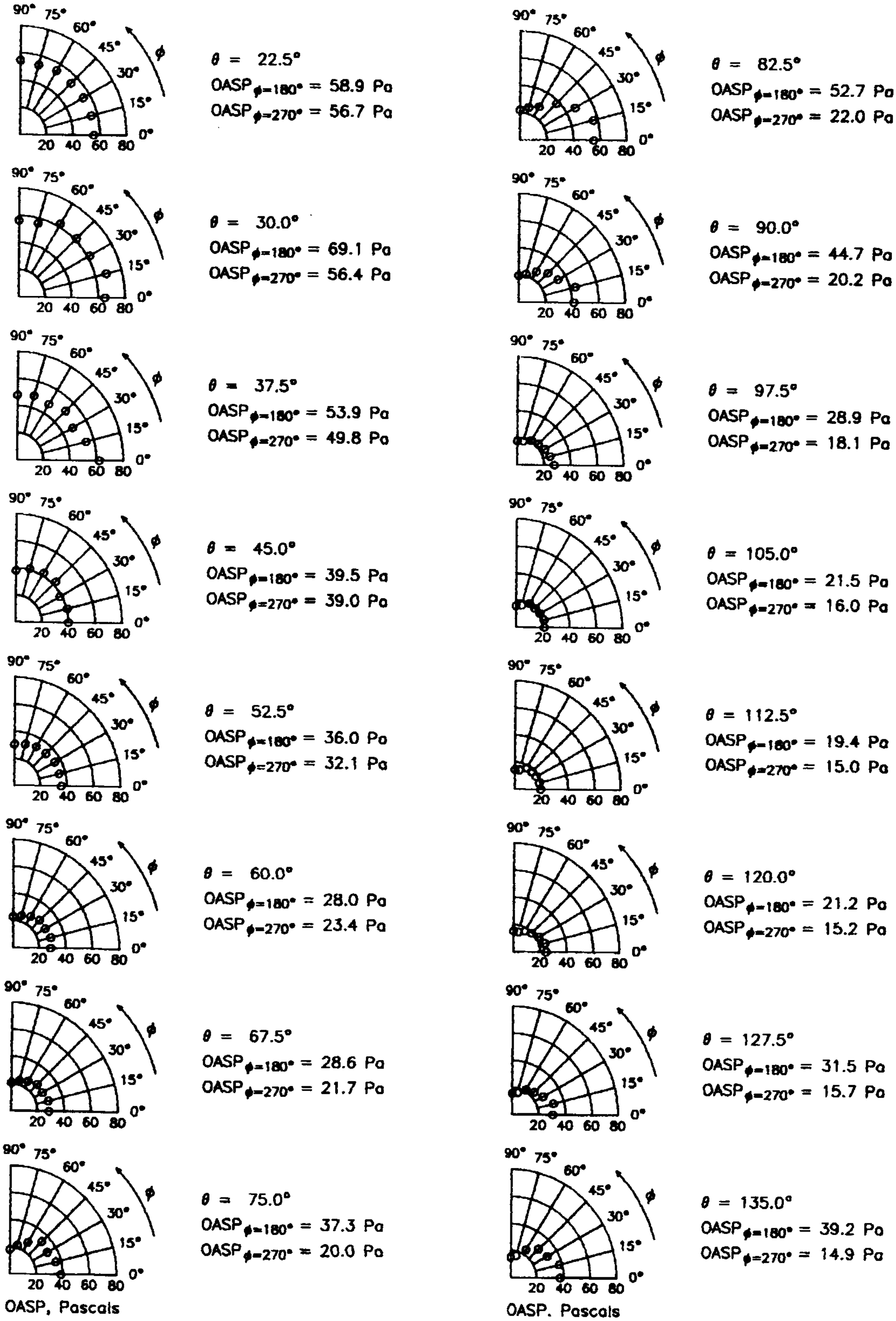

(j) $p_e/p_a = 1.35$.

Figure 9. Continued.

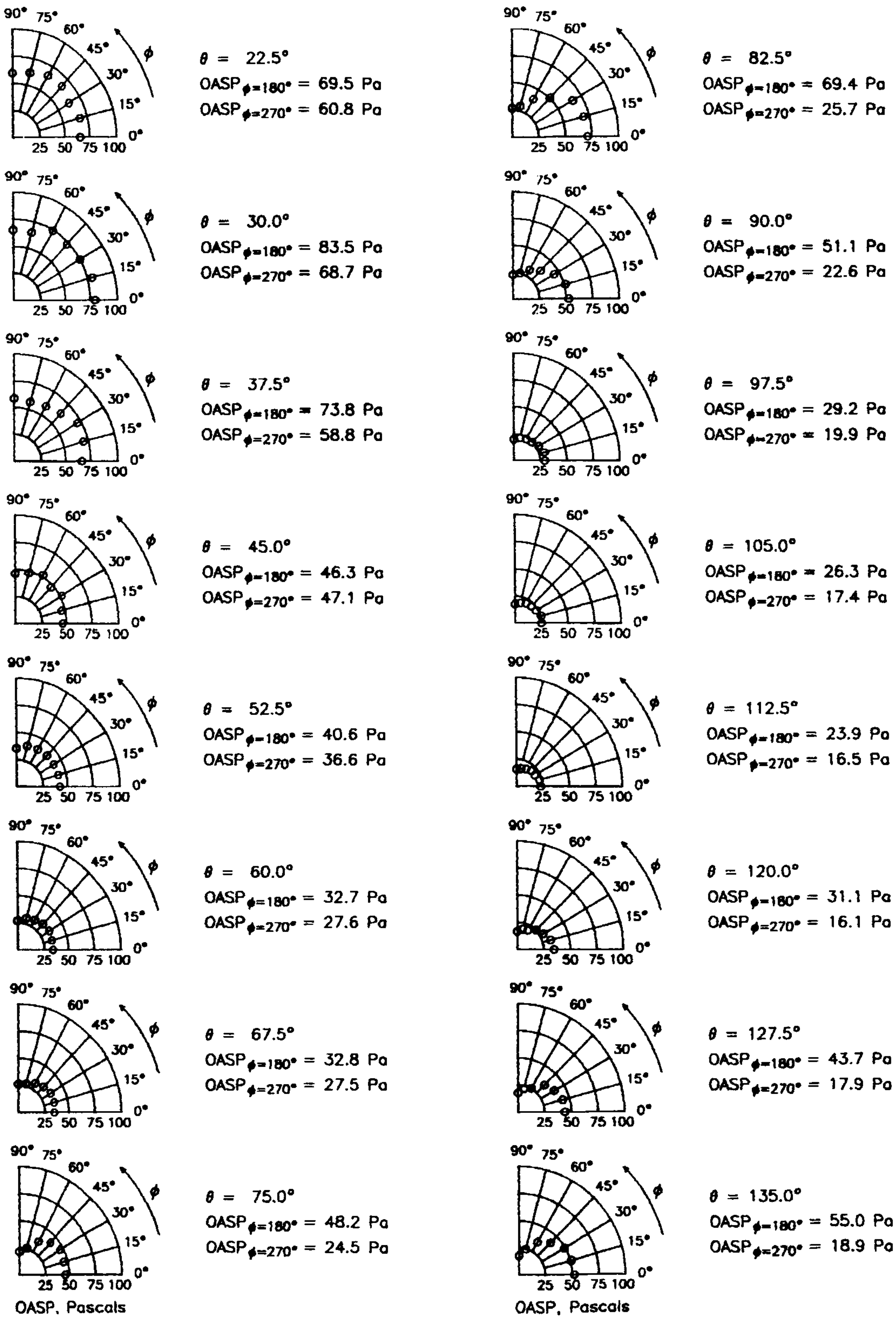

(k) $p_e/p_a = 1.45$.

Figure 9. Concluded.

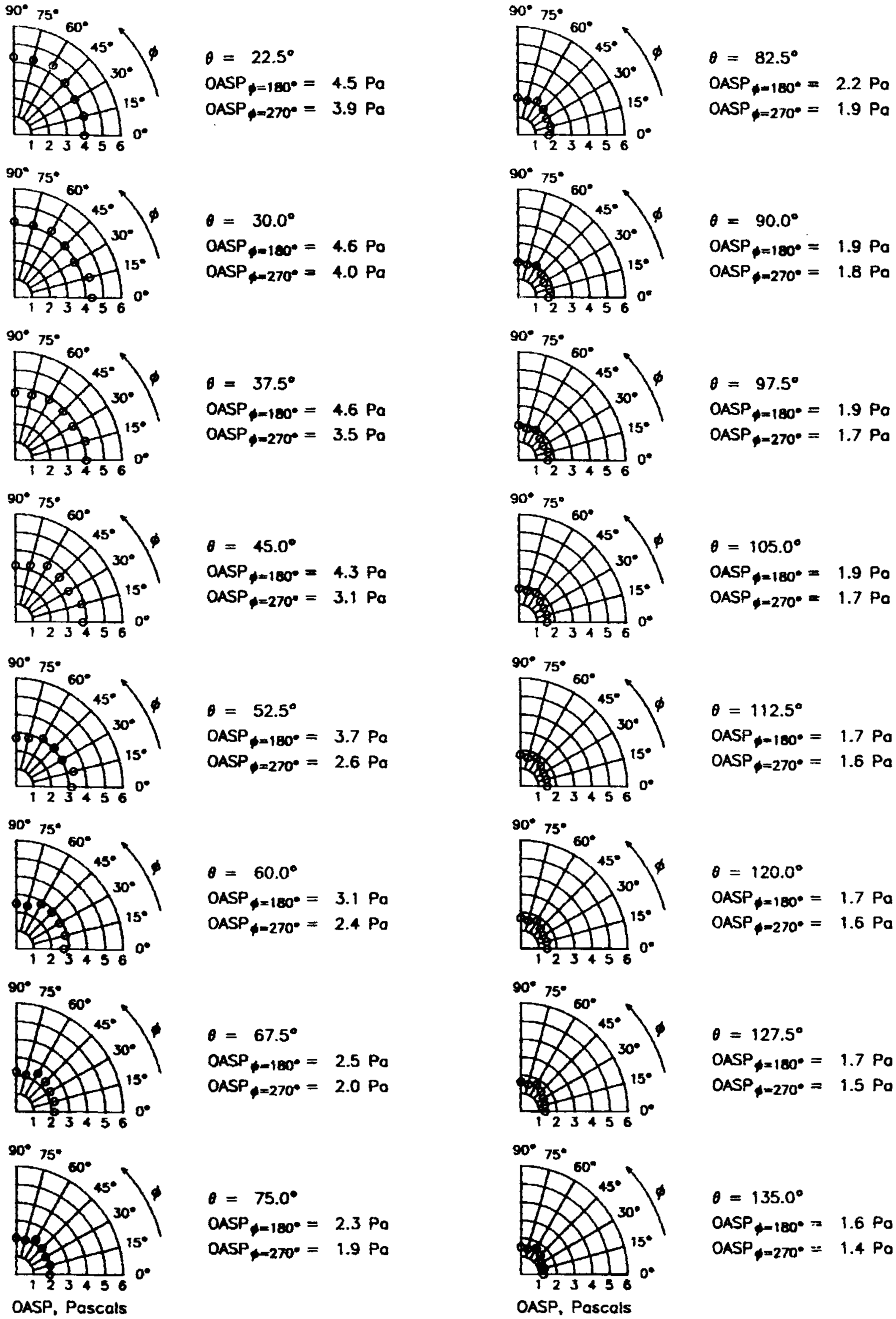

(a) $p_e/p_a = 0.65$.

Figure 10. Directivity plots for rectangular nozzle with throat aspect ratio of 5.8.

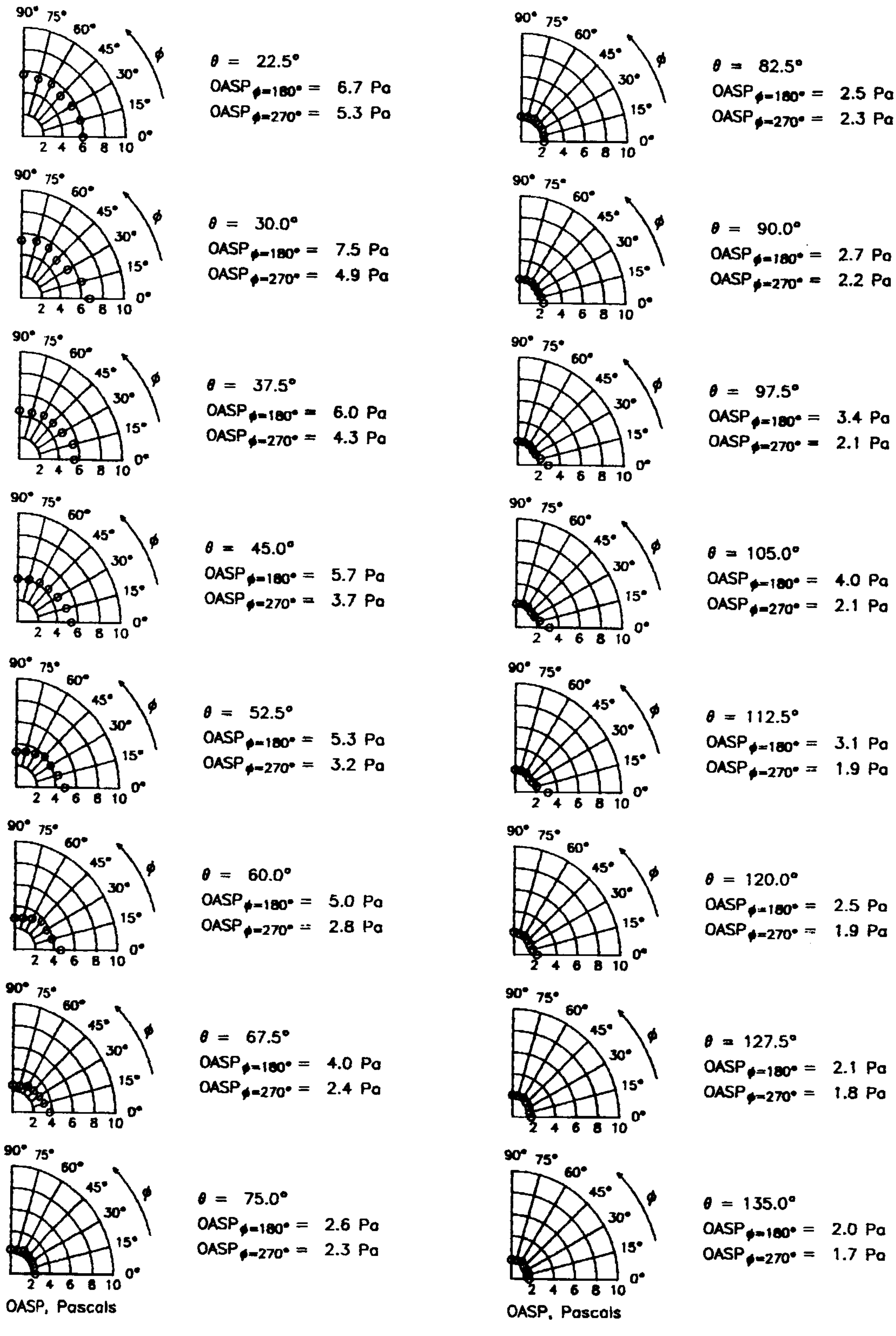

(b) $p_e/p_a = 0.70$.

Figure 10. Continued.

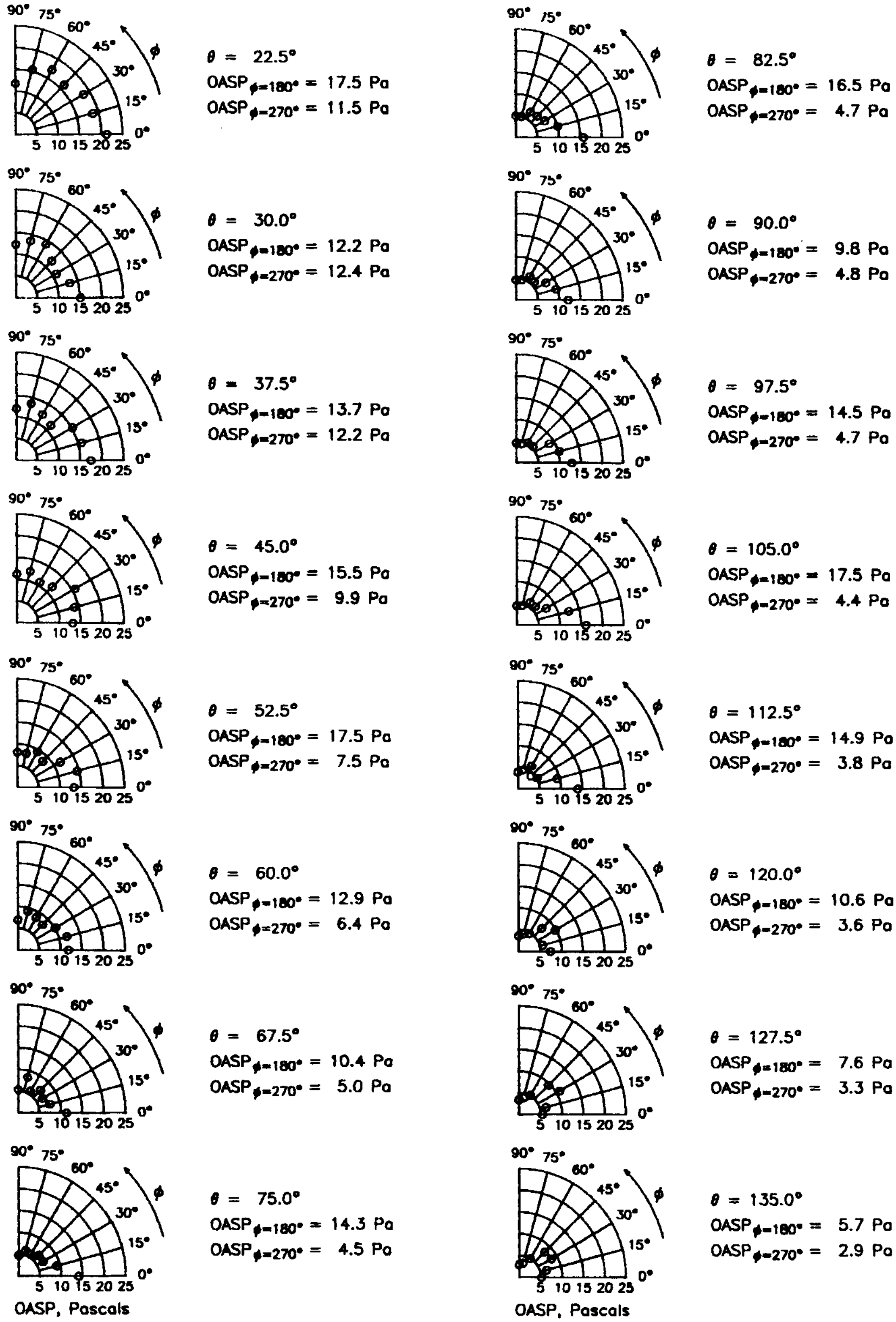

(c) $p_e/p_a = 0.80$.

Figure 10. Continued.

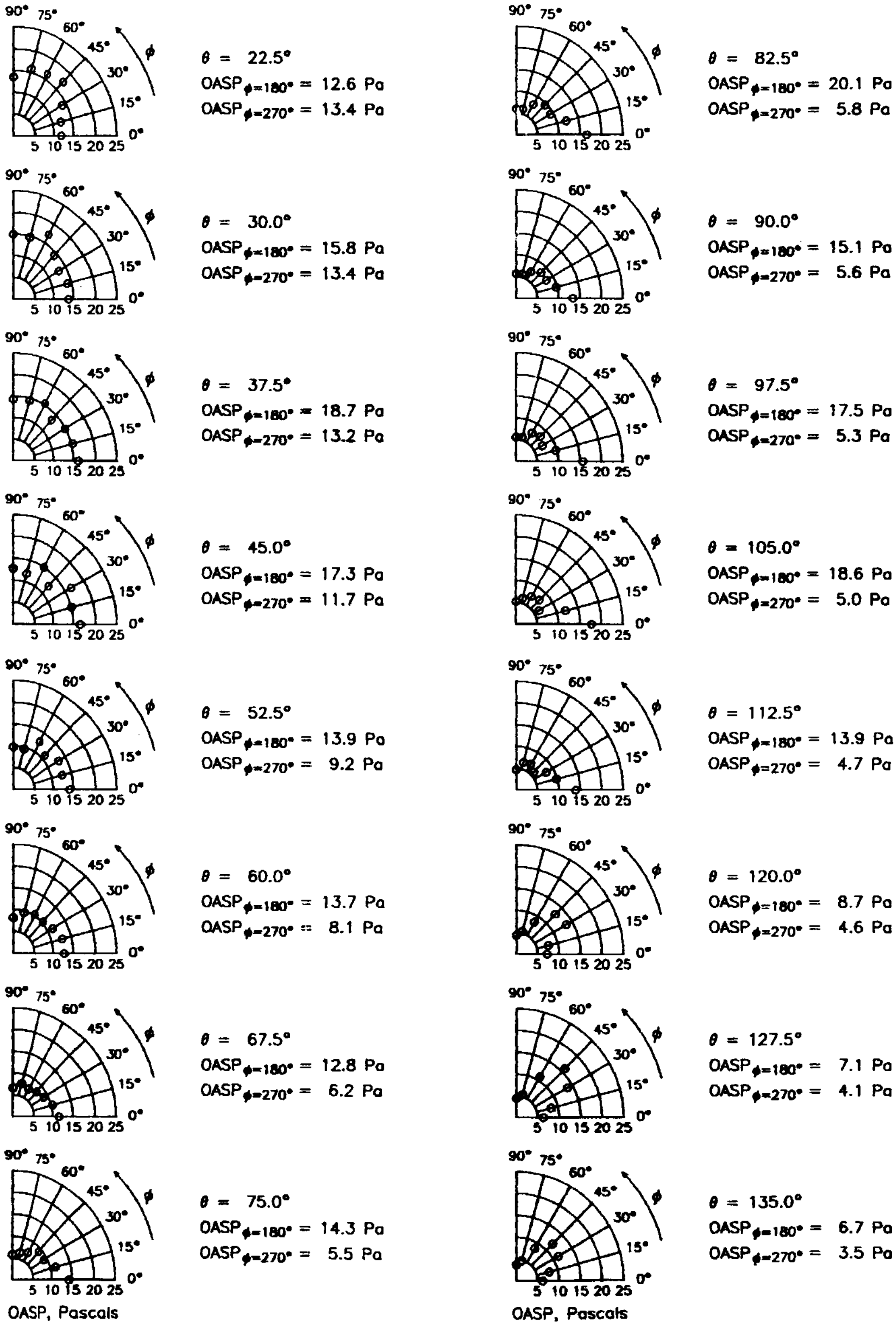

(d) $p_e/p_a = 0.85$.

Figure 10. Continued.

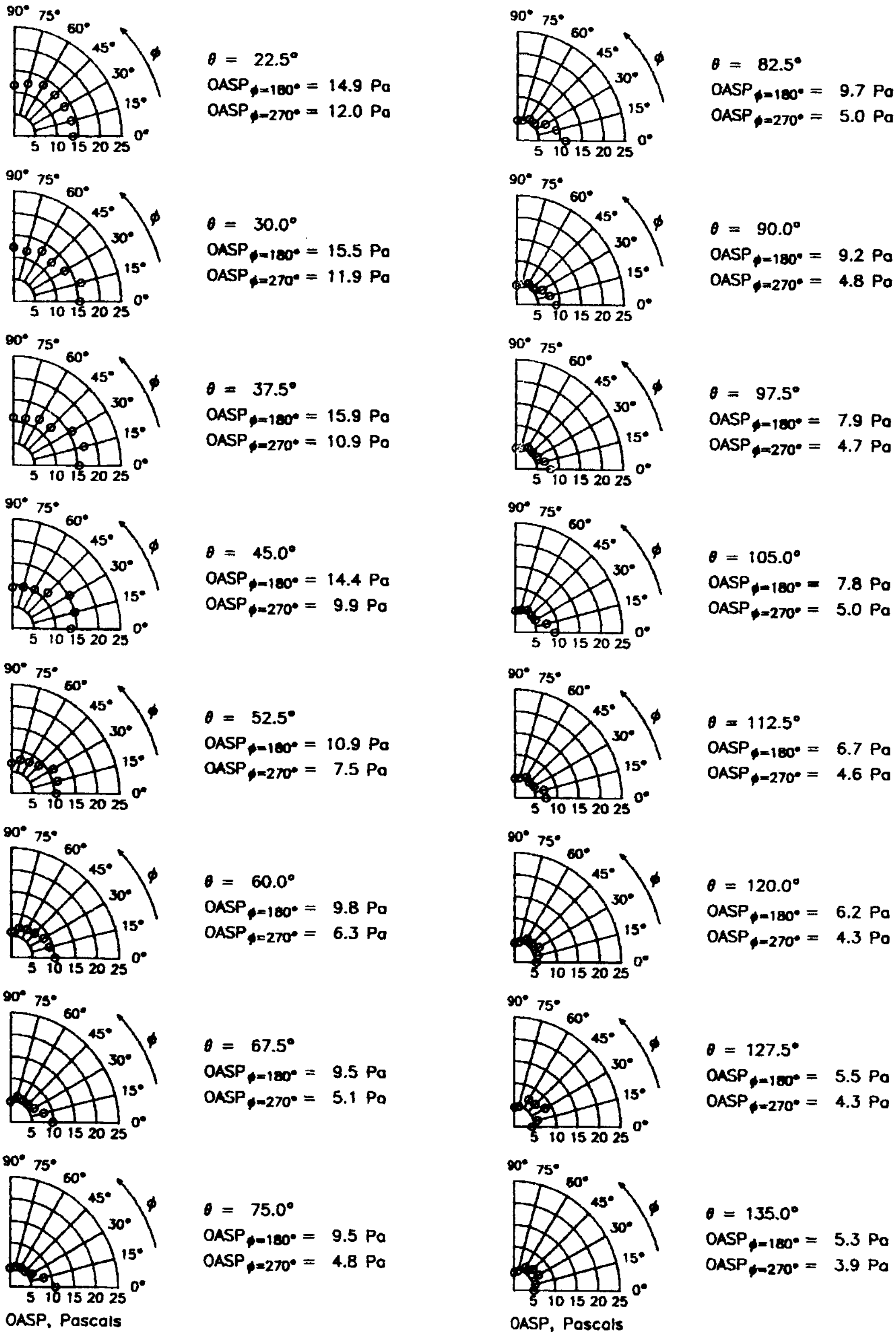

(e) $p_e/p_a = 0.90$.

Figure 10. Continued.

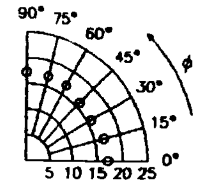

θ = 22.5°
$\mathrm{OASP}_{\phi=180°}$ = 17.2 Pa
$\mathrm{OASP}_{\phi=270°}$ = 15.5 Pa

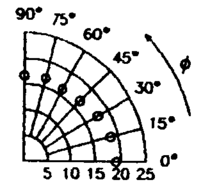

θ = 30.0°
$\mathrm{OASP}_{\phi=180°}$ = 19.0 Pa
$\mathrm{OASP}_{\phi=270°}$ = 14.8 Pa

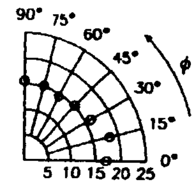

θ = 37.5°
$\mathrm{OASP}_{\phi=180°}$ = 18.5 Pa
$\mathrm{OASP}_{\phi=270°}$ = 13.4 Pa

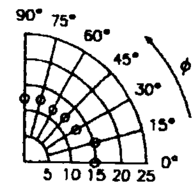

θ = 45.0°
$\mathrm{OASP}_{\phi=180°}$ = 16.2 Pa
$\mathrm{OASP}_{\phi=270°}$ = 11.3 Pa

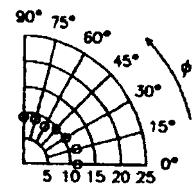

θ = 52.5°
$\mathrm{OASP}_{\phi=180°}$ = 12.1 Pa
$\mathrm{OASP}_{\phi=270°}$ = 7.9 Pa

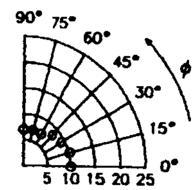

θ = 60.0°
$\mathrm{OASP}_{\phi=180°}$ = 10.7 Pa
$\mathrm{OASP}_{\phi=270°}$ = 6.5 Pa

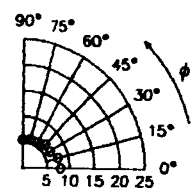

θ = 67.5°
$\mathrm{OASP}_{\phi=180°}$ = 8.8 Pa
$\mathrm{OASP}_{\phi=270°}$ = 5.3 Pa

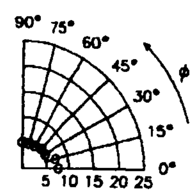

θ = 75.0°
$\mathrm{OASP}_{\phi=180°}$ = 7.6 Pa
$\mathrm{OASP}_{\phi=270°}$ = 4.8 Pa

OASP, Pascals

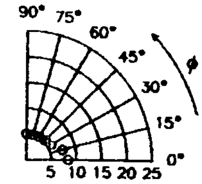

θ = 82.5°
$\mathrm{OASP}_{\phi=180°}$ = 8.4 Pa
$\mathrm{OASP}_{\phi=270°}$ = 4.9 Pa

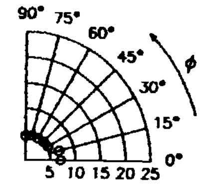

θ = 90.0°
$\mathrm{OASP}_{\phi=180°}$ = 7.7 Pa
$\mathrm{OASP}_{\phi=270°}$ = 4.9 Pa

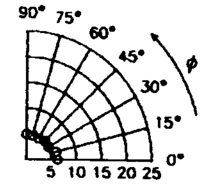

θ = 97.5°
$\mathrm{OASP}_{\phi=180°}$ = 6.9 Pa
$\mathrm{OASP}_{\phi=270°}$ = 4.7 Pa

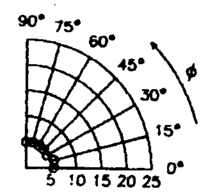

θ = 105.0°
$\mathrm{OASP}_{\phi=180°}$ = 5.8 Pa
$\mathrm{OASP}_{\phi=270°}$ = 4.8 Pa

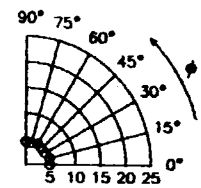

θ = 112.5°
$\mathrm{OASP}_{\phi=180°}$ = 4.9 Pa
$\mathrm{OASP}_{\phi=270°}$ = 4.7 Pa

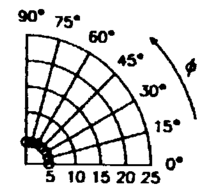

θ = 120.0°
$\mathrm{OASP}_{\phi=180°}$ = 4.6 Pa
$\mathrm{OASP}_{\phi=270°}$ = 4.3 Pa

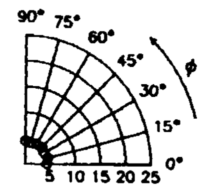

θ = 127.5°
$\mathrm{OASP}_{\phi=180°}$ = 4.9 Pa
$\mathrm{OASP}_{\phi=270°}$ = 4.0 Pa

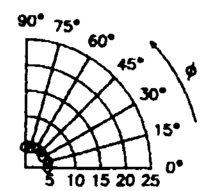

θ = 135.0°
$\mathrm{OASP}_{\phi=180°}$ = 5.2 Pa
$\mathrm{OASP}_{\phi=270°}$ = 3.8 Pa

OASP, Pascals

(f) $p_e/p_a = 1.00$.

Figure 10. Continued.

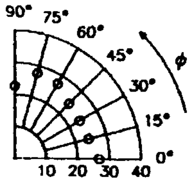

θ = 22.5°
$OASP_{\phi=180°}$ = 19.5 Pa
$OASP_{\phi=270°}$ = 25.3 Pa

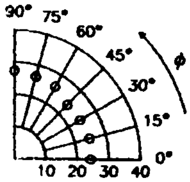

θ = 30.0°
$OASP_{\phi=180°}$ = 21.5 Pa
$OASP_{\phi=270°}$ = 26.6 Pa

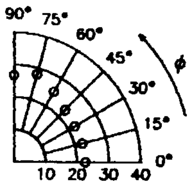

θ = 37.5°
$OASP_{\phi=180°}$ = 26.6 Pa
$OASP_{\phi=270°}$ = 25.9 Pa

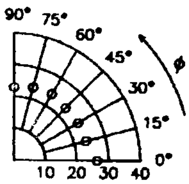

θ = 45.0°
$OASP_{\phi=180°}$ = 28.5 Pa
$OASP_{\phi=270°}$ = 22.2 Pa

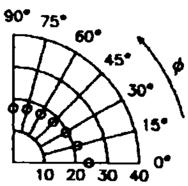

θ = 52.5°
$OASP_{\phi=180°}$ = 21.3 Pa
$OASP_{\phi=270°}$ = 16.9 Pa

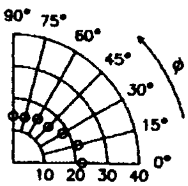

θ = 60.0°
$OASP_{\phi=180°}$ = 22.2 Pa
$OASP_{\phi=270°}$ = 13.8 Pa

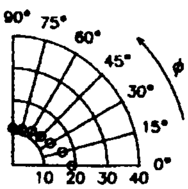

θ = 67.5°
$OASP_{\phi=180°}$ = 18.2 Pa
$OASP_{\phi=270°}$ = 10.8 Pa

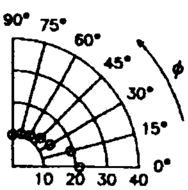

θ = 75.0°
$OASP_{\phi=180°}$ = 20.1 Pa
$OASP_{\phi=270°}$ = 9.7 Pa

OASP, Pascals

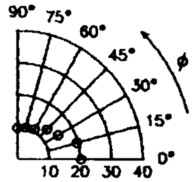

θ = 82.5°
$OASP_{\phi=180°}$ = 21.4 Pa
$OASP_{\phi=270°}$ = 9.5 Pa

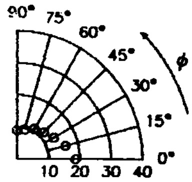

θ = 90.0°
$OASP_{\phi=180°}$ = 16.6 Pa
$OASP_{\phi=270°}$ = 8.9 Pa

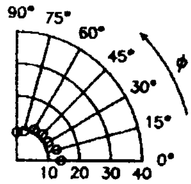

θ = 97.5°
$OASP_{\phi=180°}$ = 13.6 Pa
$OASP_{\phi=270°}$ = 8.5 Pa

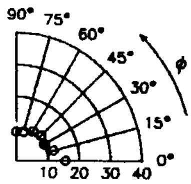

θ = 105.0°
$OASP_{\phi=180°}$ = 13.7 Pa
$OASP_{\phi=270°}$ = 8.3 Pa

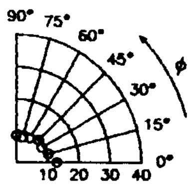

θ = 112.5°
$OASP_{\phi=180°}$ = 11.1 Pa
$OASP_{\phi=270°}$ = 8.6 Pa

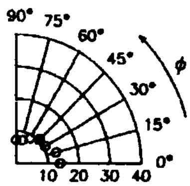

θ = 120.0°
$OASP_{\phi=180°}$ = 12.1 Pa
$OASP_{\phi=270°}$ = 7.9 Pa

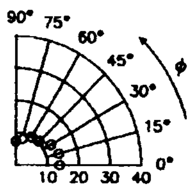

θ = 127.5°
$OASP_{\phi=180°}$ = 13.9 Pa
$OASP_{\phi=270°}$ = 8.3 Pa

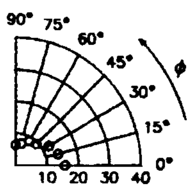

θ = 135.0°
$OASP_{\phi=180°}$ = 15.6 Pa
$OASP_{\phi=270°}$ = 6.0 Pa

OASP, Pascals

(g) $p_e/p_a = 1.10$.

Figure 10. Continued.

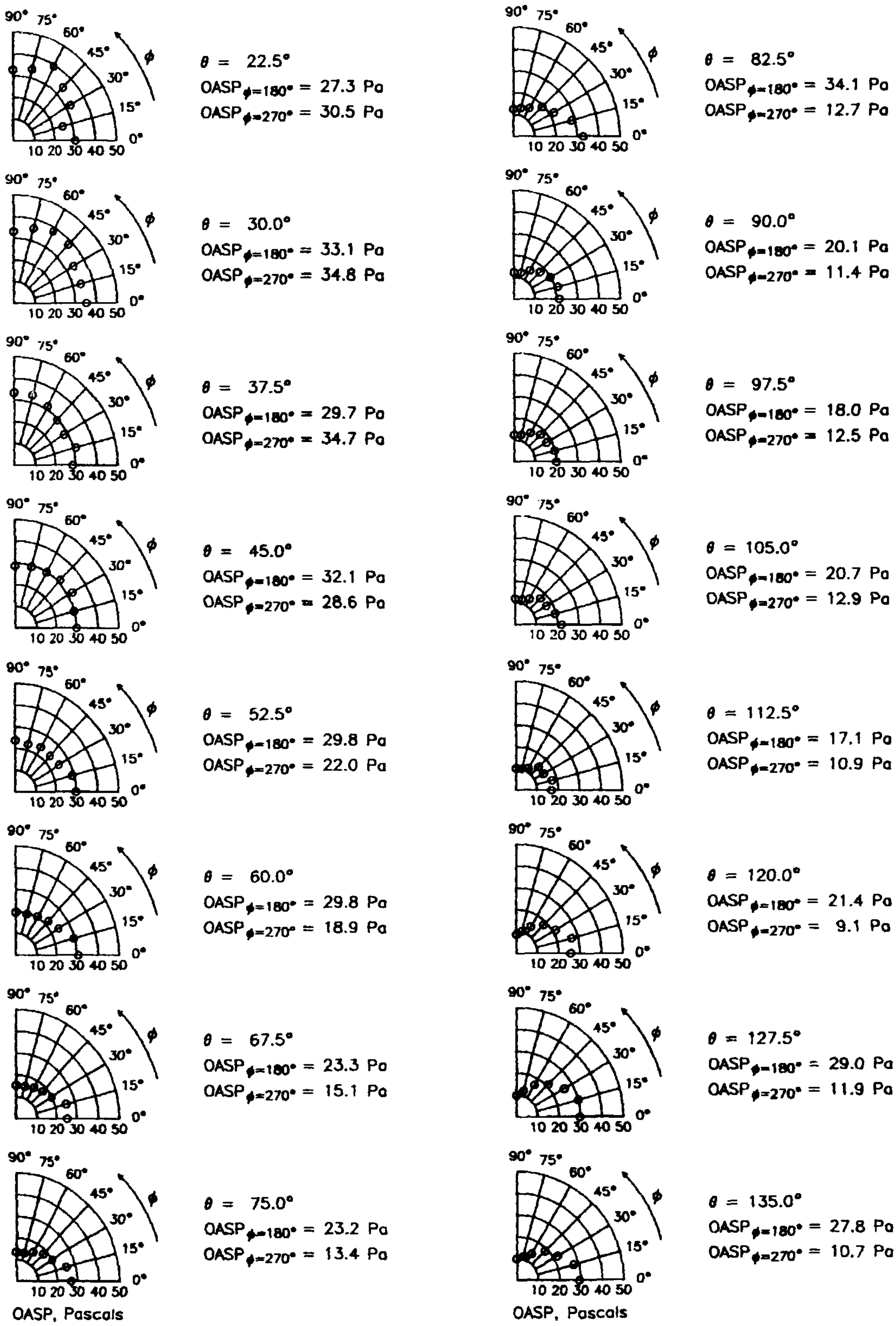

(h) $p_e/p_a = 1.20$.

Figure 10. Continued.

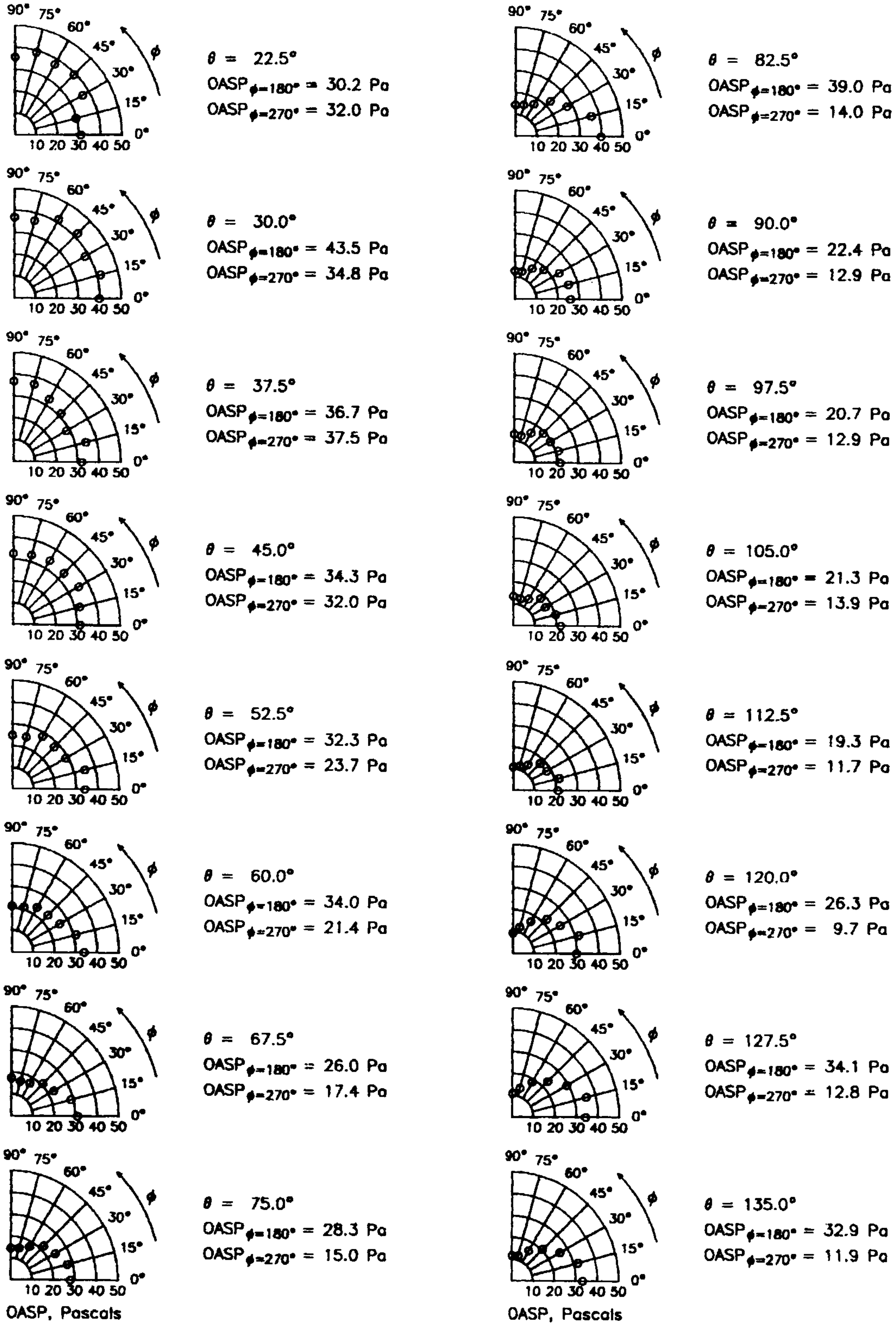

(i) $p_e/p_a = 1.25$.

Figure 10. Continued.

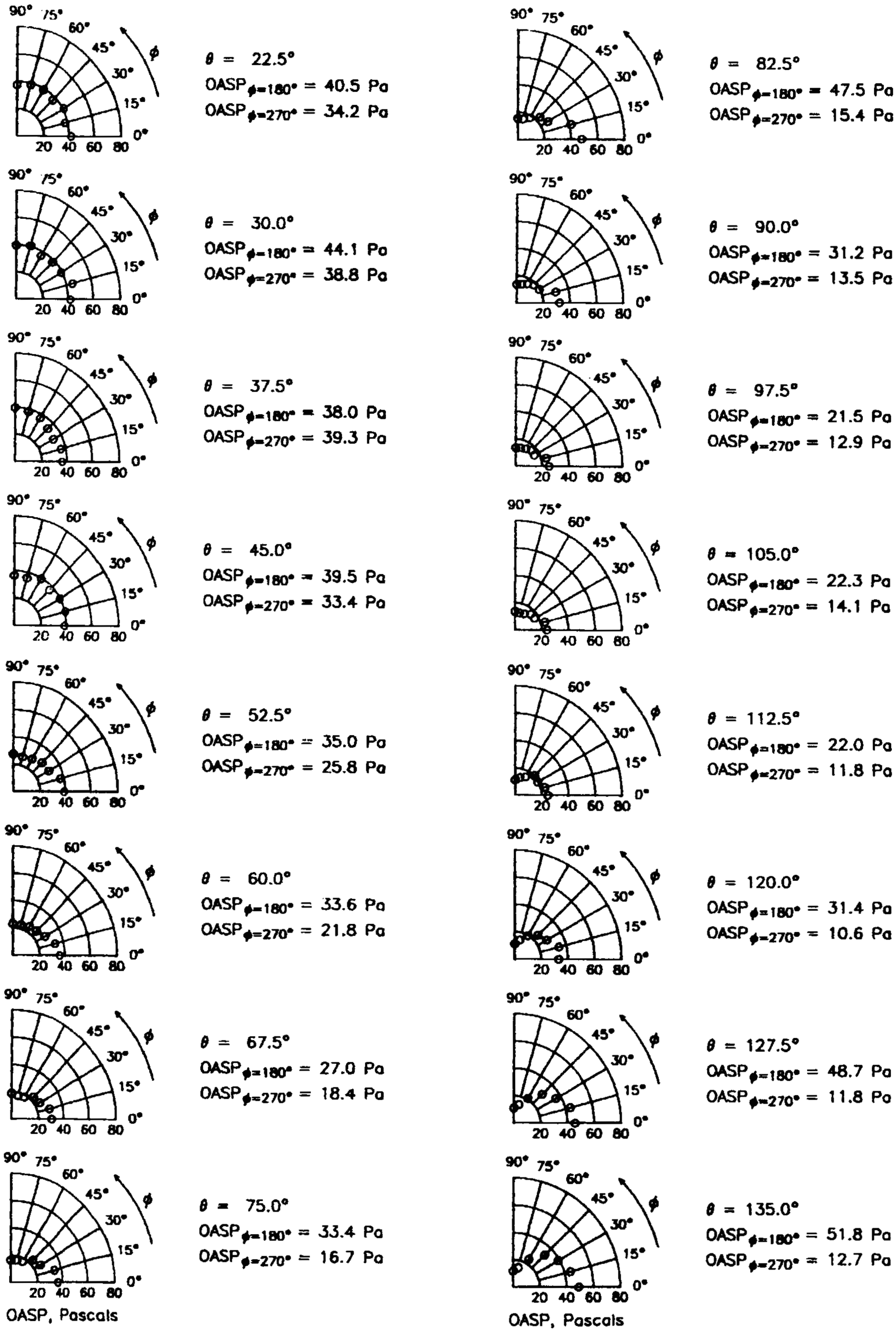

(j) $p_e/p_a = 1.35$.

Figure 10. Continued.

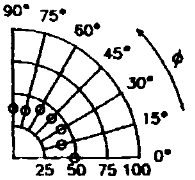

θ = 22.5°
OASP$_{\phi=180°}$ = 44.9 Pa
OASP$_{\phi=270°}$ = 38.8 Pa

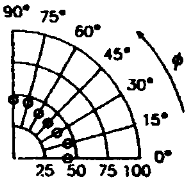

θ = 30.0°
OASP$_{\phi=180°}$ = 45.9 Pa
OASP$_{\phi=270°}$ = 42.2 Pa

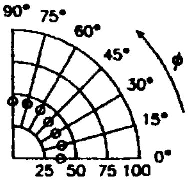

θ = 37.5°
OASP$_{\phi=180°}$ = 40.9 Pa
OASP$_{\phi=270°}$ = 39.1 Pa

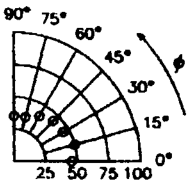

θ = 45.0°
OASP$_{\phi=180°}$ = 46.6 Pa
OASP$_{\phi=270°}$ = 31.8 Pa

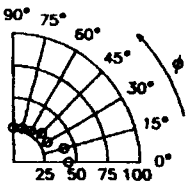

θ = 52.5°
OASP$_{\phi=180°}$ = 36.1 Pa
OASP$_{\phi=270°}$ = 23.7 Pa

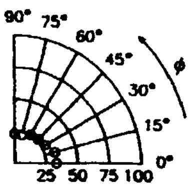

θ = 60.0°
OASP$_{\phi=180°}$ = 30.1 Pa
OASP$_{\phi=270°}$ = 20.8 Pa

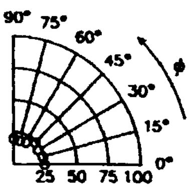

θ = 67.5°
OASP$_{\phi=180°}$ = 24.1 Pa
OASP$_{\phi=270°}$ = 16.8 Pa

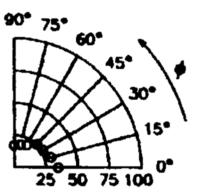

θ = 75.0°
OASP$_{\phi=180°}$ = 31.9 Pa
OASP$_{\phi=270°}$ = 15.3 Pa

OASP, Pascals

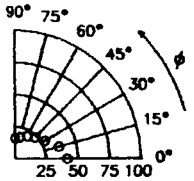

θ = 82.5°
OASP$_{\phi=180°}$ = 31.8 Pa
OASP$_{\phi=270°}$ = 15.6 Pa

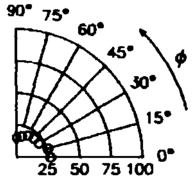

θ = 90.0°
OASP$_{\phi=180°}$ = 25.3 Pa
OASP$_{\phi=270°}$ = 14.7 Pa

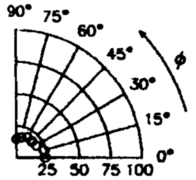

θ = 97.5°
OASP$_{\phi=180°}$ = 19.8 Pa
OASP$_{\phi=270°}$ = 14.9 Pa

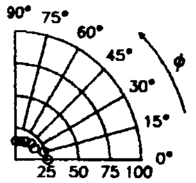

θ = 105.0°
OASP$_{\phi=180°}$ = 23.0 Pa
OASP$_{\phi=270°}$ = 14.6 Pa

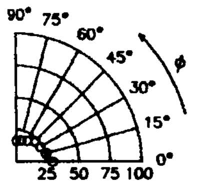

θ = 112.5°
OASP$_{\phi=180°}$ = 25.0 Pa
OASP$_{\phi=270°}$ = 16.1 Pa

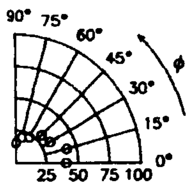

θ = 120.0°
OASP$_{\phi=180°}$ = 36.8 Pa
OASP$_{\phi=270°}$ = 14.9 Pa

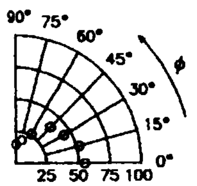

θ = 127.5°
OASP$_{\phi=180°}$ = 55.1 Pa
OASP$_{\phi=270°}$ = 13.5 Pa

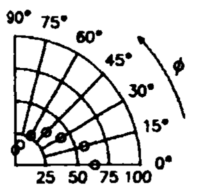

θ = 135.0°
OASP$_{\phi=180°}$ = 56.5 Pa
OASP$_{\phi=270°}$ = 12.5 Pa

OASP, Pascals

(k) $p_e/p_a = 1.45$.

Figure 10. Concluded.

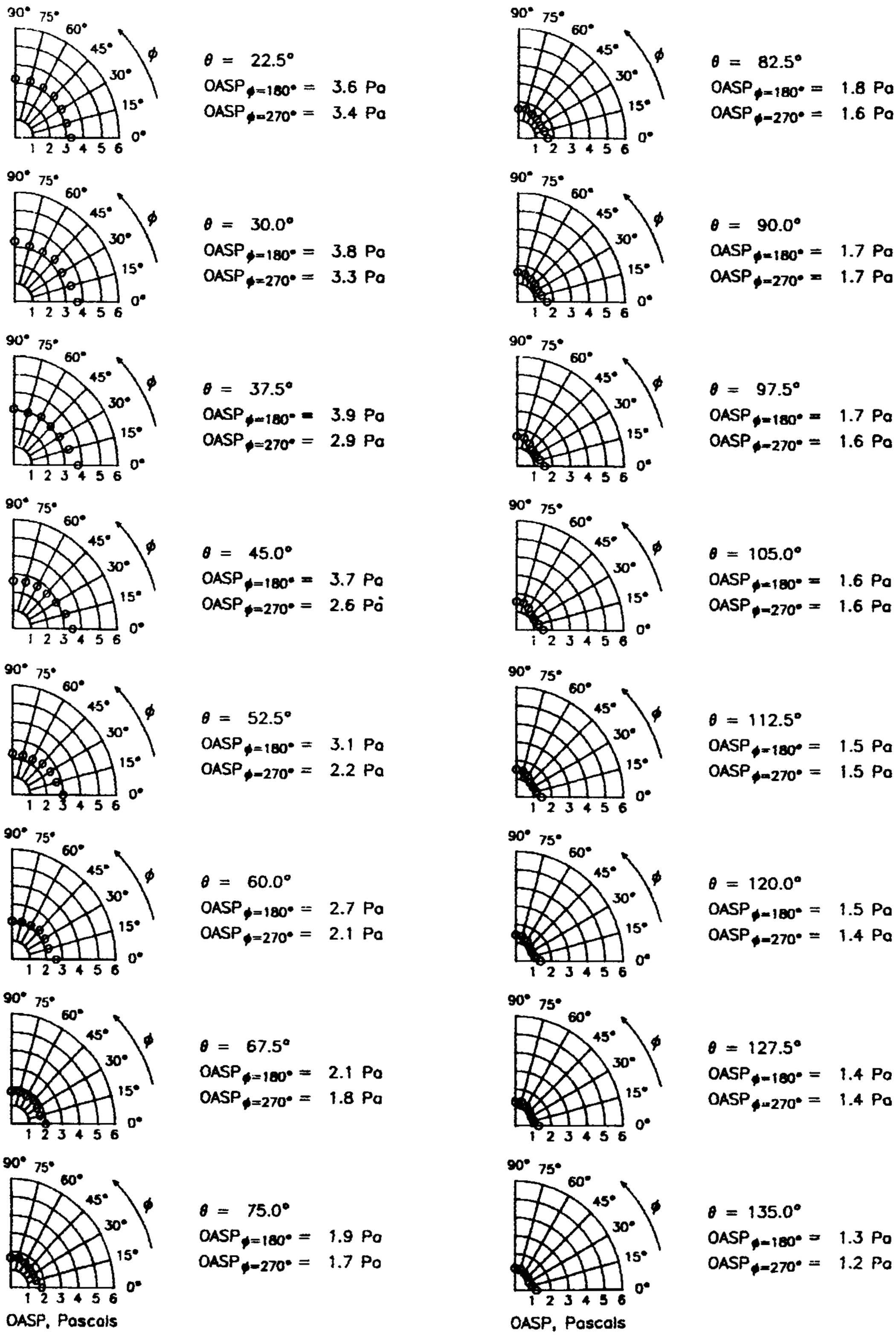

(a) $p_e/p_a = 0.65$.

Figure 11. Directivity plots for rectangular nozzle with throat aspect ratio of 7.6.

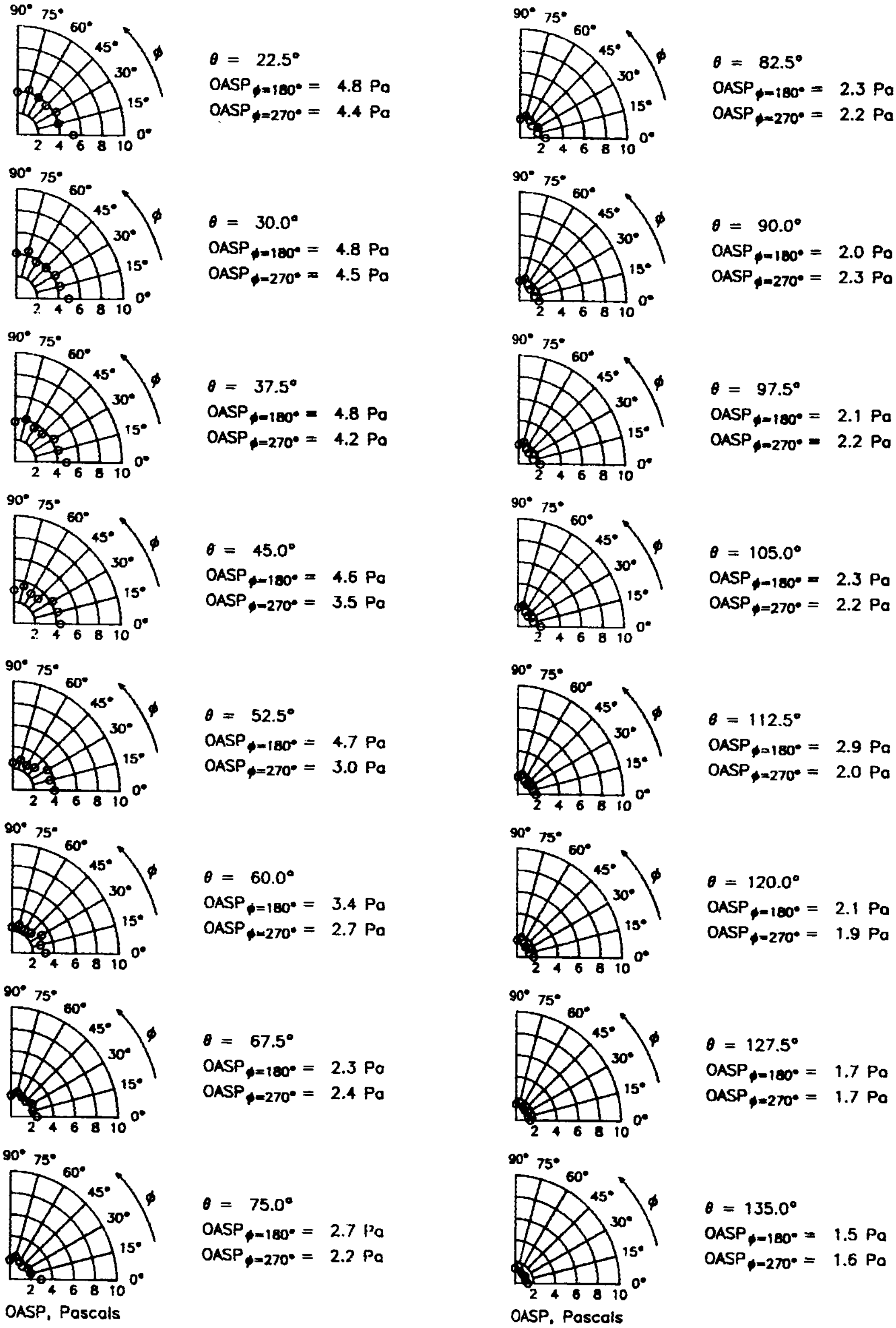

(b) $p_e/p_a = 0.70$.

Figure 11. Continued.

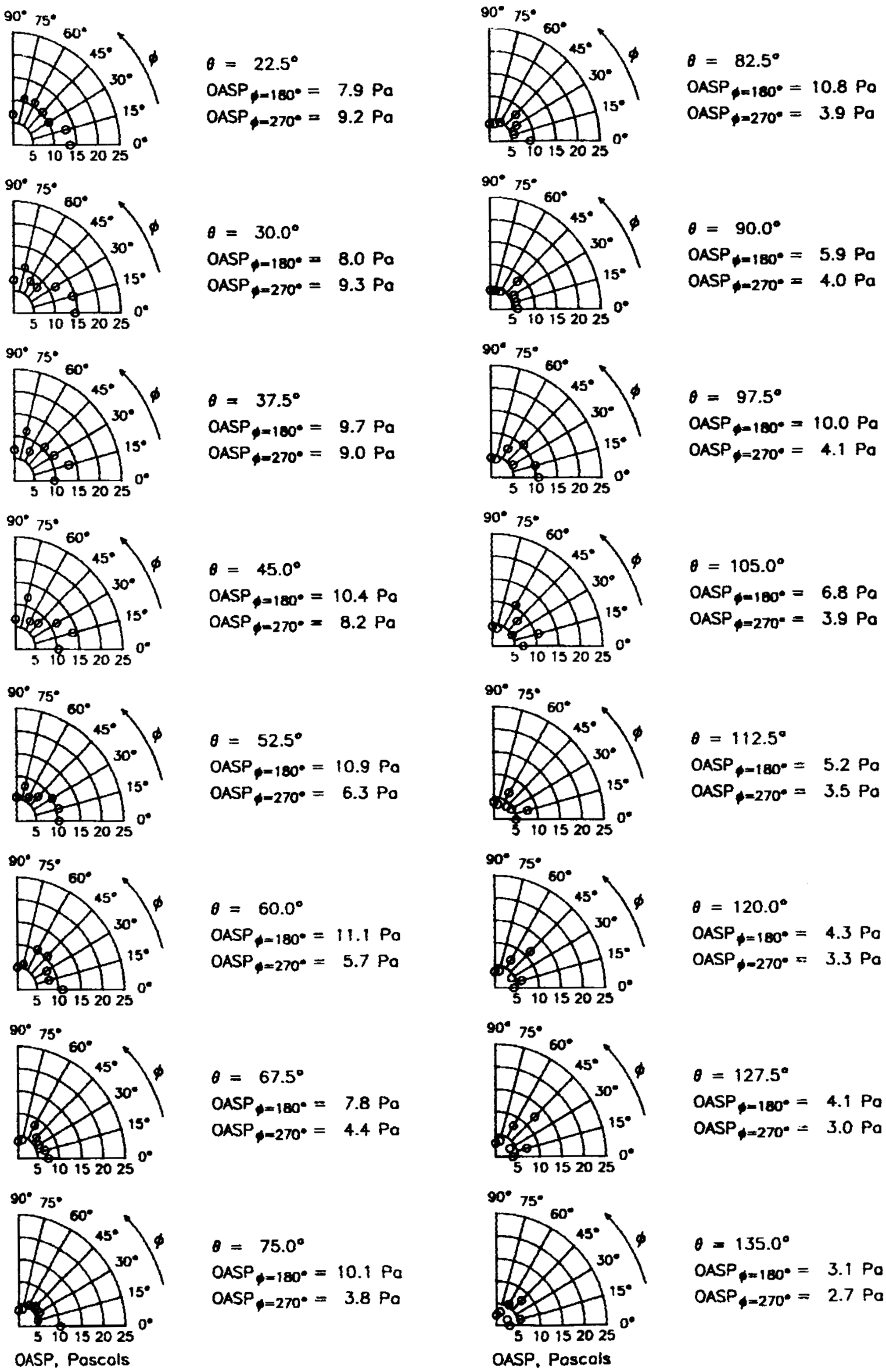

(c) $p_e/p_a = 0.80$.

Figure 11. Continued.

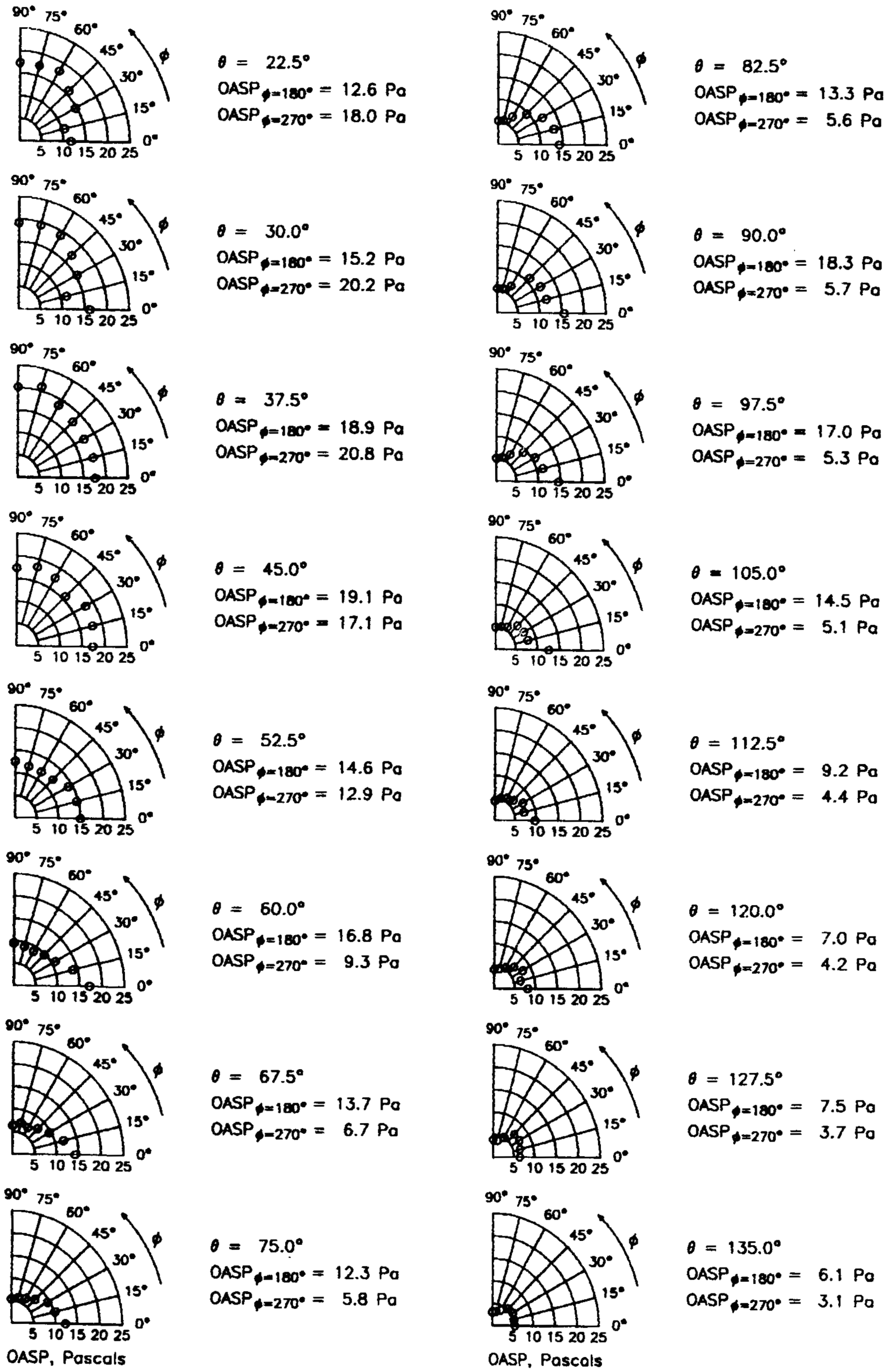

(d) $p_e/p_a = 0.85$.

Figure 11. Continued.

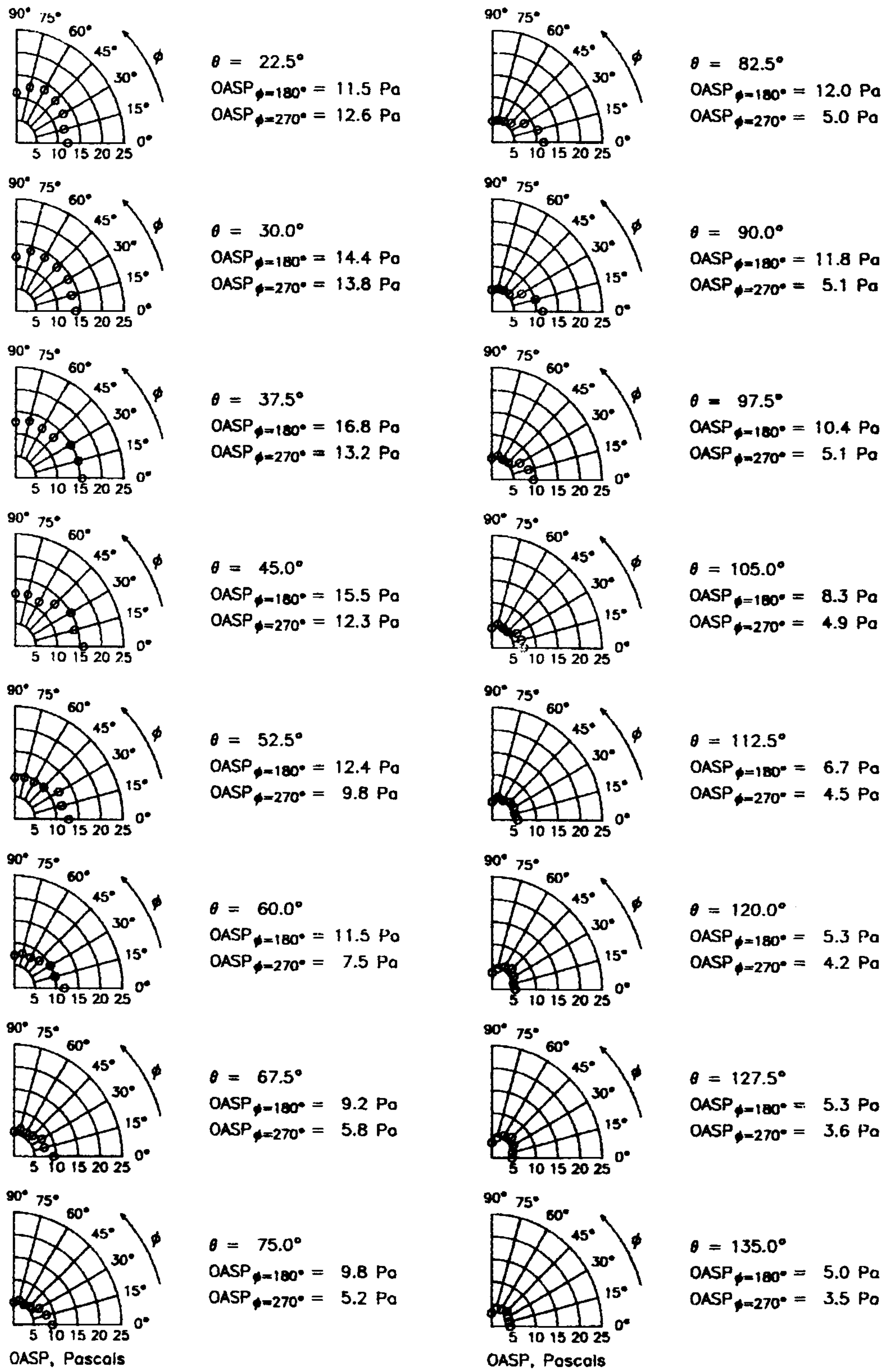

(e) $p_e/p_a = 0.90$.

Figure 11. Continued.

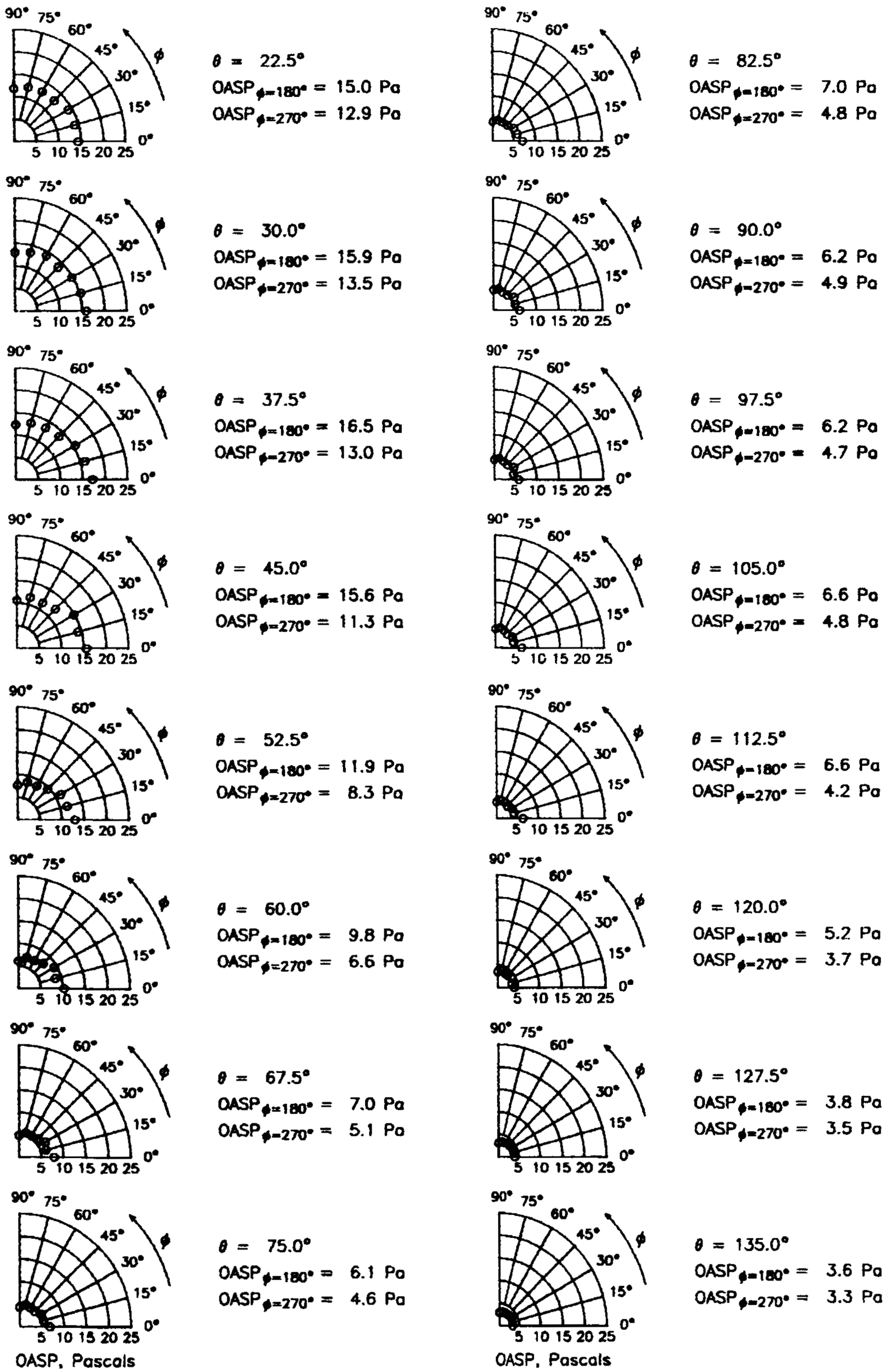

(f) $p_e/p_a = 1.00$.

Figure 11. Continued.

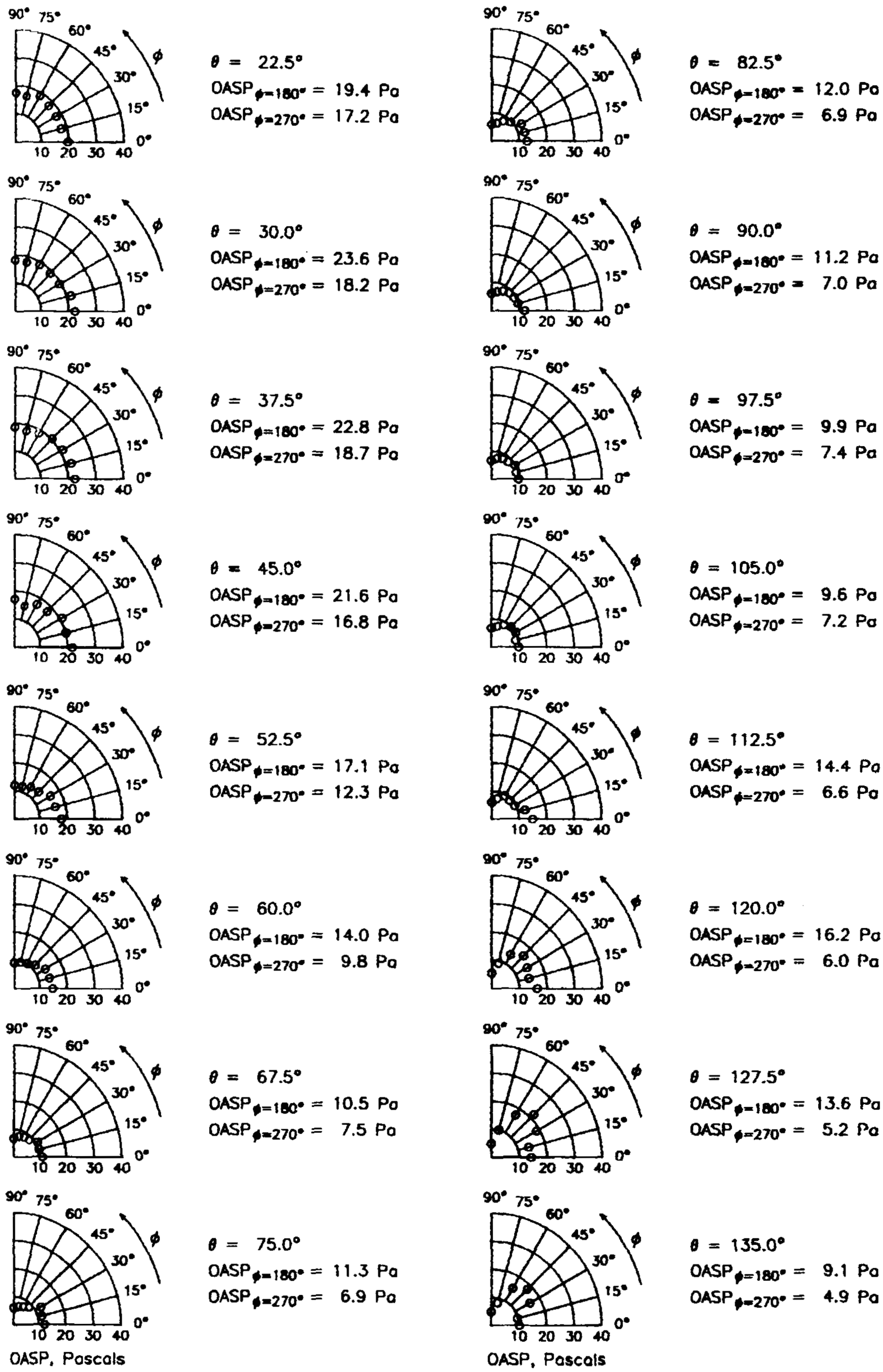

(g) $p_e/p_a = 1.10$.

Figure 11. Continued.

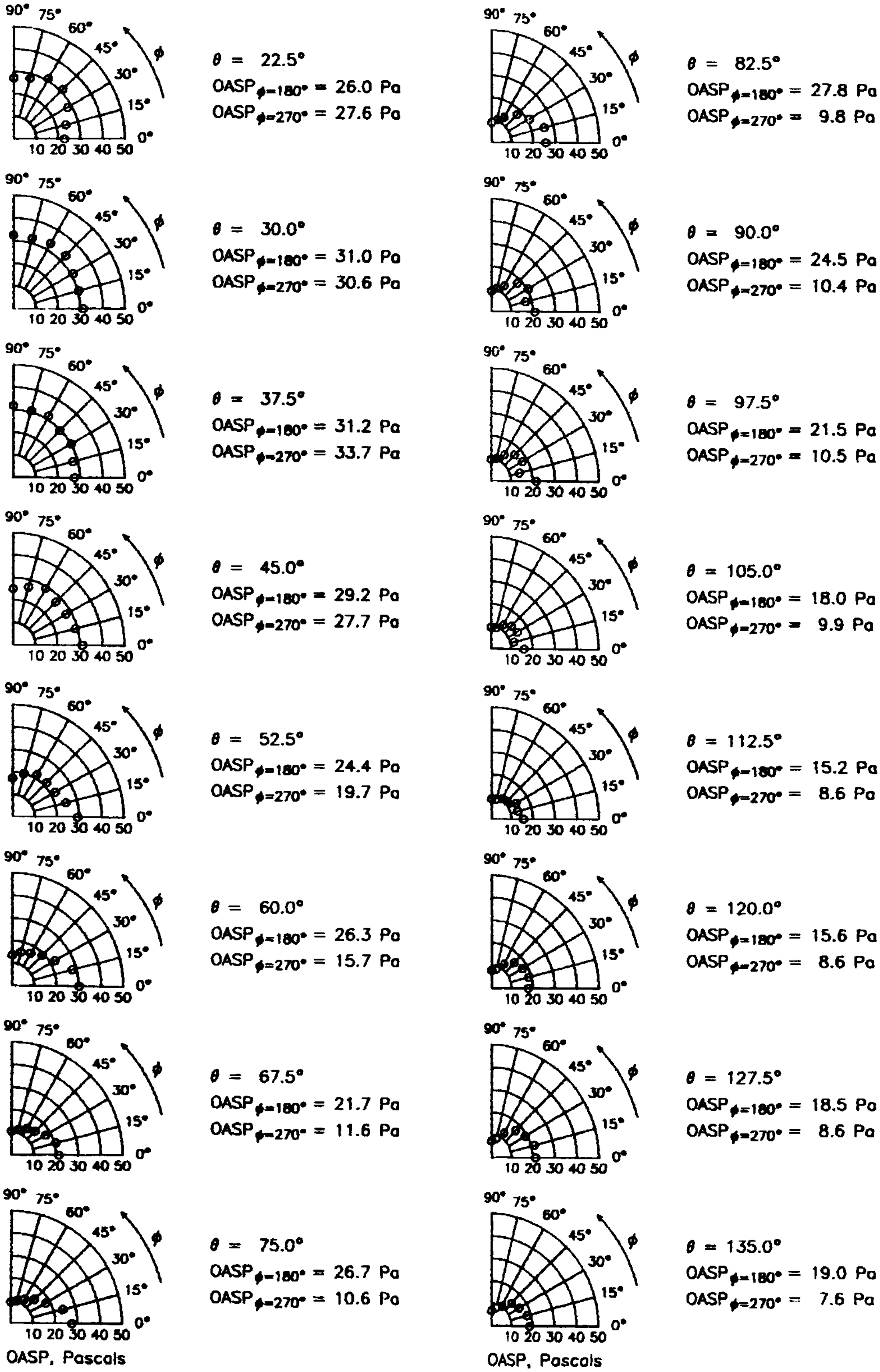

(h) $p_e/p_a = 1.20$.

Figure 11. Continued.

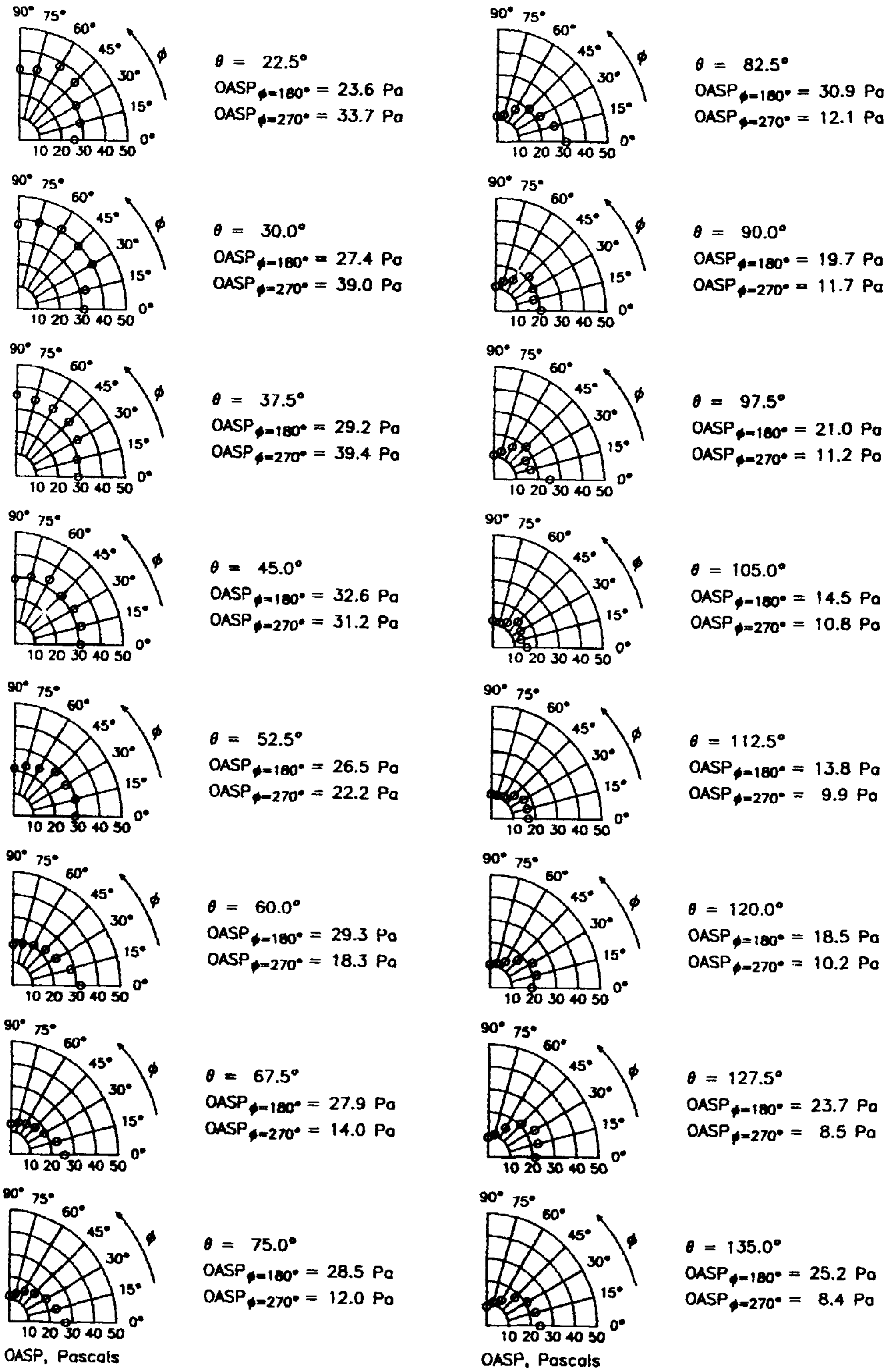

(i) $p_e/p_a = 1.25$.

Figure 11. Continued.

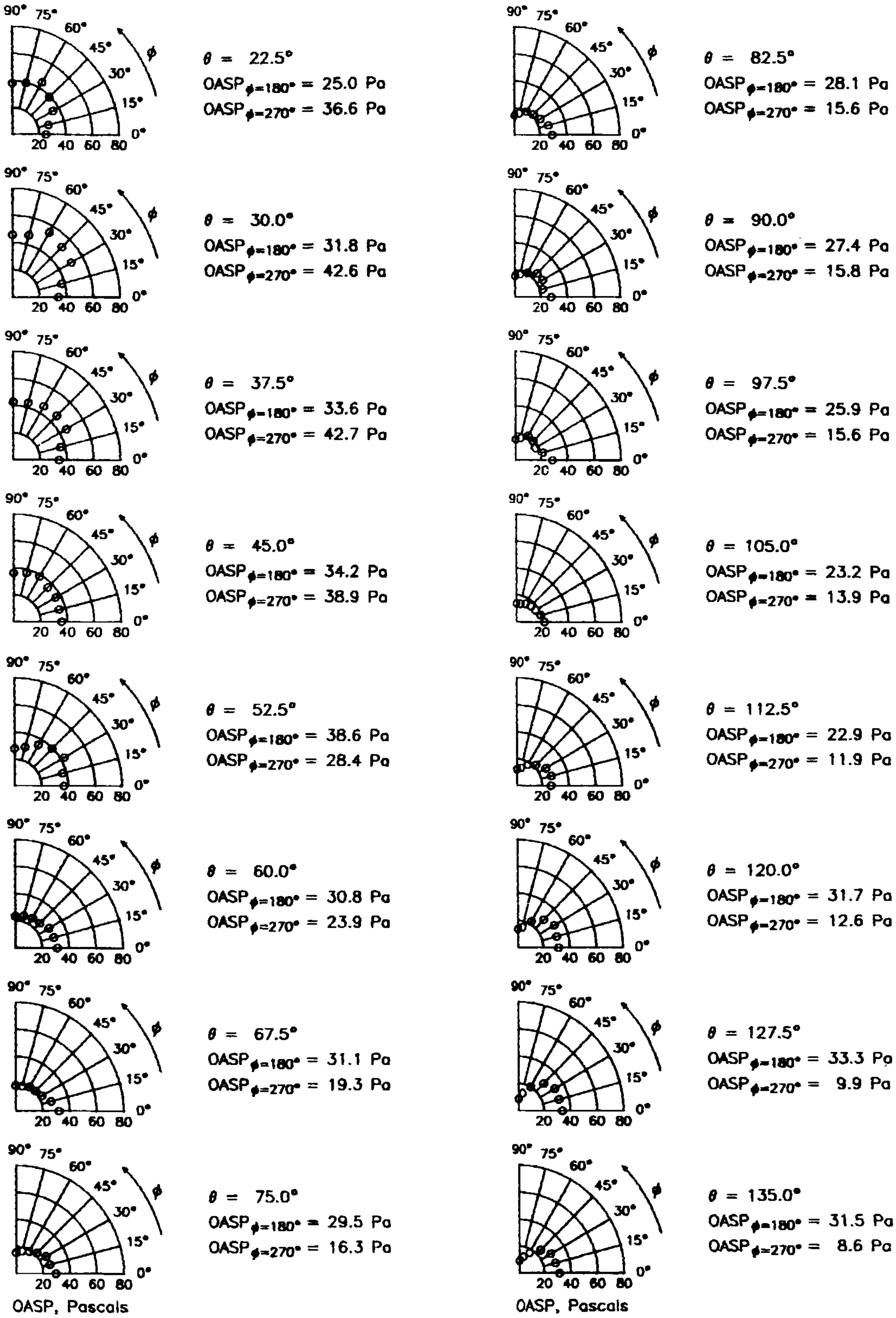

(j) $p_e/p_a = 1.35$.

Figure 11. Continued.

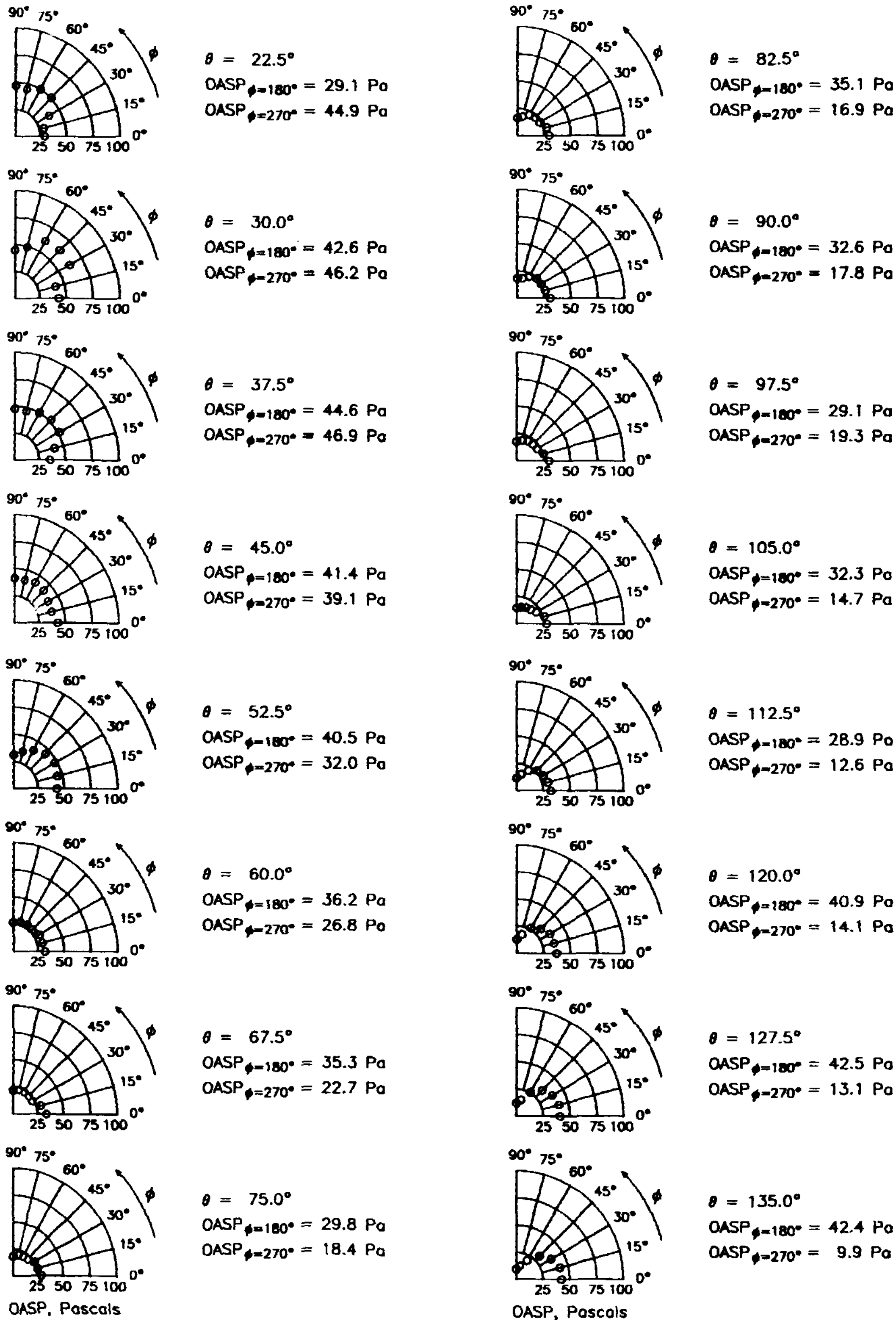

(k) $p_e/p_a = 1.45$.

Figure 11. Concluded.

Standard Bibliographic Page

1. Report No. NASA TM-89002	2. Government Accession No.	3. Recipient's Catalog No.
4. Title and Subtitle Far-Field Acoustics of Supersonic Rectangular Nozzles With Various Throat Aspect Ratios		5. Report Date December 1986
		6. Performing Organization Code 505-61-11-01
7. Author(s) Michael K. Ponton, James C. Manning, and John M. Seiner		8. Performing Organization Report No. L-16167
9. Performing Organization Name and Address NASA Langley Research Center Hampton, VA 23665-5225		10. Work Unit No.
		11. Contract or Grant No.
12. Sponsoring Agency Name and Address National Aeronautics and Space Administration Washington, DC 20546-0001		13. Type of Report and Period Covered Technical Memorandum
		14. Sponsoring Agency Code

15. Supplementary Notes
Michael K. Ponton: PRC Kentron, Inc., Hampton, Virginia.
James C. Manning and John M. Seiner: Langley Research Center, Hampton, Virginia.

16. Abstract
The far-field acoustic behavior of supersonic jets produced by four rectangular nozzles with various throat aspect ratios are reported. One nozzle tested was designed for an exit Mach number of 1.66 with throat aspect ratio of 2.0. The remaining three nozzles (throat aspect ratios of 3.7, 5.8, 7.6) were designed for an exit Mach number of 1.35. Acoustic results presented include narrowband spectra and overall sound pressures for numerous operating pressure ratios and spatial locations.

17. Key Words (Suggested by Authors(s))		18. Distribution Statement	
Acoustics Supersonic Rectangular nozzles Far field		Unclassified—Unlimited Subject Category 71	
19. Security Classif.(of this report) Unclassified	20. Security Classif.(of this page) Unclassified	21. No. of Pages 87	22. Price A05

For sale by the National Technical Information Service, Springfield, Virginia 22161

NASA-Langley, 1986